

Emergent stability in complex network dynamics

Chandrakala Meena,¹⁻³ Chittaranjan Hens,⁴ Suman Acharyya,^{1,2} Simcha Haber,¹

Stefano Boccaletti⁵⁻⁸ & Baruch Barzel^{1,2,*}

1. Department of Mathematics, Bar-Ilan University, Ramat-Gan, Israel
2. Gonda Multidisciplinary Brain Research Center, Bar-Ilan University, Ramat-Gan, Israel
3. Chemical Engineering and Process Development, CSIR-National Chemical Laboratory, Pune 411008, Maharashtra, India
4. Physics and Applied Mathematics Unit, Indian Statistical Institute, Kolkata, India
5. CNR - Institute of Complex Systems, Via Madonna del Piano 10, Sesto Fiorentino I-50019, Italy
6. Unmanned Systems Research Institute, Northwestern Polytechnical University, Xi'an 710072, China
7. Moscow Institute of Physics and Technology (National Research University), 9 Institutskiy per., Dolgoprudny, Moscow Region 141701, Russian Federation
8. Universidad Rey Juan Carlos, Calle Tulipán s/n, 28933 Móstoles, Madrid, Spain

* **Correspondence:** baruchbarzel@gmail.com

In memory of Prof. Robert May

The stable functionality of networked systems is a hallmark of their natural ability to coordinate between their multiple interacting components. Yet, strikingly, real-world networks seem random and highly irregular, apparently lacking any design for stability. What then are the naturally emerging organizing principles of complex-system stability? Encoded within the system's stability matrix, the Jacobian, the answer is obscured by the scale and diversity of the relevant systems, their broad parameter space, and their nonlinear interaction mechanisms. To make advances, here we uncover emergent patterns in the structure of the Jacobian, rooted in the interplay between the network topology and the system's intrinsic nonlinear dynamics. These patterns help us analytically identify the few relevant control parameters that determine a system's dynamic stability. Complex systems, we find, exhibit discrete stability classes, from asymptotically unstable, where stability is unattainable, to sensitive, in which stability abides within a bounded range of the system's parameters. Most crucially, alongside these two classes, we uncover a third class, asymptotically stable, in which a sufficiently large and heterogeneous network acquires a guaranteed stability, independent of parameters, and therefore insensitive to external perturbation. Hence, two of the most ubiquitous characteristics of real-world networks - scale and heterogeneity - emerge as natural organizing principles to ensure stability in the face of changing environmental conditions.

The study of complex social, biological and technological systems, is often directed towards dramatic events, such as cascading failures¹⁻⁵ or abrupt state transitions.^{2,4,6,8,10} In reality, however, these represent the exception rather than the rule. In fact, the truly intriguing phenomenon is that, despite enduring constant perturbations and local obstructions, many systems continue to sustain reliably stable dynamics.^{8,11,12,14} This is achieved in the absence of a detailed design, as indeed, the dynamics of the majority of complex systems are mediated by random, often extremely heterogeneous, networks, comprising a large number of interacting components, and driven by a vast space of microscopic parameters. What then are the roots of the observed stability?

To address this we seek the system’s linear stability matrix, namely its Jacobian J , whose principal eigenvalue λ determines its response to perturbation.^{15,16} According to linear stability theory, perturbations may either grow exponentially ($\text{Re}(\lambda) > 0$), capturing instability, or decay exponentially ($\text{Re}(\lambda) < 0$), if the system is at a stable state. These distinct behaviors depend on the detailed structure of J , and therefore predicting complex system stability boils down to two crucial challenges:

Theoretical. The first challenge is of mathematical nature - how do we uncover the structure of J , given the scale, diversity and multiple parameters characterizing real-world complex systems? Indeed, for low-dimensional systems, with just few interacting components, J can be calculated explicitly around each of the system’s potential states. However, such explicit construction becomes intractable as the number of components N is increased, making it difficult to predict the system’s stability.¹⁷ The common paradigm is to bypass this difficulty by extracting J from the random matrix ensemble, allowing a simple construction, with well-established spectral properties.^{9,19} However, this approach, we show, overlooks emergent patterns in J , rooted in the system’s dynamic mechanisms, that have profound impact on stability.

Practical. Regardless of our ability to calculate J , it remains unclear how real systems calibrate their structural/dynamic parameters to ensure that this J is stable. Indeed, random matrix theory indicates that, unless specifically designed for stability, a random J is extremely unlikely to have $\text{Re}(\lambda) < 0$. We, therefore, seek to uncover naturally emerging organizing principles that secure stability without having to *fine-tune* the system’s vast number of microscopic parameters.

Here, we address both challenges by extracting the structure of real-world Jacobian matrices directly from the system’s intrinsic nonlinear dynamics. We discover a new, non-random, Jacobian ensemble, in which topology and dynamics are deeply intertwined. Under this ensemble, stability is determined by a small set of analytically attainable parameters that capture the combined contribution of both topology *and* dynamics. Most crucially, the ensemble includes a broad class of frequently encountered dynamic mechanisms, for which stability becomes *inevitable* in the limit of $N \rightarrow \infty$. Such systems exhibit an *emergent stability*, that becomes asymptotically independent of microscopic parameters, offering a natural design principle to ensure complex system stability.²⁰⁻²²

Fixed-point dynamics

Consider a complex system of N interacting components (nodes), whose dynamic activities $\mathbf{x}(t) = (x_1(t), \dots, x_N(t))^T$ are driven by nonlinear pairwise interactions. The system’s fixed-points \mathbf{x}_α capture static states, which, unperturbed, remain independent of time. The dynamics in the vicinity of these fixed-point can be examined through the system’s response to small perturbations $\delta\mathbf{x}(t)$, which, in the linear regime, can be approximated by

$$\frac{d\delta\mathbf{x}}{dt} = J\delta\mathbf{x} + O(\delta\mathbf{x}^2). \quad (1)$$

Here J , an $N \times N$ matrix, represents the system’s Jacobian around \mathbf{x}_α , which approximates, through a set of linear equations, the original nonlinear system’s dynamics in the perturbative limit, *i.e.* small activity changes $\mathbf{x}(t) = \mathbf{x}_\alpha + \delta\mathbf{x}(t)$. Hence, J ’s spectral properties, and specifically its principal eigenvalue λ , are of crucial importance in characterizing the system’s fixed-point behavior.

Two factors shape the Jacobian - the system’s topology, *i.e.* its patterns of interaction, and its

internal dynamics, capturing the mechanisms of these interactions:

Topology. The first ingredient that impacts the structure of J is the network topology A , a binary matrix ($A_{ij} \in (0, 1), A_{ii} = 0$), which is typically sparse and, most often, highly heterogeneous.³ As J is designed to capture the *direct* response between i and j , its off-diagonal terms vanish in case there is no direct i, j link, *i.e.* $A_{ij} = 0 \iff J_{ij} = 0$ for all $i \neq j$. If, however $A_{ij} = 1$, then the relevant term is assigned a *weight* $J_{ij} = W_{ij}$ that captures the strength of the i, j linear dependence. Together, this leads to

$$J = (A - I) \otimes W, \quad (2)$$

where the Hadamard product \otimes represents matrix multiplication element by element, and I is the $N \times N$ identity matrix. In (2) the network structure (A) determines the non-vanishing off-diagonal terms in J , and W determined their weights. The diagonal entries J_{ii} are introduced through the second term in (2), $I \otimes W$, where W_{ii} quantifies $x_i(t)$'s self-linear dependence.

The random matrix paradigm. To complete the construction of (2) we must assign all weights W . In many of the traditional analyses these unknown weights are extracted from two pre-selected distributions, $P_0(w)$ and $P_1(w)$, capturing the probability density functions of the diagonal (P_0) and off-diagonal (P_1) weights. This gives rise to the Jacobian ensemble $\mathbb{E}(A, P_0, P_1)$, in which one first constructs the topology A , then assigns diagonal and off-diagonal weights from $P_0(w)$ and $P_1(w)$, respectively (Fig. 1a-c).

As a classic example for this ensemble, we consider May's⁹ construction, in which A is an Erdős-Rényi (ER) network, the off-diagonal weights are extracted via $W_{ij} \sim \mathcal{N}(0, \sigma^2)$, a zero-mean normal distribution, and the diagonal entries are taken uniformly as $W_{ii} = 1$. This captures the fact that the interaction strengths are potentially random, hence the distributed nature of W_{ij} , while the self-dynamics are driven by the system's intrinsic relaxation time-scales, as expressed by the fixed value of all W_{ii} , here set to unity.

More generally, one can consider more complex A_{ij} , *e.g.*, sparse or scale-free,¹⁹ which have, indeed, been shown to impact (2)'s spectral properties. Similarly, the weight distributions may also be generalize, allowing distributed time-scales via $P_0(w)$, or diverse, often scale-free, interaction strengths, through a fat-tailed $P_1(w)$.

Despite its simplicity, the $\mathbb{E}(A, P_0, P_1)$ ensemble has two crucial shortcomings: (i) it provides no explicit guidelines to connect $P_0(w)$ and $P_1(w)$ with the system's specific nonlinear interaction mechanisms; (ii) by assigning A and W independently, it ignores the potential interplay between the network structure and J 's dynamic weights. Consequently, in $\mathbb{E}(A, P_0, P_1)$ if two systems share a similar topology A , they will have an equally similar J (up to statistical variations), regardless of their dynamics, social, biological or technological. This, of course, stands in sharp contrast with the frequently observed fact that different nonlinear mechanisms, despite being supported by the same network, may express fundamentally distinct dynamic behaviors.^{1,25,26}

In reality, one expects J not only to distinguish between different types of dynamics, but even between different fixed-points within the *same* dynamics. Indeed, if a system has two fixed-points, a stable \mathbf{x}_α and a non-stable \mathbf{x}_β , they must each be characterized by a different J matrix, a stable J around \mathbf{x}_α and an unstable one around \mathbf{x}_β . Such distinctions are absent in the random matrix paradigm underlying the $\mathbb{E}(A, P_0, P_1)$ ensemble.

How then do we appropriately assign the wights W in (2) to capture the role of the system's

dynamics? For low dimensional systems of few components, this can be done on a case by case basis, by explicitly calculating all linear dependencies. However, for complex, often highly heterogeneous networks, in which not only is $N \gg 1$, but all individual nodes are also potentially diverse, we lack a systematic construction of J , limiting our ability to predict complex system fixed-point dynamics. We, therefore, now seek the general rules that govern the structure of J , *i.e.* the relevant J -ensemble for real-world network dynamics.

The dynamic Jacobian ensemble

Dynamic mechanisms (Fig. 1d). To construct realistic J matrices we consider each system's specific nonlinear dynamic mechanisms. For example, in epidemic dynamics, individuals interact through infection and recovery,^{10,28,29} in biological networks, proteins, genes and metabolites are linked through biochemical processes^{12,13,31,33} and in population dynamics, species undergo competitive or symbiotic interactions.^{15,17,35,37} Most generally, these dynamic mechanisms can be described by¹

$$\frac{dx_i}{dt} = M_0(x_i(t), \mathbf{f}_i) + \mathcal{G} \sum_{j=1}^N A_{ij} M_1(x_i(t)) G_{ij} M_2(x_j(t)), \quad (3)$$

where $M_0(x_i, \mathbf{f}_i)$ captures the self-dynamics of all nodes, and the product function $M_1(x_i)M_2(x_j)$ describes the i, j pairwise interaction. With the appropriate selection of these three nonlinear functions $\mathbf{M} = (M_0(x), M_1(x), M_2(x))$, Eq. (3) captures a broad range of frequently used models in social,^{10,28} biological^{12,13,15,31,33} and technological³⁸ systems (Fig. 2). The dynamics in (3) incorporate a set of tunable parameters: the self-dynamics of each node is characterized by the parameter set \mathbf{f}_i , and the global interaction rate between all nodes is controlled by \mathcal{G} , whose value increases/decreases the strength of *all* interactions. Besides that, the specific interaction strength between i and j is governed by the network weights G_{ij} , allowing potentially diverse link weights.

Equation (3) goes beyond topology A , introducing also the dynamics. It therefore allows us to capture the role of the nonlinearity and its impact on J . Before we use it to extract J , however, we wish to distinguish between the role of its different components • **Dynamic mechanisms** (Fig. 1e). The functions M_0, M_1, M_2 in \mathbf{M} describe the system's intrinsic mechanisms, ingrained into the natural processes driving its interacting units. Indeed, the functional form of \mathbf{M} distinguishes between, *e.g.*, social vs. biological dynamics, capturing built-in mechanisms that are hardwired into the *physics* of the system components. These functions are therefore fixed and uniform across all nodes/links, *i.e.* they are *intrinsic*. • **Parameters** (Fig. 1f,g). $\mathbf{f} = (f_1, \dots, f_N)$ and G_{ij} , in contrast, capture the node/link specific parameters, which may be potentially diverse, depending on the particular rates characterizing each node or the unique strength of each interaction. Similarly, the global weight \mathcal{G} , is also subject to the effect of external conditions, which may increase/decrease the typical interaction rates. Hence, f, \mathcal{G} and G are *non-intrinsic*.

To understand this distinction let us consider a specific example of epidemic spreading via the susceptible-infected-susceptible (SIS) dynamics, *i.e.* Epidemic in Fig. 2a. First, we focus on the self-dynamics $M_0(x_i, \mathbf{f}_i) = -f_i x_i$. This function describes the process of recovery, in which an infected node (\mathcal{I}) transitions to the susceptible state (\mathcal{S}) at a rate f_i , *i.e.* $\mathcal{I} \xrightarrow{f_i} \mathcal{S}$. Such transition is captured by a *linear* function $M_0(x_i) \propto x_i$, whose slope represents its single *rate* parameter f_i . The crucial point is, that while the rate f_i is idiosyncratic and changes from one individual to another, the *linear form* of M_0 is intrinsic to the nature of the recovery process, and is therefore,

uniform across all nodes. Hence M_0 's functional form is fixed (*dynamic mechanism*, Fig. 1e), while its rate constant f_i is tunable (*parameter*, Fig. 1f).

Similarly, the nonlinear interactions of Epidemic, $M_1(x_i)G_{ij}M_2(x_j) = (1-x_i)G_{ij}x_j$, are universal across all linked pairs - embedded in the nature of the SIS infection mechanism $\mathcal{I} + \mathcal{S} \xrightarrow{G_{ij}} 2\mathcal{I}$. This is while the rates G_{ij} depend on the unique strength of the i, j social tie, or on i and j 's individual propensity for contracting the disease. Therefore, in (3) the *functional form* of \mathbf{M} is fixed, representing the *built-in physical* mechanisms that drive all nodes/links, while the *parameters* $\mathbf{f}, \mathcal{G}, G$ are potentially diverse and/or tunable due to external conditions.

Below we seek patterns in J that can be traced to the nonlinear Eq. (3), distinguishing, along the lines of the above discussion, between the contribution of (i) the intrinsic nonlinear mechanisms \mathbf{M} ; (ii) the potentially diverse parameters $\mathbf{f}, \mathcal{G}, G$ and (iii) the network topology A .

Real-world Jacobians (Fig. 1h). To obtain realistic J matrices we relinquish the random matrix construction $\mathbb{E}(A, P_0, P_1)$, and extract the Jacobian directly from (3), hence incorporating not just the network structure A , but also the system's nonlinear dynamics \mathbf{M} . In Supplementary Section 1, we show that this leads to a currently unexplored matrix ensemble, in which the Jacobian weights W in (2) are strongly intertwined with the weighted topology A, G via

$$W_{ii} \sim C(\mathbf{f}, \mathcal{G}) \mathcal{D}_{\text{nn}}^n d_i^\mu \quad (4)$$

for the diagonal weights $J_{ii} = -W_{ii}$, and

$$W_{ij} \sim d_i^\nu G_{ij} d_j^\rho \quad (5)$$

for the off-diagonal weights $J_{ij} = A_{ij}W_{ij}$ ($i \neq j$).

In (4) and (5) $d_i = \sum_{j=1}^N A_{ij}G_{ij}$ represents the weighted degree of node i , and

$$\mathcal{D}_{\text{nn}} = \frac{1}{N} \sum_{i=1}^N \frac{1}{d_i} \sum_{j=1}^N A_{ij}G_{ij}d_j \quad (6)$$

represents the average weighted degree of a nearest neighbor node.² The coefficient $C = C(\mathbf{f}, \mathcal{G})$ is governed by the system's specific parameters $\mathbf{f} = (\mathbf{f}_1, \dots, \mathbf{f}_N)^\top$ and \mathcal{G} , which, as noted above, are *non-intrinsic*. Finally, the four exponents, $\Omega = (\eta, \mu, \nu, \rho)$ are fully determined by the system's *intrinsic* dynamic mechanisms, \mathbf{M} , as shown in **Appendix I**.

The resulting dynamic J in (4) and (5) is fundamentally distinct from the existing random matrix based constructions. On the one hand, the network structure A continues to determine the non-zero entries, similarly to the classic ensemble $\mathbb{E}(A, P_0, P_1)$. Also, the typical magnitude of the diagonal entries is determined by the system's rates constants through \mathbf{f} and \mathcal{G} , once again, analogous, albeit not identical, to the selection of $P_0(w)$ in the existing ensemble. However, the similarity ends there, as (4) and (5), in contrast to $\mathbb{E}(A, P_0, P_1)$, also capture the role of the *intrinsic nonlinear mechanisms*. Indeed, they predict emergent patterns in the structure of real-world Jacobian matrices, that are rooted in the interplay between topology and dynamics: The degrees $\mathcal{D}_{\text{nn}}, d_i$ are extracted from the *weighted network topology* $A \otimes G$ (Fig. 1g), while the scaling exponents Ω are derived from the *nonlinear dynamics* \mathbf{M} (Fig. 1e). Therefore, we arrive at a new Jacobian ensemble $\mathbb{E}(A, G, \Omega)$, which, unlike the random matrix based treatment of $\mathbb{E}(A, P_0, P_1)$, accounts for the effect of the system-specific nonlinear mechanisms. Consequently,

in $\mathbb{E}(A, G, \Omega)$, identical networks may give rise to highly distinctive Jacobian matrices, depending on whether the interactions are, *e.g.*, social, biological or ecological, as each of these mechanisms is characterized by its unique set of exponents Ω , and, consequently, its unique fixed-point dynamics (Fig. 1h).

Testing $\mathbb{E}(A, G, \Omega)$. To examine predictions (4) and (5) we constructed a broad testing ground, on which we implemented seven relevant dynamic models from social, biological and technological domains: *Epidemic*. The SIS model^{10,28,29} for disease spreading • *Regulatory*. The Michaelis-Menten model¹² for gene regulation • *Inhibitory*. Growth suppression in pathogen-host interactions¹⁷ • *Biochemical*. Protein-protein interactions^{13,31,33} in sub-cellular networks • *Population 1,2*. Mutualistic¹⁵ interactions in population dynamics • *Power*. Load distribution in electric transmission networks. Applying each of these dynamics to five different model and relevant empirical networks, we arrive at a total of 35 combinations of networks/dynamics, upon which we test our predicted J -ensemble (for a detailed description of all dynamic models and networks see Supplementary Sections 3 and 4).

In Fig. 2 we present, for each system, its dynamic equation (blue), and list the relevant networks upon which it was tested (violet). In some cases the system features several fixed-points, for example, Epidemic (Fig. 2a) exhibits a healthy state (inactive \mathbf{x}_0) and a pandemic state (active \mathbf{x}_1). These states are presented using a 3D visualization. The network is laid out on the x, y plane, and the activity x_i of all nodes is captured by the vertical z -axis displacement. Hence under \mathbf{x}_0 all nodes remain on the x, y plane ($z = 0$), while in the active \mathbf{x}_1 they all have $x_i > 0$. Finally, we derive the dynamic exponents $\Omega = (\eta, \mu, \nu, \rho)$ for each system around its active state (orange); see Supplementary Section 3, where we also treat the inactive states.

Perturbing the system around its active fixed-point, we constructed the Jacobian matrix J for each of our 35 systems. In Fig. 3 we find that, indeed, the diagonal (W_{ii}) and off-diagonal (W_{ij}) weights of J follow the predicted scaling of (4) and (5). For example, in Epidemic we predict $\mu = 1$, while for Regulatory we have $\mu = 0$, both scaling relationships clearly evident in Fig. 3b and d. This means that extracting all diagonal terms independently from $P_0(w)$, as in $\mathbb{E}(A, P_0, P_1)$, misses the actual patterns that arise from the nonlinear Epidemic/Regulatory dynamics. Similarly, the off-diagonal terms are proportional to $d_i^{-1}G_{ij}d_j^0$ in Epidemic (Fig. 3c) and $d_i^0G_{ij}d_j^{-2}$ in Regulatory (Fig. 3e), once again overruling the random construction in which W_{ij} are extracted from an arbitrary $P_1(w)$.

Our analysis further predicts that these scaling relationships, encapsulated within our analytically predicted Ω , are intrinsic to the nonlinear dynamics \mathbf{M} , thus independent of the network structure A or the specific parameters \mathbf{f}, \mathcal{G} and G . We examine this in Fig. 3, by testing each of our dynamics on a diverse set of networks, with different degree/weight distributions. As predicted, we find that η, μ, ν and ρ are, indeed, universal, conserved across our distinct model (Erdős-Rényi, Scale-free 1, Scale-free 2) and relevant empirical (Social 1,2, PPI 1,2, etc.) networks. Hence, Ω captures the intrinsic, and most crucially, hitherto overlooked, contribution of the nonlinear *dynamics* to the structure of J .

Together, our derivation demonstrates that: (i) actual J matrices, extracted from real nonlinear dynamics are fundamentally distinct from the commonly used random ensembles; (ii) contrary to the random J ensembles, real Jacobians feature non-random scaling patterns in which topology ($\mathcal{D}_{\text{nn}}, d_i$) and dynamics (Ω) are deeply intertwined; (iii) these patterns can be analytically traced to the system's intrinsic nonlinear mechanisms (\mathbf{M}) through Eqs. (4) and (5), giving rise to our new ensemble $\mathbb{E}(A, G, \Omega)$. Next, we use $\mathbb{E}(A, G, \Omega)$ to derive the conditions for Eq. (3)'s dynamic

stability.

Topology, dynamics and the emergence of stability

The dynamic stability of (3) around a given fixed-point is governed by J 's principal eigenvalue λ , requiring that $\text{Re}(\lambda) < 0$. We, therefore, seek the contribution of the weighted topology (A, G , Fig. 1g), the system specific parameters (\mathbf{f}, \mathcal{G} , Fig. 1f) and its nonlinear dynamic mechanisms (\mathbf{M} , Fig. 1e) to the value of $\text{Re}(\lambda)$.

First, let us focus on the weighted topology. The ingredients of $J \in \mathbb{E}(A, G, \Omega)$, as expressed in Eqs. (4) and (5), suggest that λ is strongly linked to the network's weighted degree distribution $P(d)$. This is indicated directly through the dependence on d_i and d_j , but also indirectly through the nearest neighbor degree \mathcal{D}_{nn} , whose magnitude depends on the system's degree-heterogeneity.⁵ For instance, in a random network with uniform weights we have $\mathcal{D}_{\text{nn}} = \langle d^2 \rangle / \langle d \rangle$,^{2,19} in which the second moment $\langle d^2 \rangle$ increases with $P(d)$'s variance, and consequently with A 's heterogeneity. Most generally, for a fat-tailed $P(d)$, we have⁵

$$\mathcal{D}_{\text{nn}} \sim N^\beta, \quad (7)$$

an asymptotic divergence with system size. Hence, β is driven by the network heterogeneity, being $\beta = 0$ for homogeneous networks, in which $P(d)$ is bounded, and $\beta > 0$ for heterogeneous A, G , where $P(d)$ is fat-tailed.

The second ingredient which impacts λ in $\mathbb{E}(A, G, \Omega)$ is $\Omega = (\eta, \mu, \nu, \rho)$, designed to capture the role of the dynamics \mathbf{M} . Finally, $C(\mathbf{f}, \mathcal{G})$, the pre-factor in the scaling relationship of (4), encapsulates the contribution of the non-intrinsic, potentially tunable, parameters. Combining all three contributions together, we show in Supplementary Section 2 that in $\mathbb{E}(A, G, \Omega)$, the principal eigenvalue asymptotically follows

$$\text{Re}(\lambda) \sim N^Q \left(1 - \frac{C}{N^S} \right), \quad (8)$$

where $Q = \beta(1 + \nu + \rho - \eta/2)$ and

$$S = \beta(\mathbf{s} + \nu + \rho - \mu - \eta). \quad (9)$$

In (9), the parameter \mathbf{s} depends on the *sign* of the interactions, being $\mathbf{s} = 1$ under cooperative interactions (positive J_{ij}), such as in Epidemic or Regulatory, and $\mathbf{s} = 0$ if the interactions are adversarial (negative J_{ij}), *e.g.* Inhibitory or Biochemical.

Equations (8)-(9), our key result, uncover the asymptotic behavior of λ in the limit of a large complex system $N \rightarrow \infty$. Contrary to $\mathbb{E}(A, P_0, P_1)$, in which λ is fully determined by A and G , here the exponents S and Q capture the interplay of structure *and* dynamics, via Ω . Most importantly, these equations have crucial implications regarding the system's fixed-point stability, giving rise to three potential stability classes (Fig. 1i):

- **Asymptotic instability** ($S > 0$, red). In case S in (8) is positive, we have, for sufficiently large N , $\text{Re}(\lambda) \sim N^Q > 0$. This asymptotic behavior is independent of C , which represents the only term in (8) that depends on \mathbf{f}, \mathcal{G} . Therefore, such fixed-points, in a large enough system, become intrinsically unstable, regardless of the model parameters.

- **Asymptotic stability** ($S < 0$, blue). For $S < 0$ we have $N^S \rightarrow 0$, the r.h.s. of (8) is dominated by the negative term, and hence $\text{Re}(\lambda) < 0$, independently of C . Hence, here in the limit $N \rightarrow \infty$, stability becomes unconditionally guaranteed, once again unaffected by the system’s specific parameters \mathbf{f}, \mathcal{G} .
- **Sensitive stability** ($S = 0$, green). Under $S = 0$ the system lacks an asymptotic behavior, and therefore, its stability depends on C in (8). If $C > 1$ the system is stable, otherwise it becomes unstable. Consequently, in this class stability is not an intrinsic characteristic of the *system*. Rather it is driven by Eq. (3)’s specific tunable parameters.

Stability classifier. The *stability classifier* S in (9) helps group all $J \in \mathbb{E}(A, G, \Omega)$ into distinct stability classes. It achieves this by identifying the relevant topological (β) and dynamic (Ω) control parameters that help analytically predict the stability of any system within the form (3). We can therefore use S to predict *a priori* whether a specific combination of topology and dynamics will exhibit stable functionality or not.

To examine S ’s predictive power we used our model and real networks to extract 7,387 Jacobian matrices from the $\mathbb{E}(A, G, \Omega)$ ensemble, with different sets of η, μ, ν and ρ . In Fig. 4a we show the principal eigenvalue λ vs. S for the entire 7,387 Jacobian sample. As predicted, we find that the parameter S sharply splits the sample into three classes. The asymptotically unstable class (red, top-right) has $S > 0$ and consequently also $\lambda > 0$, a guaranteed instability. The asymptotically stable class (blue, bottom-left) is observed for $S < 0$, and has, in all cases $\lambda < 0$, *i.e.* stable dynamics. Finally, for $S = 0$ we observe sensitive stability, with λ having no asymptotic positive/negative assignment (green). A small fraction ($\sim 8\%$) of our sampled J matrices were inaccurately classified by S (grey), a consequence of the approximate nature of our derivations (Supplementary Section 2).

Figures 3 and 4, together, demonstrate our theoretical path up to this point: First, Fig. 3 shows that real J matrices exhibit the internal scaling patterns predicted in (4) and (5) - representing a steep departure from the broadly applied random matrix paradigm of $\mathbb{E}(A, P_0, P_1)$. Next, Fig. 4 shows that the resulting Jacobian ensemble $\mathbb{E}(A, G, \Omega)$ has a rich stability profile, profoundly distinct from the currently considered $\mathbb{E}(A, P_0, P_1)$, and, most importantly, fully characterized by a single parameter - our analytically predicted classifier S . We can now use S to analyze the structural and dynamic ingredients that contribute to complex system stability.

The ingredients of dynamic stability

The parameter S in (9) reduces a network’s dynamic stability into five relevant exponents. The first four $\Omega = (\eta, \mu, \nu, \rho)$ are determined by the nonlinear dynamics **M**, Epidemic, Regulatory, Population etc., and are therefore intrinsic to the system’s inherent interaction mechanisms. These exponents are independent of the topology A , its weights G , or of the microscopic model parameters \mathbf{f} and \mathcal{G} . Therefore they are *hardwired* into the system’s dynamic behavior.

The remaining exponent in (9), β , is independent of the dynamics, determined solely by A, G , specifically by the weighted degree distribution $P(d)$, through (7). Therefore, together, S captures the roles of both topology *and* dynamics, whose interplay determines the system’s stability class around a specific fixed-point - stable, unstable or sensitive.

The role of degree-heterogeneity. The prevalence of fat-tailed $P(d)$ is among the defining features of real-world complex systems, from biological⁴⁰ to social^{21,22} and technological^{43,44} networks, with far-reaching implications on their observed dynamic behavior.^{1,2,19} Our analysis indicates that this universal network characteristic may also play a crucial role in the context

of dynamic stability.

To understand this, consider a bounded $P(d)$, such as an ER network with uniform weights. Here the weighted degrees follow a Poisson distribution, having $\beta = 0$. Under these conditions we have $S = 0$ in (9), the system has no defined asymptotic behavior, and hence it is sensitively stable - *i.e.* its stability depends on model parameters via C . Therefore, our predicted asymptotically stable/unstable classes, which depend on $\beta > 0$, are, in fact, a direct consequence of degree-heterogeneity.

This uncovers a new, previously overlooked, layer to the dynamic impact of $P(d)$ on complex system functionality. Consider, for example, the factors that drive a system towards the loss of stability. Most often such events result from external stress or changes in environmental conditions.² Such forces impact the system by perturbing its dynamic parameters, namely they affect the coefficient C . Seldom, however, do these environmental perturbations affect the system's built-in interaction mechanisms. Indeed, as discussed above, these mechanisms are ingrained in the *physics* of the interacting components, therefore unaffected by external conditions. The crucial point is, that under $S < 0$, a state only possible if $P(d)$ is fat-tailed, stability becomes asymptotically independent of C , driven solely by Ω , which is insensitive to the non-intrinsic model parameters. Hence, for a sufficiently large system ($N \rightarrow \infty$), if $P(d)$ is fat-tailed, stability becomes asymptotically robust against any external perturbation. *This suggests that degree/weight-heterogeneity serves as a dynamically stabilizing topological characteristics, in the face of a persistently fluctuating environment.*

Our framework settles this dichotomy, quite naturally, by departing from the prevailing random matrix paradigm, captured via $\mathbb{E}(A, P_0, P_1)$, in favor of our analytically derived $\mathbb{E}(A, G, \Omega)$. In this new J -ensemble, the system's intrinsic dynamic mechanisms lead to the emergence of built-in scaling patterns in J , that are absent in the random matrix framework. These patterns, in turn, predict a broad class of *asymptotically stable dynamics*, in which May's original question receives a clear answer: large complex systems not only *can*, but, often *must* be stable.

Will a large complex system be stable? To gain deeper insight into roots of asymptotic stability/instability, we consider again $\mathbb{E}(A, G, \Omega)$'s principal eigenvalue λ in (8). Its structure portrays stability as a balance between the positive, *i.e.* destabilizing, effect mediated by the network interactions, vs. the negative, stabilizing, feedback, driven by the parameter C in J 's diagonal (4); Fig. 4b. It is therefore, natural to enhance stability by increasing C , which, in

BOX I. Solving a 50 year old puzzle

Will a large complex system be stable? This question, first posed by May in 1972,⁹ captures a long standing challenge, fueled by the seeming contradiction between theory and practice. While empirical reality answers with an astounding yes, May's mathematical analysis, based on random matrix theory, suggests the contrary, giving rise to the *diversity-stability paradox*. What, then, are the organizing principles, or in May's original wording - *nature's devious strategies*, that enable complex system stability.

Initial clues began to unveil with the mapping of empirical networks, which uncovered universally recurring topological characteristics^{3,45} that can potentially impact the system's dynamics.¹⁷ For example, degree heterogeneity,⁴⁶ community structure⁵ or topological symmetries⁴⁷⁻⁴⁹ - all naturally emerging features of real-world networks - were suggested as potentially stabilizing structures. In ecology, constraints on populations sizes offered additional paths to stability.^{21,22}

Our framework settles this dichotomy, quite naturally, by departing from the prevailing random matrix paradigm, captured via $\mathbb{E}(A, P_0, P_1)$, in favor of our analytically derived $\mathbb{E}(A, G, \Omega)$. In this new J -ensemble, the system's intrinsic dynamic mechanisms lead to the emergence of built-in scaling patterns in J , that are absent in the random matrix framework. These patterns, in turn, predict a broad class of *asymptotically stable dynamics*, in which May's original question receives a clear answer: large complex systems not only *can*, but, often *must* be stable.

effect, translates to strengthening each node’s intrinsic negative feedback. Equation (8) predicts that J becomes stable if C exceeds a critical value

$$C_0 \sim N^S, \quad (10)$$

beyond which λ becomes negative. For asymptotically stable systems ($S < 0$) we have, for sufficiently large N , $C_0 \rightarrow 0$, a guaranteed stability even under arbitrarily small C . In contrast, for asymptotically unstable systems ($S > 0$) we have $C_0 \rightarrow \infty$, hence such systems are impossible to stabilize even under extremely large C . We emphasize that $C = C(\mathbf{f}, \mathcal{G})$ is the only component in (8) that is dependent on the system’s tunable parameters, and therefore having an unbounded range of C values under which the system remains stable (or unstable) guarantees that λ is unaffected by parameter perturbation, *e.g.*, changing environmental conditions.

To test Eq. (10) in Fig. 4c-k we extract a set of three specific J matrices from $\mathbb{E}(A, G, \Omega)$, representing systems from our three stability classes: J_{AS} , asymptotically stable with $\Omega = (2, 2, 2, -1)$; J_{SS} , sensitively stable with $\Omega = (0, -1, -2, 0)$; and J_{AU} , asymptotically unstable with $\Omega = (1, -2, -1, 2)$. For each of these we plot C_0 vs. N , capturing the level of negative feedback required to ensure the system’s stability. Under ER ($\beta = 0$) we do not observe a defined asymptotic behavior. The critical C_0 does not scale with N , indicating that sufficient perturbation to the model parameters can, indeed, affect the system’s stability (Fig. 4i-k, green circles).

Constructing the same J matrices from our scale-free network SF1 ($\beta = 0.6$), we now observe a clear asymptotic behavior, congruent with prediction (10). For J_{AS} we have $C_0 \sim N^{-1.2}$, while under J_{AU} we observe $C_0 \sim N^{1.8}$ (Fig. 4f-h), capturing the intrinsic stability/instability of these two systems. Finally, in J_{SS} , having $S = 0$, the system, again lacks an asymptotic behavior, and therefore can be stabilized under finite C_0 , independently of system size N (Fig. 4g). Together, Eq. (10) helps us link the scale N of a complex system with its observed stability. As opposed to the random matrix viewpoint of $\mathbb{E}(A, P_0, P_1)$, in which N has a *destabilizing* effect,⁹ our dynamic ensemble uncovers broad conditions where the contrary is true, and $N \rightarrow \infty$, is, in fact, what anchors the system’s stability (**Box I**).

Emergent stability. This observation on the stabilizing/destabilizing effect of N and $P(d)$ is especially relevant if (3) exhibits multiple fixed-points, for example, an undesirable \mathbf{x}_0 and a desirable \mathbf{x}_1 . For a low-dimensional system (N small) transitions between these points are controlled by the system *parameters*. This is also the case if the system is large ($N \rightarrow \infty$) but homogeneous ($\beta = 0$). Indeed, both cases belong to the sensitively stable class ($S = 0$), in which λ in (8) shows no asymptotic trend - either due to the finite value of N or due to the fact that $\beta = 0$. Such parameter-driven state transitions capture the classic view of dynamic stability: the potential fixed-points are rooted in the system’s intrinsic nonlinear dynamics, their stability, on the other hand, is determined by its specific, and most crucially, tunable parameters.²

The picture, however, changes fundamentally when the network is large and heterogeneous, *i.e.* $N \rightarrow \infty$ and $\beta > 0$. This is because in $\mathbb{E}(A, G, \Omega)$ each of the system’s fixed-points may be potentially characterized by a unique set of dynamic exponents, \mathbf{x}_0 ’s Jacobian having the set Ω_0 and \mathbf{x}_1 having Ω_1 (Fig. 5a,b). If, for instance, Ω_0 has $S > 0$ in (9) and Ω_1 has $S < 0$, then \mathbf{x}_0 becomes asymptotically *unstable* and \mathbf{x}_1 becomes asymptotically *stable*. Such systems will be guaranteed to reside only in \mathbf{x}_1 , unaffected by perturbation to their parameters.

To observe this we return to our testing ground of Fig. 2, this time focusing on dynamic models that have multiple fixed-points. This includes Regulatory, Epidemic and Inhibitory, each of

which exhibits on top of its *active* state \mathbf{x}_1 , in which all $x_i > 0$, an *inactive* state $\mathbf{x}_0 = (0, \dots, 0)^\top$, where all activities vanish (Population 1,2 also exhibit an inactive \mathbf{x}_0 , however it is never stable, see Supplementary Section 3.3).

First, we simulated Regulatory 1 ($a = h = 1$) on an ER network, and varied the model's two parameters \mathbf{f}, \mathcal{G} . We find that when the average $\langle \mathbf{f} \rangle$ is large or, alternatively, when \mathcal{G} is small the system resides in \mathbf{x}_0 , whereas in the opposite limit, it favors \mathbf{x}_1 (Fig. 5c-e, diamonds). This is precisely the *sensitive stability*, in which the system's fixed-point behavior is driven by its tunable parameters. Repeating the same experiment on our scale-free network SF1, we observe that \mathbf{x}_1 is sustained for a broader range of $\langle f \rangle$ and \mathcal{G} , hence SF1 is comparably insensitive to these parameters (Fig. 5d-f, triangles). This robustness is a direct outcome of our classifier: \mathbf{x}_0 has $\Omega_0 = (0, 0, 0, 0)$, which in (9) predicts $S = \beta > 0$, while \mathbf{x}_1 has $\Omega_1 = (0, 1, 0, -2)$, and hence $S = -\beta < 0$. Therefore, on a large scale-free network \mathbf{x}_0 becomes asymptotically unstable, and the system is forced to reside in the asymptotically stable \mathbf{x}_1 .

To observe this systematically we seek the critical global weight \mathcal{G}_c , below which \mathbf{x}_1 becomes unstable, and the system transitions to \mathbf{x}_0 . Varying the system size N over ~ 4 orders of magnitude, we observe first hand \mathbf{x}_1 's asymptotic stability: while under ER \mathcal{G}_c is almost independent of N (Fig. 5g, diamonds), in SF1 it scales negatively with system size, approaching $\mathcal{G}_c \rightarrow 0$ in the limit $N \rightarrow \infty$ (triangles). Hence, as predicted SF1 remains stable even under arbitrarily small \mathcal{G}_c . This reconfirms prediction (10), but this time, not on theoretically constructed J from $\mathbb{E}(A, G, \Omega)$, as shown in Fig. 4f-k, but rather on the actual numerically calculated dynamics of Eq. (3). Similar stability patterns are also observed in Epidemic and Inhibitory (Fig. 5h,i and Supplementary Sections 3.1 and 3.5).

Hence, we observe a qualitative difference between bounded vs. scale-free $P(d)$, in which degree-heterogeneity can potentially afford the network a guaranteed stability, that is asymptotically independent of microscopic parameters.

Equivalence classes of dynamic stability. While stability is, in its essence, a binary classification - a fixed-point is either stable or not, we can use S to quantify the *level* of the system's stability around a given fixed-point. Consider again C_0 in (10), capturing the critical value of C in (4) required to stabilize the system's dynamics. For large N , it either vanishes (stable) or diverges (unstable). These asymptotic effects are pronounced more strongly as S becomes more negative or more positive. As an example, let us compare Regulatory with $h = 1, a = 2$, under which we have $S = -\beta/2$, vs. Population 1, where $S = -\beta$. Both are asymptotically stable, yet Eq. (10) indicates that Population 1 is *more* stable: to destabilize Population 1 one needs $C_0^{\text{Pop}} \sim N^{-\beta}$, while for Regulatory it is sufficient to have $C_0^{\text{Reg}} \sim N^{-\beta/2}$, *i.e.* $C_0^{\text{Pop}} \ll C_0^{\text{Reg}}$. The meaning is that to destabilize Population 1 we much push C further towards zero, namely set more extreme parameters, than what is needed for Regulatory.

In Fig. 6b we show the lines of *equi-stability*, comprising all dynamics with the same S value, and hence a similar level of stability/instability. These equi-stable classes may group together highly distinct dynamics, that despite their different Ω may have identical S . For example, Epidemic and Population 1, two dynamics from fundamentally different domains, exhibit a similar level of stability, belonging to the *equivalence stability class* $S = -\beta$.

Generality and limitations the $\mathbb{E}(A, G, \Omega)$ ensemble. Our ensemble $\mathbb{E}(A, G, \Omega)$ was obtained and analyzed under the conditions defined by Eq. (3), whose structure allowed us to achieve the reported analytical advances. Despite its general structure, this equation excludes several families of dynamics. For example, non-additive interactions or threshold models.⁵⁰ Similarly,

if the system incorporates a mixture of distinct interaction mechanisms its dynamics cannot be cast into the form \mathbf{M} .

We note, however, that while our analytical derivations are, indeed, bounded by these restrictions, the family of potential dynamics included in $\mathbb{E}(A, G, \Omega)$ may, in fact, be broader. Specifically, in Supplementary Section 4 we consider three expansions to Eq. (3) • *Non-factorizable interactions*. Our testing ground includes Power dynamics, in which the interaction term cannot be partitioned into a product $M_1(x_i)M_2(x_j)$, but rather incorporates a diffusive mechanism of the form $M(x_j - x_i)$. Such dynamics, excluded from (3), arise in different contexts, from reaction-diffusion to synchronization,^{51,52} and despite the fact that they are not covered by our analytical framework, our analysis of Power indicates that they continue to fall within $\mathbb{E}(A, G, \Omega)$ • *Non-additive interactions*. Another outlier in Fig. 2 is Population 2, in which the linear sum over $M_2(x_j)$ is replaced by $M_2(\sum_{j=1}^N x_j)$. This represents a common structure in population dynamics, which, as our analysis shows, is also within the $\mathbb{E}(A, G, \Omega)$ family • *Mixed s dynamics*. While Eq. (3) is limited to uniform dynamics, either cooperative ($\mathbf{s} = 1$) or adversarial ($\mathbf{s} = 0$), in Supplementary Section 4.3 we numerically analyze the case of mixed dynamics, in which a fraction ϕ of cooperative interactions coexists alongside a $1 - \phi$ fraction of adversarial ones. We find that for a broad range of ϕ values, our predicted Jacobian patterns remain valid. This is thanks to a constraint relevant in many real-world systems: the fact that the activities $x_i(t)$ in (3) are, by definition, non-negative.^{21,22} Therefore, as the system evolves in time, at any instance where a node reaches $x_i(t) = 0$ it becomes extinct, and permanently removed from the network. This *ratchet-motion* prunes out nodes with many adversarial interacting partners, as their activities are naturally driven towards zero. As a result, the system reaches a fixed-point in which the majority of remaining links are positive, which continue to approximately follow Eqs. (4) and (5) of the $\mathbb{E}(A, G, \Omega)$ ensemble.

Discussion and outlook

The linear stability matrix J carries crucial information on the dynamic behavior of complex systems. Here, we exposed distinct patterns in the structure of J that (i) arise from the nature of the system's interaction dynamics; (ii) affect its principal eigenvalue, and thus, its stability profile. These patterns are expressed through the four dynamic exponents $\Omega = (\eta, \mu, \nu, \rho)$, which we link to the system's dynamics, \mathbf{M} , through the leading powers of the expansions in Eq. (12). This dependence on the *powers* ($\Psi(n), \Gamma(n)$, etc.), rather than the *coefficients* (G_n, C_n , etc.) indicates that Ω is hardwired into the interaction dynamics. Indeed, the powers in (12) are determined by the dynamic model, *e.g.*, Epidemic or Regulatory, but not by the specific model parameters, which only impact the coefficients. Therefore, our predicted Jacobian ensemble in (4) and (5), as well as its associated stability classifier S in (9), both capture highly robust and distinctive characteristics of the system's dynamics, that cannot be perturbed or otherwise affected by shifting environmental conditions.

External forces, however, may not only impact the system's structure (A, G) or parameters (\mathbf{f}, \mathcal{G}), but also directly act on the node dynamics. This, for example, arises in non-autonomous systems, in which the nodes interact with components outside the network. Such effects can be captured in Eq. (3) by coupling it with a *virtual* node/s, whose activities $z_i(t)$ are designed to encapsulate the dynamic impact of the external signals. As long as the number of these external coupling terms is small, *i.e.* weak environmental forces, our J will only be marginally affected.

Graph spectral analysis represents a central mathematical tool to translate network structure into dynamic predictions.^{53–55} A network's spectrum, *i.e.* its set of eigenvalues and eigenvectors,

captures information on its dynamic time-scales, potential states, and - in the present context - its dynamic stability. Most often, spectral analysis is applied to the network *topology*, namely we seek the *graph's* eigenvalues. Focusing on the graph topology, however, loses information on the nonlinear dynamics that occur *on* that graph. As an alternative, our $\mathbb{E}(A, G, \Omega)$ ensemble suggests to apply spectral analysis, not to the topology A (or the weighted $A \otimes G$), but rather to the derived Jacobian in (4) and (5), which, thanks to Ω preserves the information of both structure *and* dynamics.

In a broader perspective, the interplay between topology and dynamics is one of the major theoretical obstacles along the path to predict, understand and control complex system behavior.^{56–59} The problem is that we lack sufficient theoretical tools to treat the challenging combination of nonlinear dynamics with complex, random and often highly heterogeneous network structures. Consequently, advances are often system specific, requiring dedicated tools, and hence, lacking the breadth of a general network dynamics theory. The Jacobian ensemble presented here, transforms the nonlinear Eq. (3) into an effective linear system, whose weights incorporate the nonlinear \mathbf{M} through Ω . It can, therefore, allow us to utilize the powerful tools of spectral graph theory, even in a nonlinear dynamic setting. This may offer a basis for systematic analysis of nonlinear network dynamics.

Code and data availability. Upon acceptance, all codes/data to reproduce our analysis will be made freely available online.

Acknowledgments. C.M. thanks the Planning and Budgeting Committee (PBC) of the Council for Higher Education, Israel for support. C.M. is also supported by the INSPIRE-Faculty grant (code: IFA19-PH248) of the Dept. of Science and Technology, India. C.H. is supported by the INSPIRE-Faculty grant (code: IFA17-PH193) of the Dept. of Science and Technology, India. S.B. acknowledges funding from the project EXPLICS granted by the Italian Ministry of Foreign Affairs and International Cooperation. This research was also supported by the Israel Science Foundation (grant No. 499/19), the US National Science Foundation-CRISP award No. 1735505, and by the Bar-Ilan University Data Science Institute grant for data science research.

Appendix I. The ensemble $\mathbb{E}(A, G, \Omega)$ - how to calculate Ω

To construct J as appears in Eqs. (4) and (5) we must extract the exponents $\Omega = (\eta, \mu, \nu, \rho)$ from Eq. (3). First we use the dynamic functions $M_0(x), M_1(x)$ and $M_2(x)$ to construct three new functions

$$R(x) = -\frac{M_1(x)}{M_0(x)}, \quad Y(x) = M_1(x)R'(x), \quad Z(x) = R(x)M_2(x), \quad (11)$$

where $R'(x)$ represents a derivative dR/dx around the fixed-point \mathbf{x} . From these we extract four additional functions, which we express through a Hahn power-series expansion as

$$\begin{aligned} M_2(Z^{-1}(x)) &= \sum_{n=0}^{\infty} G_n x^{\Psi(n)}, & Y(R^{-1}(x)) &= \sum_{n=0}^{\infty} C_n x^{\Gamma(n)}, \\ M_1(R^{-1}(x)) &= \sum_{n=0}^{\infty} K_n x^{\Pi(n)}, & M_2'(R^{-1}(x)) &= \sum_{n=0}^{\infty} L_n x^{\Theta(n)} \end{aligned}, \quad (12)$$

where $R^{-1}(x)$ and $Z^{-1}(x)$ represent the inverse functions of $R(x)$ and $Z(x)$. The Hahn expansion⁶ is a generalization of the Taylor expansion to include negative and real powers. Hence $\Psi(n), \Gamma(n), \Pi(n)$ and $\Theta(n)$ represent series of real powers in ascending order, the leading (*i.e.* smallest) powers assigned the index $n = 0$. These leading powers directly provide Ω via

$$\mu = 2 - \Gamma(0), \quad \nu = -\Pi(0), \quad \rho = -\Theta(0), \quad \eta = -\Psi(0)(\mu - \nu - \rho). \quad (13)$$

Hence, to construct $J \in \mathbb{E}(A, G, \Omega)$ we first generate the weighted network $A \otimes G$, then extract the weighted degrees d_i of all nodes and the nearest neighbor degree \mathcal{D}_{nn} of Eq. (6). The resulting J satisfies

$$J_{ii} \sim -C(\mathbf{f}, \mathcal{G}) \mathcal{D}_{\text{nn}}^{\eta} d_i^{\mu} \quad (14)$$

$$J_{ij} \sim d_i^{\nu} A_{ij} G_{ij} d_j^{\rho}, \quad (15)$$

where the constant $C > 0$ captures the system's specific dynamic time-scales. Note that Ω , as opposed to C , depends only on the leading *powers* of (12), and not on the *coefficients*. Therefore it is unaffected by Eq. (3)'s microscopic parameters, but rather captures an intrinsic characteristic of each dynamic *model*. Namely Ω distinguished between, *e.g.*, Epidemic and Regulatory, but remains the same under two Epidemic systems with different recovery/infection rates. The detailed derivation of Ω appears in Supplementary Section 1, followed by a step by step application on all our testing ground dynamics (Fig. 2) in Supplementary Section 3.

In the above formulation we have assumed that $R(x)$ and $Z(x)$ are invertible, writing $R^{-1}(x)$ and $Z^{-1}(x)$ in (12). In Supplementary Section 1 we explain how to properly treat non-invertible $R(x), Z(x)$. In these sections, we also demonstrate how to extract J for system's with multiple fixed-points, and, specifically, in Supplementary Section 1.5, how to construct J around a trivial fixed-point $\mathbf{x} = (0, \dots, 0)^{\top}$.

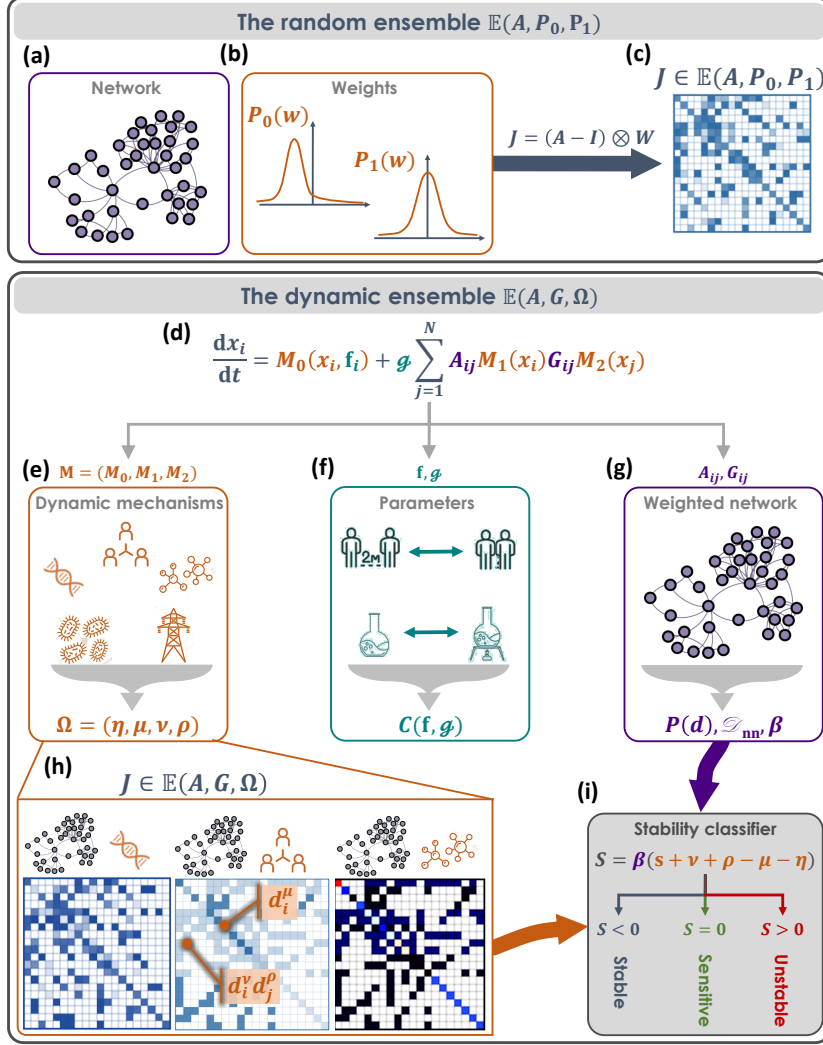


Figure 1: The dynamic Jacobian ensemble. To predict dynamic stability we seek the system's stability matrix J . (a)-(b) The classic approach is to structure J around the network topology A , with weights extracted from two distributions: $P_0(w)$ for the diagonal entries J_{ii} (typically negative) and $P_1(w)$ for the interactions strengths J_{ij} , $i \neq j$. $P_0(w), P_1(w)$ are designed to capture the typical time-scales of the system's self/interaction dynamics. (c) Together this provides $J \in \mathbb{E}(A, P_0, P_1)$, a random matrix based construction, whose stability is determined by the the structure A and the random weights W . (d) Such construction, however, disregards the system's intrinsic interaction *mechanisms*, e.g., infection/recovery (Epidemic) or activation/inhibition (Regulatory). We therefore derive J directly from the nonlinear Eq. (3), which models network dynamics using a composition of three distinct factors: (e) The dynamic mechanisms (orange) are captured by the nonlinear form of the functions \mathbf{M} . These mechanisms are *hardwired* into the system's interacting components, hence unaffected by external perturbations. Our formalism derives the exponents Ω in Eqs. (4) and (5) directly from \mathbf{M} . (f) The system's microscopic parameters \mathbf{f}, \mathcal{G} (turquoise) provide the specific rate-constants for (3)'s dynamic processes. For example, the infection rate in Epidemic (top), or the degradation rate in Biochemical (bottom). These parameters are non-intrinsic, and therefore, influenced by external conditions, such as changes in social behavior (Epidemic) or temperature (Biochemical). Their impact on J is encapsulated within the coefficient $C(\mathbf{f}, \mathcal{G})$ in Eq. (4). (g) A, G represent the weighted network (purple), which is expressed in J via the weighted degree distribution $P(d)$, the nearest neighbor degree \mathcal{Z}_{nn} in (6) and β in (7). (h) The resulting J -ensemble, $\mathbb{E}(A, G, \Omega)$, exhibits non-random scaling patterns driven by the interplay between A, G and Ω . Similar to the random $\mathbb{E}(A, P_0, P_1)$, the non-vanishing terms correspond to the network links, however, in contrast to the random weight assignment of $\mathbb{E}(A, P_0, P_1)$, here the weight of the i, j entry depends on d_i and d_j , as well as on Ω (orange captions). The result is a *dynamic* ensemble, in which identical networks (A, G) yield highly distinctive J matrices depending on \mathbf{M} , e.g., Regulatory (left), Epidemic (center) or Biochemical (right). (i) The stability of J can be reduced to the classifier S in (9), whose value depends only on the degree heterogeneity (β , purple) and on the dynamic exponents (orange terms), but not the parameters \mathbf{f}, \mathcal{G} . Therefore, it provides a robust classification into stable (blue) or unstable (red) dynamics, that are asymptotically insensitive to changes in environmental conditions, i.e. parameters \mathbf{f}, \mathcal{G} . Under $S = 0$ the system becomes sensitive (green), in which case stability is driven by the potentially tunable parameters.

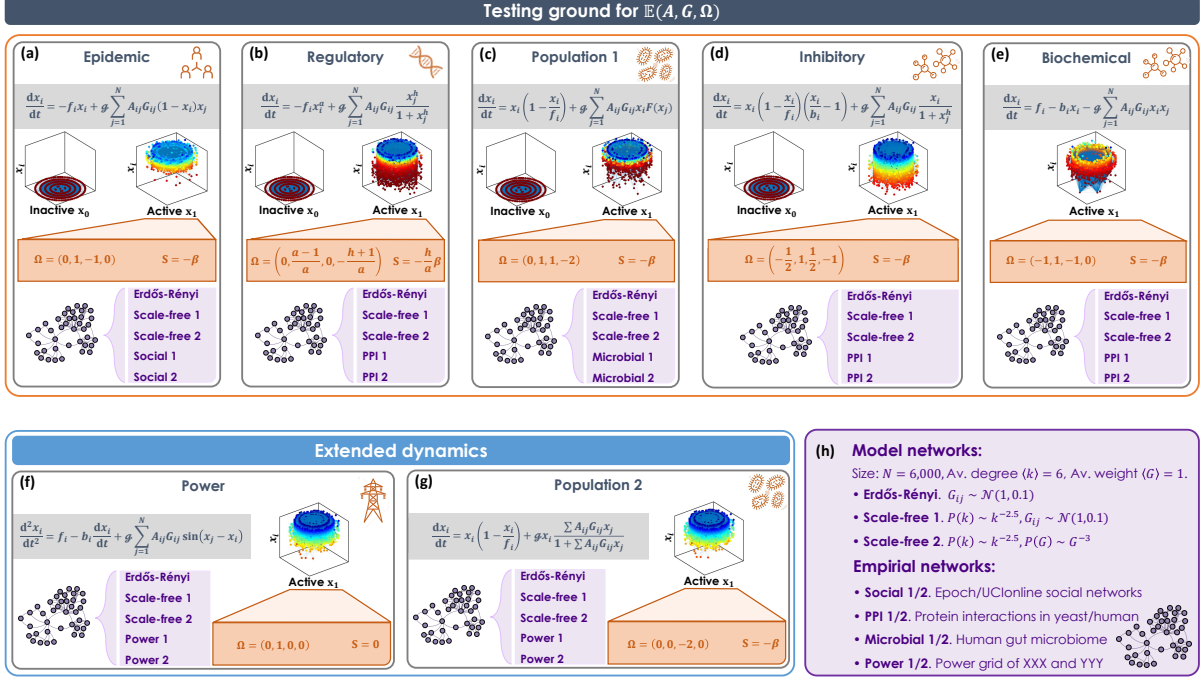


Figure 2: Testing ground for the $\mathbb{E}(A, G, \Omega)$ ensemble. We constructed different combinations of (weighted) networks A, G and dynamics M to examine our J -ensemble. (a) Epidemic. We implemented the susceptible-infected-susceptible (SIS) dynamics (grey box) on a set of model and real-world networks (violet box). This system exhibits two potential fixed-points (3D plots): the inactive \mathbf{x}_0 , in which all activities vanish, *i.e.* healthy, and the active \mathbf{x}_1 , in which all $x_i > 0$, namely the pandemic state. In this 3D visualization the nodes $i = 1, \dots, N$ are laid out on the x, y plane and their fixed-point activity x_i is represented by color (red - low, blue - high) and vertical displacement (z -axis). Therefore, in \mathbf{x}_0 all nodes are on the x, y plane ($x_i = 0$), and in \mathbf{x}_1 they are distributed along $z > 0$ and range from red to blue. In each of these states the system has a different set of exponents Ω and hence a different Jacobian J . Here we present Ω and S for the non-vanishing state \mathbf{x}_1 (orange box). The remaining panels follow a similar format. (b) Regulatory. Sub-cellular dynamics following the Michaelis-Menten model. (c) Population 1. Mutualistic interactions in, *e.g.*, microbial communities. (d) Inhibitory. Suppression dynamics, *e.g.*, between hosts and pathogens. (e) Biochemical. Protein-protein interactions modeled via mass-action kinetics. This system exhibits a single fixed-point, and therefore includes a single 3D plot. (f) Power. Synchronization dynamics between power system components. (g) Population 2. Mutualistic population dynamics with non-additive interactions, namely replacing the term $\sum_{j=1}^N A_{ij} G_{ij} M_2(x_j)$ in Eq. (3) by $M_2(\sum_{j=1}^N A_{ij} G_{ij} x_j)$. (h) Our model and empirical networks. For a detailed description of all networks see Supplementary Section 5.4. Together we arrive at a set of 35 combinations of networks/dynamics upon which we test our theoretical framework. A detailed analysis of all dynamic models appears in Supplementary Section 3. Note that Population 2 and Power are not in the form of Eq. (3), and hence they expand our testing ground beyond the bounds of our analytical framework. We provide a dedicated analysis of these models, together with a mixed-dynamics scenario in Supplementary Section 4.

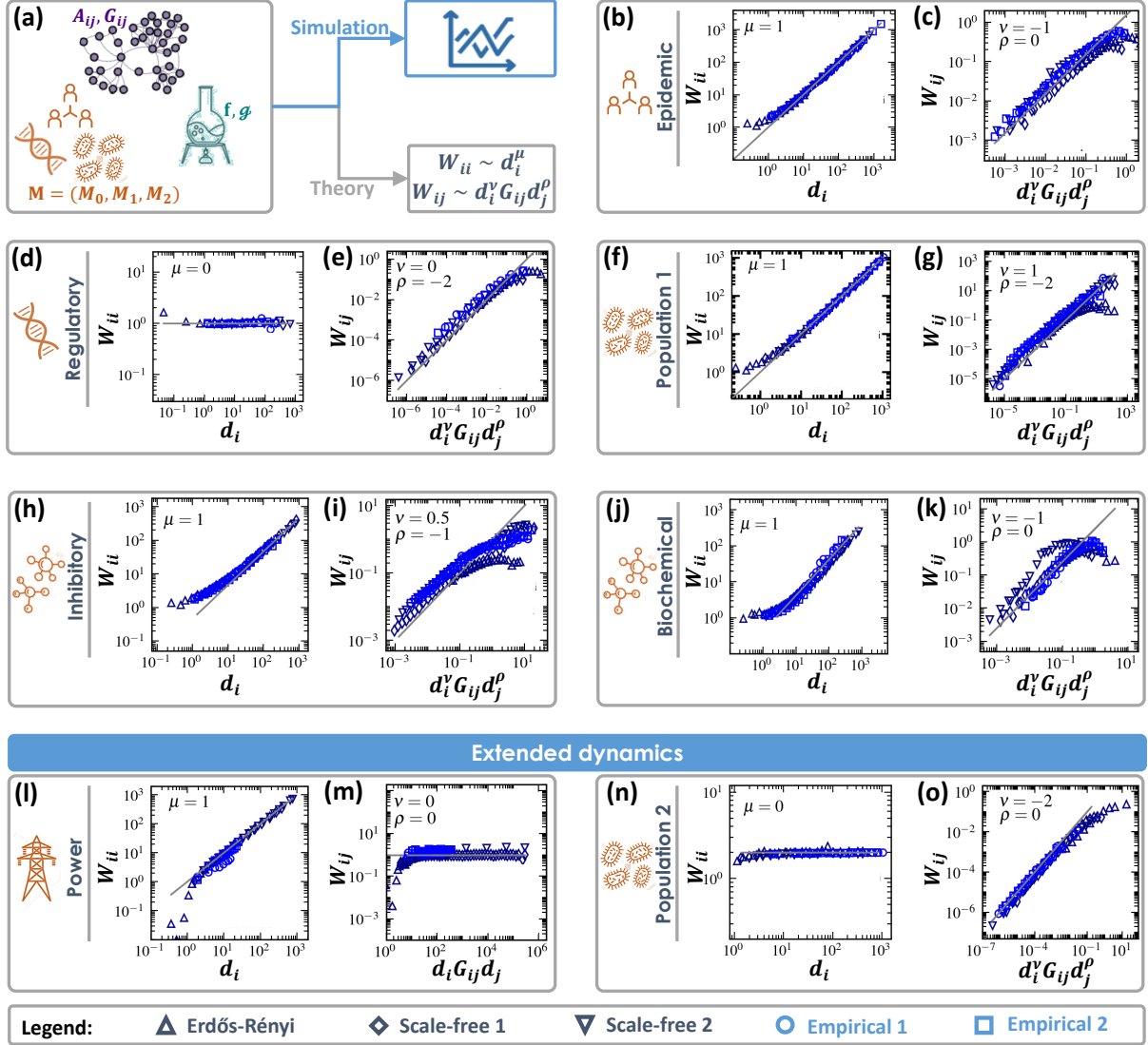


Figure 3: **Emergent patterns in the dynamic ensemble** $\mathbb{E}(A, G, \Omega)$. We implemented our seven dynamic models, Epidemic, Regulatory, Population 1 etc., on a set of relevant model and empirical networks, as detailed in our testing ground of Fig. 2. Focusing on the non-vanishing state \mathbf{x}_1 , we perturbed all nodes around their numerically obtained fixed-point to construct the Jacobian, J . (a) The numerical simulations incorporate the full complexity of Eq. (3), including the weighted network (purple), the diverse parameters (green) and the nonlinear mechanisms (orange). This helps us observe the *real* Jacobian matrices for each of our systems, as obtained from actual numerical runs of the nonlinear network models (Simulation, blue, top). We then compare in each panel the simulation results with our theoretical predictions based on the $\mathbb{E}(A, G, \Omega)$ ensemble (Theory, grey, bottom). (b) The diagonal weights W_{ii} vs. the weighted degree d_i as obtained from Epidemic dynamics (symbols). We observe the scaling relationship of Eq. (4) with $\mu = 1$ (grey solid line) confirming our predicted J -patterns for this dynamics. We also find that this scaling is independent of the specific network, intrinsic to the Epidemic dynamics, as predicted. (c) The off-diagonal weights W_{ij} vs. prediction (5) with $\nu = -1, \rho = 0$ (symbols). Once again, we observe a perfect agreement with our theoretical prediction (grey solid line). We also include results obtained from two relevant empirical networks, Social 1 and Social 2 (light blue circles/squares), capturing online social dynamics. (d)-(e) Similar results are observed under Regulatory dynamics ($\mu = \nu = 0, \rho = -2$) on both model and real networks (PPI 1 and PPI 2); (f)-(g) Population 1 dynamics ($\mu = \nu = 1, \rho = -2$, empirical networks: Microbial 1 and Microbial 2); (h)-(i) Inhibitory dynamics ($\mu = 1, \nu = 1/2, \rho = -1$, empirical networks: PPI 1 and PPI 2); (j)-(k) Biochemical dynamics ($\mu = 1, \nu = -1, \rho = 0$, empirical networks: PPI 1 and PPI 2). (l)-(m) Power dynamics ($\mu = 1, \nu = \rho = 0$, empirical networks: Power 1 and Power 2); (n)-(o) Population 2 dynamics ($\mu = 0, \nu = -2, \rho = 0$, empirical networks: Microbial 1 and Microbial 2); As predicted, we find that real Jacobian matrices exhibit the non-random patterns of Eqs. (4) and (5), and therefore cannot be modeled via the random ensemble $\mathbb{E}(A, P_0, P_1)$, but rather through our dynamic Jacobian family $\mathbb{E}(A, G, \Omega)$. Data in all panels are logarithmically binned.²⁰ Details on the numerical calculation of J , log-binning and the construction of all model/real networks appear in Supplementary Section 5.

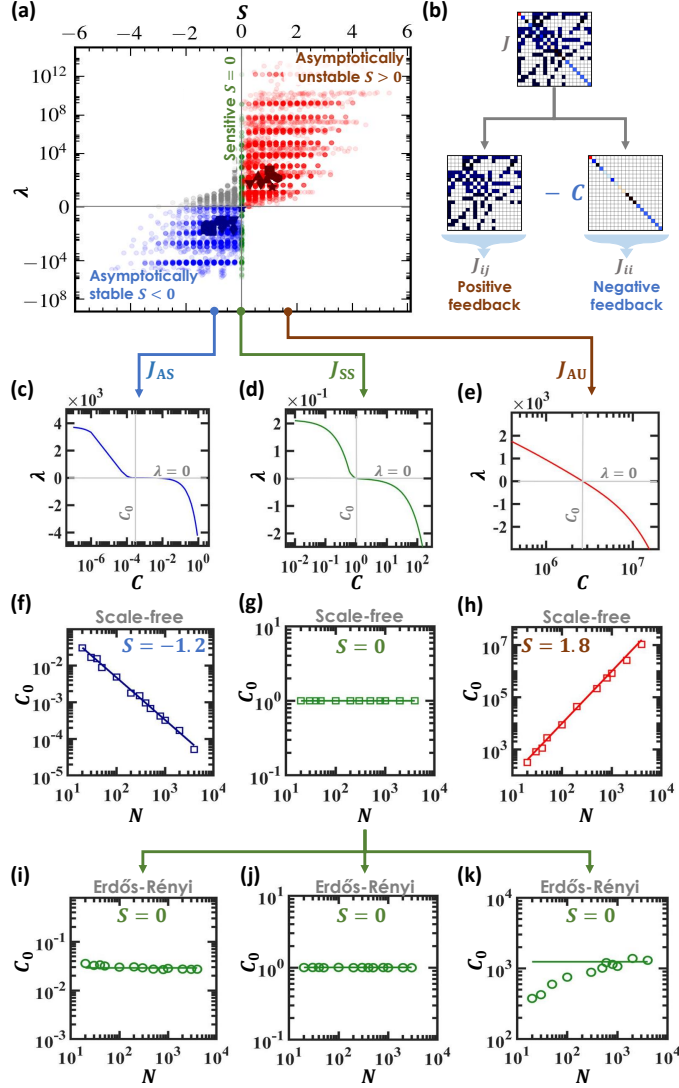


Figure 4: **Three classes of dynamic stability in real and model networks.** We extracted 7,387 Jacobian matrices from the $\mathbb{E}(A, G, \Omega)$ ensemble, using combinations of model/real networks with different dynamic exponents Ω . For each J we calculated the principal eigenvalue λ and the stability classifier S in (9). (a) λ vs. S for all 7,387 J -matrices. We observe the three predicted classes: Asymptotically unstable (red) in which $S > 0$ and hence also $\lambda > 0$; Sensitively stable (green), where $S = 0$ and λ can be both positive or negative; Asymptotically stable (blue), where $S < 0$ and therefore $\lambda < 0$. Our classification was inaccurate in $\sim 4\%$ of the cases on binary networks, $\sim 5\%$ on weighted networks and $\sim 15\%$ on weighted/negative networks, amounting to a total discrepancy of $\sim 8\%$ over the entire ensemble (grey dots). Empirical networks (solid symbols): Under the random ensemble $\mathbb{E}(A, P_0, P_1)$ all our empirical networks are classified as unstable (red symbols). This is a consequence of the diversity-stability principal that predicts, for random networks, an asymptotic instability (see **Box I**). However, the same networks under $\mathbb{E}(A, G, \Omega)$, each with its relevant Ω , become dynamically stable (blue symbols). Hence, networks rendered unstable via the existing random matrix paradigm, are, in fact, stable, when accounting for the nonlinearity through Ω . (b) The value of λ emerges from the competition between J 's off-diagonal terms, representing positive feedback, and the strength of the diagonal terms J_{ii} (negative feedback). Therefore one can force a system towards stability ($\lambda < 0$) by increasing C in (4). (c)-(e) Taking three specific J matrices from each class, we plot λ vs. C , seeking the critical C_0 , in which λ becomes negative (grey lines). (f) For the stable J_{AS} ($S = -1.2$) we find that C_0 decreases with N (squares), capturing the asymptotic stability, in which for large systems ($N \rightarrow \infty$) stability is sustained even under arbitrarily small C . The theoretical scaling predicted in Eq. (10) is also shown (solid line, slope -1.2). (g) For J_{SS} we have $S = 0$, the critical C_0 is independent of N , hence the system's stability can be affected by finite changes to its dynamic parameters, *e.g.*, environmental perturbations. (h) The asymptotically unstable J_{AU} ($S = 1.8$) has $C_0 \rightarrow \infty$ in the limit of large N , in perfect agreement with Eq. (10) (solid line). (i)-(k) For a bounded $P(d)$, *e.g.*, Erdős-Rényi, β vanishes and hence $S = 0$ in (9). Under these conditions, regardless of Ω , the system is always sensitively stable and therefore C_0 does not scale with N . This demonstrates the role of degree-heterogeneity in ensuring stability, in the face of changing environmental conditions.

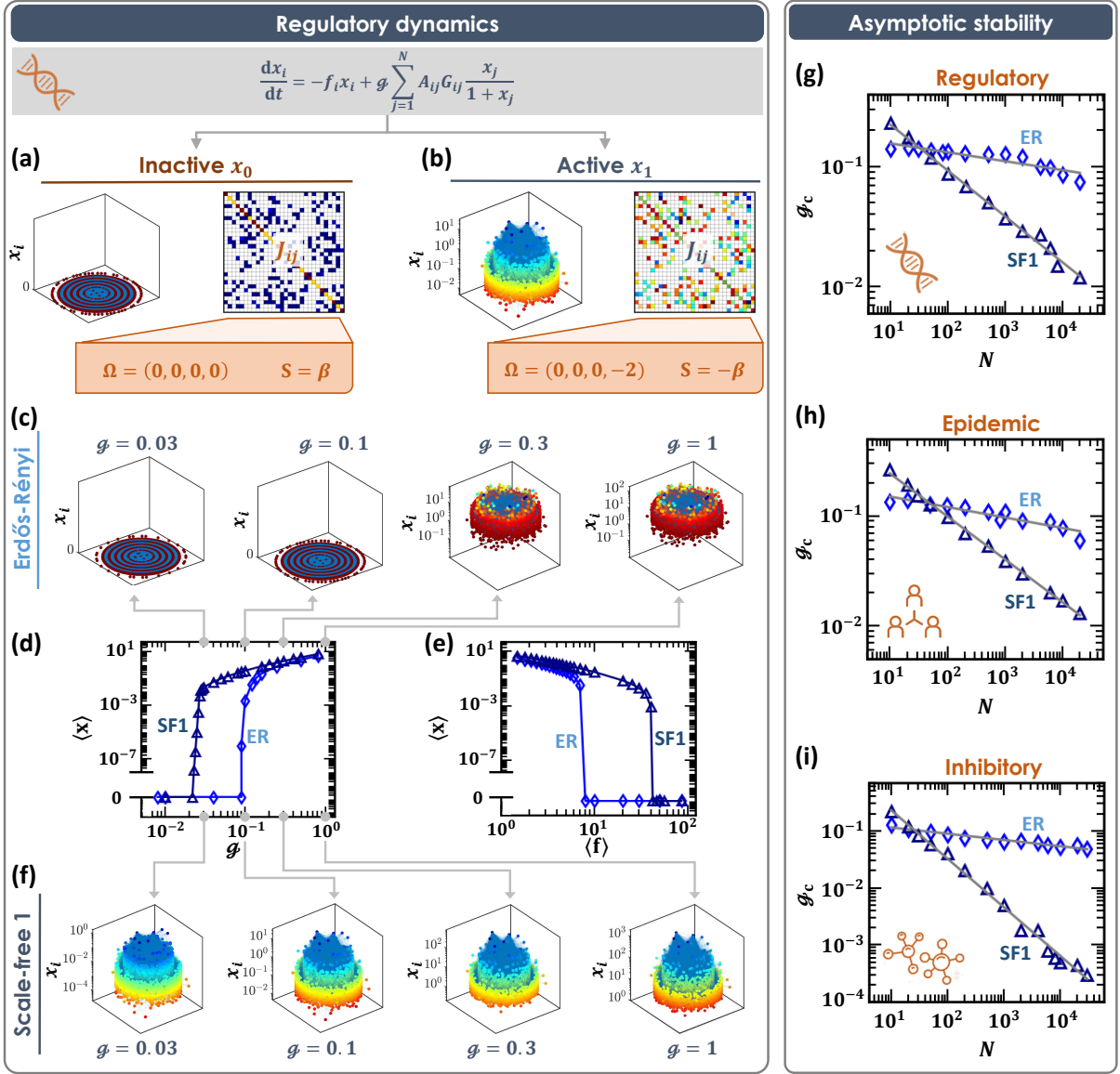


Figure 5: **Emergent stability in large heterogeneous networks.** (a)-(b) Regulatory dynamics exhibit two fixed points (3D plots), each with its own $J \in \mathbb{E}(A, G, \Omega)$, shown to the right of each plot. The inactive \mathbf{x}_0 has $\Omega = (0, 0, 0, 0)$ and $S = \beta > 0$, and hence it is asymptotically unstable. The active \mathbf{x}_1 has a different J , with $\Omega = (0, 0, 0, -2)$ and $S = -\beta < 0$, asymptotically stable. (c) The state of Regulatory as obtained from numerical simulations on our ER network under varying \mathcal{G} . The system transitions from \mathbf{x}_1 (right) to \mathbf{x}_0 (left) under small \mathcal{G} . This represents sensitive stability, as indeed predicted for ER, in which parameters, here \mathcal{G} , affect the state of the system. (d) To examine this systematically we plot the mean activity $\langle \mathbf{x} \rangle$ vs. \mathcal{G} as obtained for ER (diamonds) and for our scale-free network SF1 (triangles). Both systems exhibit a critical \mathcal{G}_c , below which \mathbf{x}_1 becomes unstable and the system transitions to \mathbf{x}_0 . The crucial point is, however, that thanks to its heterogeneity SF1 exhibits an increased robustness against \mathcal{G} variations, with \mathcal{G}_c an order of magnitude lower than that observed for ER. (e) $\langle \mathbf{x} \rangle$ vs. $\langle \mathbf{f} \rangle$ shows a similar behavior. Here *increasing* $\langle \mathbf{f} \rangle$ causes the system to collapse to \mathbf{x}_0 , and, as predicted, SF1 can incur higher $\langle \mathbf{f} \rangle$ than ER. (f) The state of SF1 under the same four conditions ($\langle \mathbf{f} \rangle, \mathcal{G}$) as shown in panel (c) for ER. Indeed, SF1 remains at \mathbf{x}_1 even when ER has already collapsed to \mathbf{x}_0 . (g) \mathcal{G}_c vs. the system size N as obtained from numerically simulating Regulatory dynamics. For ER we observe $\mathcal{G}_c \sim \text{const}$ (diamonds), *i.e.* the system *can* be destabilized via parameter perturbation. Indeed, while N spans over four orders of magnitude, \mathcal{G}_c varies by a mere $\sim 40\%$. In contrast, for SF1 we find that \mathcal{G}_c exhibits negative scaling with N , approaching $\mathcal{G}_c \rightarrow 0$ in the limit $N \rightarrow \infty$. This captures precisely the predicted asymptotic stability, in which a sufficiently large and heterogeneous network is guaranteed to stably reside in \mathbf{x}_1 . (h)-(i) Repeating this experiment for Epidemic and Inhibitory, we continue to observe our predicted asymptotic stability. For $N \rightarrow \infty$ we have $\mathcal{G}_c \rightarrow 0$ under the heterogeneous SF1, vs. \mathcal{G}_c independent of N under the homogeneous ER.

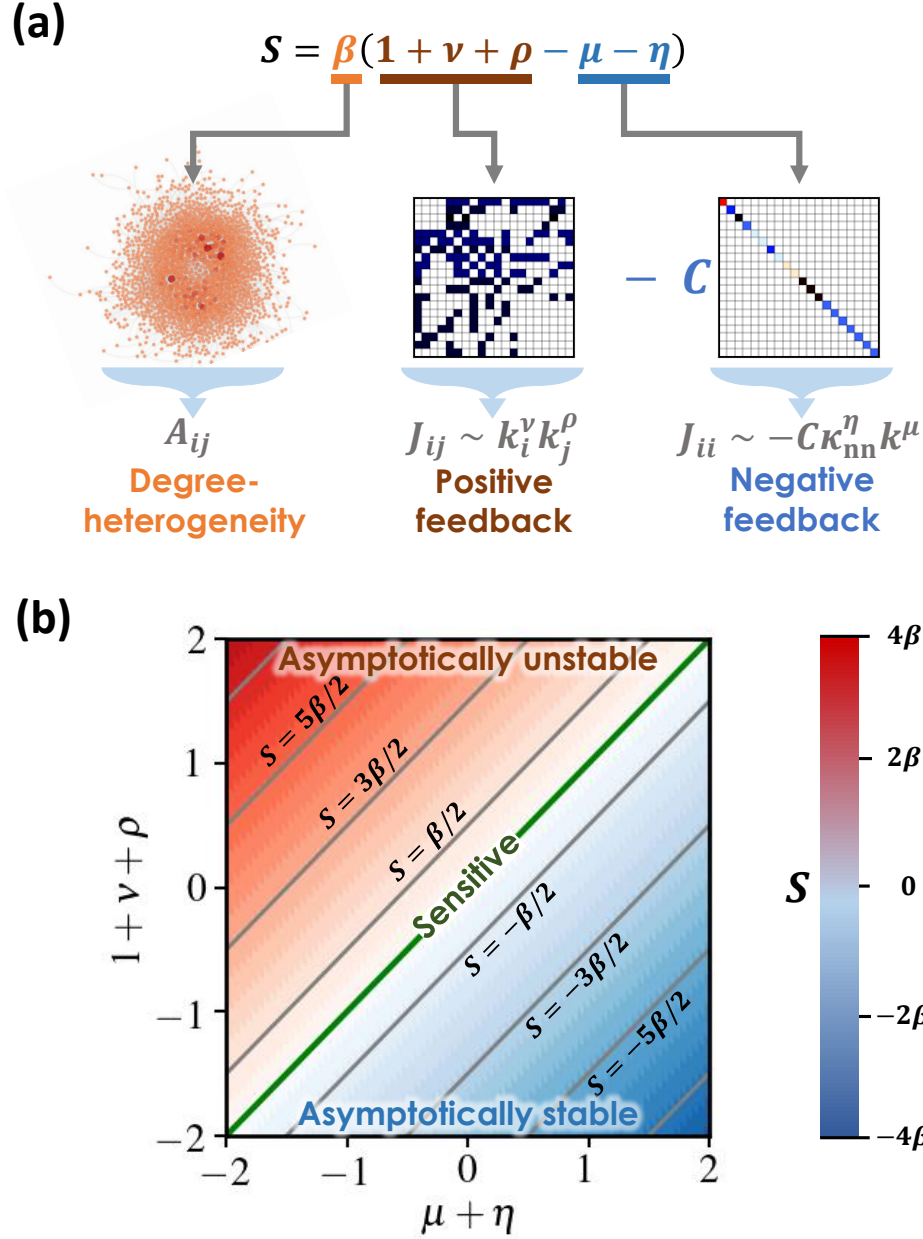


Figure 6: **The ingredients of dynamic stability.** (a) The stability classifier S (9) comprises five exponents: β characterizes the network topology and its degree heterogeneity via (7); ν, ρ determine the magnitude of J 's off-diagonal terms J_{ij} ; μ, η characterize the diagonal terms J_{ii} , *i.e.* each node's self-regulation. This portrays stability as a balance between the positive feedback mediated by the system's interactions, strengthened with increasing ν, ρ , vs. the stabilizing effect of the diagonal terms, that are reinforced by η, μ . Indeed, S in (9) tends to be positive, *i.e.* unstable, with increasing ν, ρ , and negative, *i.e.* stable, with increasing η, μ . (b) S (color-bar) vs. the exponents $\Omega = (\eta, \mu, \nu, \rho)$. Indeed, increasing ν, ρ drives the system towards the unstable class ($S > 0$, red), while increasing μ, η enhances the system's stability (blue). In addition to the discrete classification of stable dynamics (blue, $S < 0$), unstable dynamics (red, $S > 0$) and sensitive dynamics (green, $S = 0$), S also helps quantify the continuum *level* of stability, where the more negative/positive is S , the more stable/unstable is the system. Grey lines represent *equi-stable* systems. We find that highly distinct dynamical systems may reside within the same equi-stability class.

References

- [1] S.V. Buldyrev, R. Parshani, G. Paul, H.E. Stanley and S. Havlin. Catastrophic cascade of failures in interdependent networks. *Nature*, 464:1025–1028, 2010.
- [2] I. Dobson, B.A. Carreras, V.E. Lynch and D.E. Newman. Complex systems analysis of series of blackouts: Cascading failure, critical points, and self-organization. *Chaos*, 17:026103, 2007.
- [3] D. Duan, C. Lv, S. Si, Z. Wang, D. Li, J. Gao, S. Havlin, H.E. Stanley and S. Boccaletti. Universal behavior of cascading failures in interdependent networks. *Proc. Natl. Acad. Sci. USA*, 116:22452–57, 2019.
- [4] A.E. Motter and Y.-C. Lai. Cascade-based attacks on complex networks. *Physical Review E*, 66:065102, 2002.
- [5] P. Crucitti, V. Latora and M. Marchiori. Model for cascading failures in complex networks. *Phys. Rev. E*, 69:045104–7, 2004.
- [6] D. Achlioptas, R.M. D’Souza and J. Spencer. Explosive percolation in random networks. *Science*, 323:1453–1455, 2009.
- [7] J. Gao, B. Barzel and A.-L. Barabási. Universal resilience patterns in complex networks. *Nature*, 530:307—312, 2016.
- [8] S. Boccaletti, J.A. Almendral, S. Guana, I. Leyvad, Z. Liua, I.S. Nadal, Z. Wang and Y. Zou. Explosive transitions in complex networks’ structure and dynamics: Percolation and synchronization. *Physics Reports*, 660:1–94, 2016.
- [9] S. Boccaletti, V. Latora, Y. Moreno, M. Chavez and D.-U. Hwang. Complex networks: Structure and dynamics. *Physics Reports*, 424:175–308, 2006.
- [10] Michael M Danziger, Ivan Bonamassa, Stefano Boccaletti, and Shlomo Havlin. Dynamic interdependence and competition in multilayer networks. *Nature Physics*, 15(2):178–185, 2019.
- [11] K.Z. Coyte, J. Schluter and K.R. Foster. The ecology of the microbiome: Networks, competition, and stability. *Science*, 350:663–666, 2015.
- [12] R.V. Solé and J.M. Montoya. Complexity and fragility in ecological networks. *Proc. R. Soc. London Ser. B*, 268:2039–2045, 2001.
- [13] H.I. Schreier, Y. Soen and N. Brenner. Exploratory adaptation in large random networks. *Nature Communications*, 8:14826, 2017.
- [14] L.M. Pecora and T.L. Carroll. Master stability functions for synchronized coupled systems. *Phys. Rev. Lett.*, 80:2109, 1998.
- [15] V.I. Arnold. *Ordinary Differential Equations*. MIT Press, Cambridge, MA, 1973.
- [16] M.W. Hirsch and S. Smale. *Differential Equations, Dynamical Systems and Linear Algebra*. Academic Press, New York, 1974.
- [17] B. Barzel and O. Biham. Quantifying the connectivity of a network: The network correlation function method. *Phys. Rev. E*, 80:046104–15, 2009.

- [18] R.M. May. Will a large complex system be stable? *Nature*, 238:413 – 414, 1972.
- [19] G. Yan, N.D. Martinez and Y.-Y. Liu. Degree heterogeneity and stability of ecological networks. *Journal of The Royal Society Interface*, 14:131, 2017.
- [20] K.S. McCann. The diversity–stability debate. *Nature*, 405(6783):228–233, 2000.
- [21] J.D. O’Sullivan, R.J. Knell and A.G. Rossberg. Metacommunity-scale biodiversity regulation and the self-organised emergence of macroecological patterns. *Ecology Letters*, 22:1428, 2019.
- [22] M. Barbier, C. de Mazancourt, M. Loreau and G. Bunin. *Phys. Rev. X*, 11:011009, 2021.
- [23] G. Caldarelli. *Scale-free networks: complex webs in nature and technology*. Oxford University Press, New York, 2007.
- [24] B. Barzel and A.-L. Barabási. Universality in network dynamics. *Nature Physics*, 9:673 – 681, 2013.
- [25] U. Harush and B. Barzel. Dynamic patterns of information flow in complex networks. *Nature Communications*, 8:2181, 2017.
- [26] C. Hens, U. Harush, R. Cohen, S. Haber and B. Barzel . Spatiotemporal propagation of signals in complex networks. *Nature Physics*, 15:403, 2019.
- [27] R. Pastor-Satorras, C. Castellano, P. Van Mieghem and A. Vespignani. Epidemic processes in complex networks. *Rev. Mod. Phys.*, 87:925–958, 2015.
- [28] P.S. Dodds, R. Muhamad and D.J. Watts. An experimental study of search in global social networks. *Science*, 301:827–829, 2003.
- [29] D. Brockmann, V. David and A.M. Gallardo. Human mobility and spatial disease dynamics. *Reviews of Nonlinear Dynamics and Complexity*, 2:1, 2009.
- [30] G. Karlebach and R. Shamir. Modelling and analysis of gene regulatory networks. *Nature Reviews*, 9:770–780, 2008.
- [31] J.D. Murray. *Mathematical Biology*. Springer, Berlin, 1989.
- [32] B. Barzel and O. Biham. Binomial moment equations for stochastic reaction systems. *Phys. Rev. Lett.*, 106:150602–5, 2011.
- [33] B. Barzel and O. Biham. Stochastic analysis of complex reaction networks using binomial moment equations. *Phys. Rev. E*, 86:031126, 2012.
- [34] C.S. Holling. Some characteristics of simple types of predation and parasitism. *The Canadian Entomologist*, 91:385–398, 1959.
- [35] J.N. Holland, D.L. DeAngelis and J.L. Bronstein. Population dynamics and mutualism: functional responses of benefits and costs. *American Naturalist*, 159:231–244, 2002.
- [36] D. Wodarz, J.P. Christensen and A.R. Thomsen. The importance of lytic and nonlytic immune responses in viral infections. *Trends in Immunology*, 23:194–200, 2002.

- [37] E.L. Berlow, J.A. Dunne, N.D. Martinez, P.B. Stark, R.J. Williams and U. Brose. Simple prediction of interaction strengths in complex food webs. *Proceedings of the National Academy of Sciences*, 106:187–191, 2009.
- [38] J.F. Hayes and T.V.J. Ganesh Babu. *Modeling and Analysis of Telecommunications Networks*. John Wiley & Sons, Inc., Hoboken, NJ, USA, 2004.
- [39] M.E.J. Newman. *Networks - an introduction*. Oxford University Press, New York, 2010.
- [40] A.-L. Barabási and Z.N. Oltvai. Network biology: understanding the cell’s functional organization. *Nat. Rev. Gen.*, 5:101, 2004.
- [41] T. Opsahl and P. Panzarasa. Clustering in weighted networks. *Social Networks*, 31:155–163, 2009.
- [42] J.-P. Eckmann, E. Moses and D. Sergi. Entropy of dialogues creates coherent structures in e-mail traffic. *Proc. Natl. Acad. Sci. USA*, 101:14333–7, 2004.
- [43] M. Faloutsos, P. Faloutsos and C. Faloutsos. On power-law relationships of the Internet topology. *Compute. Commun. Rev.*, 29:251–262, 1999.
- [44] G. Caldarelli and M. Catanzaro. *Networks: A very short introduction*. Oxford University Press, New York, 2012.
- [45] A.-L. Barabási, H. Jeong, E. Ravasz, Z. Néda, A. Schubert and T. Vicsek. *Physica A*, 311:590, 2002.
- [46] A.-L. Barabási and R. Albert. Emergence of scaling in random networks. *Science*, 286:509–512, 1999.
- [47] S. Allesina and S. Tang. Stability criteria for complex ecosystems. *Nature*, 483:205–208, 2012.
- [48] W. Tarnowski, I. Neri and P. Vivo. Universal transient behavior in large dynamical systems on networks. *Phys. Rev. Research*, 2:023333, 2020.
- [49] S. Sinha and S. Sinha. Evidence of universality for the May-Wigner stability theorem for random networks with local dynamics. *Phys. Rev. E*, 71(2):020902, 2005.
- [50] M. Granovetter. Threshold models of collective behavior. *The American journal of Sociology*, 83:6, 1420–43, 2002.
- [51] Y. Kuramoto. *Chemical oscillations, waves and turbulence*. Springer-Verlag Berlin, Heidelberg, 1984.
- [52] P. Kundu, C. Hens, B. Barzel and P. Pal. Perfect synchronization in networks of phase-frustrated oscillators. *Europhysics Letters*, 120:40002, 2018.
- [53] J.A. Almendral and A. Díaz-Guilera. Dynamical and spectral properties of complex networks. *New Journal of Physics*, 9:187–187, 2007.
- [54] P. Van Mieghem. Epidemic phase transition of the SIS type in network. *Europhysics Letters*, 97(4):48004, 2012.

- [55] P. Van Mieghem. *Graph Spectra for Complex Networks*. Cambridge University Press, Cambridge, UK, 2010.
- [56] V.S. Afraimovich and L.A. Bunimovich. Dynamical networks: interplay of topology, interactions and local dynamics. *Nonlinearity*, 20:1761–1771, 2007.
- [57] C. Kirst, M. Timme and D. Battaglia. Dynamic information routing in complex networks. *Nature Communications*, 7:11061, 2016.
- [58] A. Barrat, M. Barthélemy and A. Vespignani. *Dynamical Processes on Complex Networks*. Cambridge University Press, Cambridge, 2008.
- [59] G. Yan, G. Tsekenis, B. Barzel, J.-J. Slotine, Y.-Y. Liu and A.-L. Barabási. Spectrum of controlling and observing complex networks. *Nature Physics*, 11:779–786, 2015.
- [60] L. Schmetterer and K. Sigmund (Eds.). *Hans Hahn Gesammelte Abhandlungen Band 1/Hans Hahn Collected Works Volume 1*. Springer, Vienna, Austria, 1995.
- [61] S. Milojević. Power-law distributions in information science: making the case for logarithmic binning. *Journal of the American Society for Information Science and Technology*, 61:2417–2425, 2010.

**Emergent stability in
complex network dynamics**

Supplementary information

May 18, 2021

Contents

1	The Jacobian ensemble $\mathbb{E}(A, G, \Omega)$	1
1.1	The fixed-points \mathbf{x}^*	2
1.1.1	From x_i to $x(d)$	3
1.1.2	Evaluating $\langle M_2(x) \rangle_{\odot}$	6
1.2	Diagonal terms W_{ii}	9
1.3	The off-diagonal terms W_{ij}	11
1.4	Piecing together the J_{ij} puzzle	13
1.4.1	Impact of $P(d)$ and \mathcal{D}_{nn}	14
1.5	J around a trivial fixed-point	15
2	Principle eigenvalue of $J \in \mathbb{E}(A, G, \Omega)$	19
2.1	Jacobians with positive weights $\mathbf{s} = 1$	20
2.2	Jacobians with negative weights $\mathbf{s} = 0$	25
2.3	The role of topology vs. dynamics	26
3	Analyzing the dynamic models	26
3.1	Epidemic dynamics	26
3.2	Regulatory dynamics	28
3.3	Population 1 dynamics	33
3.4	Biochemical dynamics	35
3.5	Inhibitory dynamics	37
4	Extended dynamics	40
4.1	Power dynamics	40
4.2	Non-additive dynamics	41
4.3	Mixed dynamics	43
5	Methods and data analysis	45
5.1	Numerical integration	45
5.1.1	Numerical analysis of Power dynamics	45
5.2	Numerically estimating J	46
5.3	Logarithmic binning	46
5.4	Model and empirical networks	47

1 The Jacobian ensemble $\mathbb{E}(A, G, \Omega)$

To analyze complex system stability we seek the *real* Jacobian matrix J , as extracted from the system's specific nonlinear interaction mechanisms. We first rewrite Eq. (3) of the main text as

$$\frac{dx_i}{dt} = F_i(\mathbf{x}(t)), \quad (16)$$

where

$$F_i(\mathbf{x}(t)) = M_0(x_i(t), \mathbf{f}_i) + \mathcal{G} \sum_{j=1}^N A_{ij} M_1(x_i(t)) G_{ij} M_2(x_j(t)). \quad (17)$$

The self dynamics M_0 is characterized by parameters \mathbf{f}_i , assigned randomly to all nodes via the density function $P(\mathbf{f})$, whose ensemble average is denoted by $\langle \mathbf{f} \rangle$. The network structure is captured by the $N \times N$ binary matrix A , whose, typically fat-tailed, degree distribution is $P(k)$. The weights of all existing links G_{ij} are extracted at random from the probability density function $P(G)$, which may be bounded, capturing a homogeneous interaction strength, or fat-tailed, describing systems in which the strength of all interactions varies broadly. The average weight in $P(G)$ is normalized to $\langle G \rangle = 1$, and hence the average interaction strength in (17) is governed by the tunable parameter \mathcal{G} . In other words, $P(G)$ governs the variability in link weights; \mathcal{G} controls their typical strength.

Together, the system's dynamics is characterized by three components: The nonlinear mechanisms are captured by the three functions

$$\mathbf{M} = (M_0(x), M_1(x), M_2(x)), \quad (18)$$

the node/link parameters are given by $\mathbf{f}_i, \mathcal{G}$, and the weighted network $\mathbb{G} = A \otimes G$ captures the distribution of degrees/weights in the system (\otimes denotes the Hadamard element-by-element matrix product). The unweighted degrees can be extracted from A through

$$k_i = \sum_{j=1}^N A_{ij}, \quad (19)$$

counting the discrete number of neighbors of linked to node i . The weighted-degrees are taken from \mathbb{G} as

$$d_i = \sum_{j=1}^N \mathbb{G}_{ij} = \sum_{j=1}^N A_{ij} G_{ij}, \quad (20)$$

together providing the weighted degree distribution $P(d)$, which captures the probability density for a randomly selected node i to have $d_i \in (d, d + \delta d)$.

We denote (16)'s fixed-point(s) by $\mathbf{x}^* = (x_1, \dots, x_N)^\top$, where we omit the term t to capture their independence on time. These fixed-points are obtained by solving the equilibrium equation

$$F_i(\mathbf{x}^*) = 0. \quad (21)$$

To assess the dynamic stability of each of Eq. (21)'s solutions we track their response to small perturbations, via the Jacobian

$$J_{ij} = \left. \frac{\partial F_i(\mathbf{x})}{\partial x_j} \right|_{\mathbf{x}=\mathbf{x}^*}, \quad (22)$$

whose structure we obtain below. Writing

$$J = (A - I) \otimes W \quad (23)$$

we treat separately the diagonal terms $J_{ii} = -W_{ii}$ and the off-diagonal terms $J_{ij} = A_{ij}W_{ij}$ (in (23) I represents the identity matrix).

1.1 The fixed-points \mathbf{x}^*

We consider systems of the form (16) that exhibit at least one fully positive fixed-point \mathbf{x}^* . First, using Eq. (24) we write

$$M_0(x_i, \mathbf{f}_i) + \mathcal{G} \sum_{j=1}^N A_{ij} M_1(x_i) G_{ij} M_2(x_j) = 0, \quad (24)$$

seeking the potentially multiple equilibrium solutions of the system. To express the sum on the r.h.s. of the equation we use

$$\langle M_2(x) \rangle_{i,\odot} = \frac{1}{d_i} \sum_{j=1}^N A_{ij} G_{ij} M_2(x_j), \quad (25)$$

capturing the weighted average of the function $M_2(x_j)$ over all of node i 's direct network *neighborhood*; d_i is i 's weighted-degree as defined in (20). Such averaging over a node's neighborhood is denoted, here and below, by the \odot symbol. This allows us to write Eq. (24) as

$$M_0(x_i, \mathbf{f}_i) + M_1(x_i) \mathcal{G} d_i \langle M_2(x) \rangle_{i,\odot} = 0, \quad (26)$$

a direct equation for i 's fixed-point value x_i . For certain dynamics Eq. (26) has a *trivial* solution in which $M_0(x_i, \mathbf{f}_i) = M_1(x_i) = 0$. Most often this solution captures an inactive state in which all $x_i = 0$. Such solutions are treated separately in Sec. 1.5, as here we focus on the Jacobian around the non-trivial states of the system.

For these non-trivial cases, *i.e.* where $M_0(x_i, \mathbf{f}_i) \neq 0$, we rewrite (26) as

$$R_i(x_i) = \frac{1}{d_i \mathcal{G} \langle M_2(x) \rangle_{i,\odot}}, \quad (27)$$

where

$$R_i(x) = -\frac{M_1(x)}{M_0(x, \mathbf{f}_i)}. \quad (28)$$

To extract x_i we invert the function $R_i(x)$, providing i 's fixed-point activity as

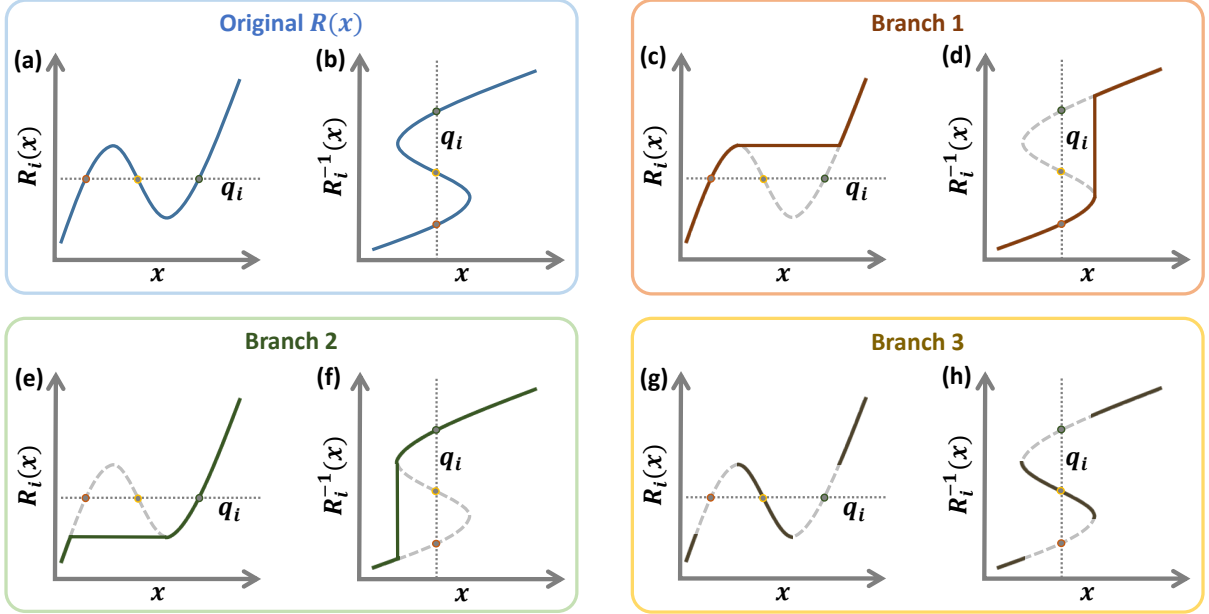


Figure 7: **Inverting a non-monotonic $R_i(x)$.** (a) In case $R_i(x)$ in (27) is non-monotonic its inverse function is ill-defined. (b) This leads in Eq. (29) to multiple solutions (orange, yellow, green), describing a potentially multi-stable system. To treat this we construct three functions, corresponding to the different branches of $R_i(x)$: (c)-(d) Branch 1, in which the only solution to (29) is the orange fixed-point; (e)-(f) Branch 2, providing the green fixed-point; (g)-(h) Branch 3, for the intermediate yellow fixed-point.

$$x_i = R_i^{-1}(q_i), \quad (29)$$

where $R_i^{-1}(x)$ is the inverse function of $R_i(x)$ and

$$q_i = \frac{1}{\mathcal{G}\langle M_2(x) \rangle_{i, \odot} d_i} \quad (30)$$

is i 's inverse weighted degree.

In certain cases $R_i(x)$ is non-monotonic, and hence $R_i^{-1}(x)$ is ill-defined. This indicates that Eq. (24) has several solutions, capturing multiple fixed-points of the system. For example, in Fig. 7a we illustrate a function in which $R_i(x) = q_i$ has three distinct solutions, represented by the red, yellow and green dots. Therefore, $R_i^{-1}(x)$ assumes three separate values at $x = q_i$, formally, an undefined function (Fig. 7b). To observe each of these solutions via (29) we focus on the different *branches* of $R_i(x)$ separately: first we take $R_i(x)$ from (40) and, if non-monotonous, we identify its extremum points. We then generate the different invertible branches of $R(x)$, for instance the one including only the maximum point (Branch 1, Fig. 7c,d), the one including only the minimum point (Branch 2, Fig. 7e,f) or the branch traversing through the intermediate point between these two extrema (Branch 3, Fig. 7g,h). Each of these constructions is invertible, and allows us to analyze all fixed-points independently using Eq. (29).

1.1.1 From x_i to $x(d)$

To understand the dependence of a node's activity on its weighted degree, we seek the average fixed-point x_i over all nodes with degree d . We express this as

$$x(d) = \frac{1}{|\mathcal{G}(d)|} \sum_{i \in \mathcal{G}(d)} x_i, \quad (31)$$

where

$$\mathcal{G}(d) = \left\{ i \in \{1, \dots, N\} \mid d_i \in (d, d + \delta d) \right\} \quad (32)$$

is the group of all nodes whose weighted degree is in the range $(d, d + \delta d)$, and $|\mathcal{G}(d)|$ is the number of nodes in that group. Such binning within $(d, d + \delta d)$ is required since d is a continuous variable, and hence writing $d_i = d$ yields a group of measure zero.

To approximate $x(d)$ we first evaluate the average neighborhood activity of all nodes in $\mathcal{G}(d)$ via

$$\langle M_2(x) \rangle_{d, \odot} = \frac{1}{|\mathcal{G}(d)|} \sum_{i \in \mathcal{G}(d)} \langle M_2(x) \rangle_{i, \odot}, \quad (33)$$

capturing the average value of $M_2(x)$ surrounding nodes with weighted degree around d , *i.e.* nodes in $\mathcal{G}(d)$. Most generally, the activities x_j may depend, to some extent, on the degree d_i of their neighbor i , however this dependence is often unknown. We therefore, capture this dependence via (33) as

$$\langle M_2(x) \rangle_{d, \odot} \approx f(d) \langle M_2(x) \rangle_{\odot}, \quad (34)$$

where

$$\langle M_2(x) \rangle_{\odot} = \frac{1}{N} \sum_{i=1}^N \frac{1}{d_i} \sum_{j=1}^N A_{ij} G_{ij} M_2(x_j) \quad (35)$$

represents the average of the function $M_2(x_j)$ over *all* network neighborhoods, independent of i or d . In (34) the term $\langle M_2(x) \rangle_{\odot}$ describes a characteristic aggregated function of the *system's* fixed-point, capturing the value of $M_2(x_j)$ averaged over all nearest neighbor nodes. Such averaging over *all* nodes is not specific to i 's neighborhood, neglecting potential dependencies between i and its neighbors - hence the approximation sign \approx , rather than $=$. The function $f(d)$ corrects this average to account for the fact that in the l.h.s. of (34) the average is carried out selectively over nodes whose neighbor has degree d , while $\langle M_2(x) \rangle_{\odot}$ in (35) averages indiscriminately over all nodes.

The function $f(d)$ is driven by two effects: (i) *Degree-correlations*. The activity x_j , and hence $M_2(x_j)$ may depend on its neighbor's degree d due to the potential correlation between j 's degree d_j and its neighbor's degree d . For example, under positive degree-correlations, if d is large, then d_j also tends to be large, and, as a consequence the average $\langle M_2(x) \rangle_{d, \odot}$ will be biased towards the high degree activities. (ii) *Dynamic-correlations*. The second effect that is captured by $f(d)$ is due to the dynamic interaction between the neighboring activities $x(d)$ and x_j . This leads to an indirect correlation, for example if $x(d)$ increases with d , this may impact j 's activity x_j , who is affected by its highly active d degree neighbor.

Both effects (i) and (ii) are indirect, and, as we show below, are quite weak¹. Indeed, the individual node i , whose degree is d , is but one of j 's k_j neighbors, and therefore, especially

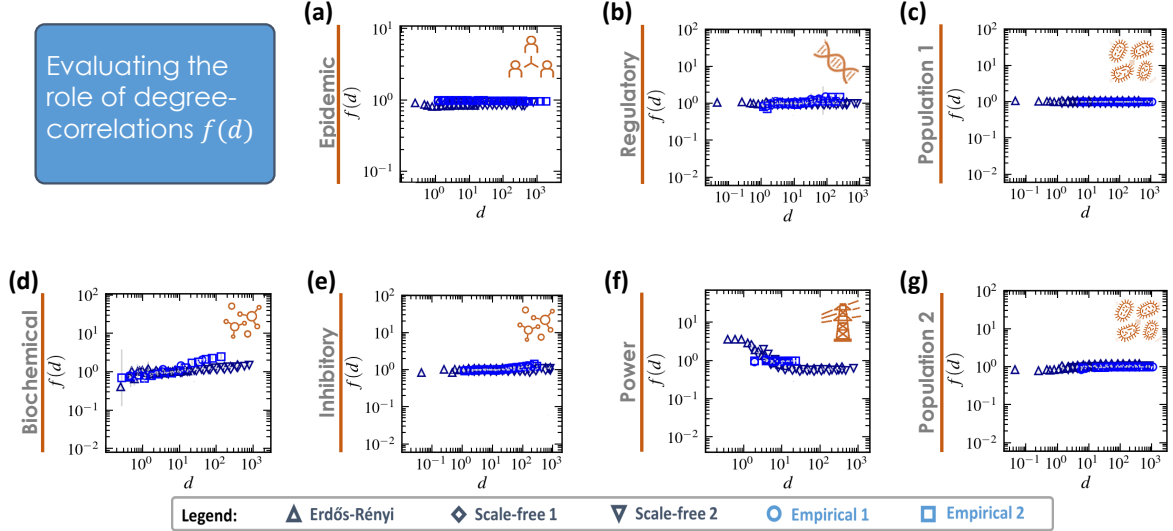


Figure 8: **Evaluating the degree correction function $f(d)$.** We used Eq. (34) to numerically evaluate $f(d) = \langle M_2(x) \rangle_{d,\odot} / \langle M_2(x) \rangle_{\odot}$, capturing the role of degree/dynamic-correlations on the average neighbor activity. Results were obtained for each of our dynamic models implemented on both model and relevant real-world networks. In all cases we find that $f(d)$ is largely independent of d , roughly following $f(d) \sim 1$. This indicates that $\langle M_2(x) \rangle_{d,\odot}$ can indeed be well-approximated by $\langle M_2(x) \rangle_{\odot}$.

when k_j is large, it has a minor contribution to j 's activity x_j . We emphasize that $f(d)$ captures the indirect contribution of i 's degree (not j) d to j 's activity $M_2(x_j)$. This is as opposed to j 's degree d_j , whose impact on $M_2(x_j)$ is direct and clearly significant. Moreover, these indirect effects are aggregated in (33), further smoothing out any local correlations between specific i, j node pairs. We therefore take $f(d)$ to be a *weak* function, *i.e.* sub-polynomial in d , for example

$$f(d) \sim \log^n(d), \quad (36)$$

potentially overridden by the *stronger* polynomial dependencies we seek below.

In Fig. 8 we numerically measure $f(d)$ for each of our different combinations of networks/dynamics. The results clearly indicate that $f(d)$ is indeed sub-polynomial, and, in most cases follows $f(d) \approx 1$. We note that in these simulations we used both model and real networks, some that have been shown to exhibit non-negligible degree-correlations. Still, we find that the role of such correlations is marginal, and has little impact on the distinction between $\langle M_2(x) \rangle_{d,\odot}$ in (33) and its approximation in (34).

We can now approximate $x(d)$ in (31), taking x_i from (29), and $\langle M_2(x) \rangle_{i,\odot}$ from (34) to obtain

$$x(d) = \frac{1}{|\mathcal{G}(d)|} \sum_{i \in \mathcal{G}(d)} R_i^{-1}(q), \quad (37)$$

where

$$q = \frac{1}{\mathcal{G} f(d) \langle M_2(x) \rangle_{\odot} d}, \quad (38)$$

now independent of i , determined solely by d . The sum in (37) incorporates an average of all self-dynamic parameters \mathbf{f}_i , through $R_i(q)$, which depends on \mathbf{f}_i as appears in (40). However, as

we aggregate over all nodes in $\mathcal{G}(d)$ we also average over the randomly distributed \mathbf{f}_i , allowing us to replace $R_i(x)$ in (37) with the ensemble averaged

$$R(x) = \frac{1}{|\mathcal{G}(d)|} \sum_{i \in \mathcal{G}(d)} R_i(x). \quad (39)$$

Roughly speaking, $R(x)$ replaces \mathbf{f}_i in (37) by $\langle \mathbf{f} \rangle$. More accurately, we have

$$R(x) = \frac{1}{|\mathcal{G}(d)|} \sum_{i \in \mathcal{G}(d)} \frac{M_1(x)}{M_0(x, \mathbf{f}_i)} = -\frac{M_1(x)}{M_0(x)}, \quad (40)$$

in which $M_0(x) = M_0(x, \langle \mathbf{f} \rangle)$ is the average self-dynamic function. Such approximate treatment is enabled thanks to our assumption that \mathbf{f}_i are assigned at random, independently of d_i , and hence averaging over all nodes in $\mathcal{G}(d)$ *smooths* out the effect of the \mathbf{f}_i heterogeneity, replacing it with the ensemble average $\langle \mathbf{f} \rangle$. Relaxing this assumption may require further correcting terms *a la* $f(d)$ in (50). Namely, we must write $R(x) = h(P(\mathbf{f}), d) \times (-M_1(x)/M_0(x))$, where the correction h is driven by the nature of the \mathbf{f}_i density function $P(\mathbf{f})$ and by the potential correlations between \mathbf{f}_i and d_i . However, as below we are focused only on scaling relationships, such corrections, as long as they are sub-polynomial, *i.e.* do not contribute to the scaling, have an asymptotically marginal effect. Therefore, to avoid cumbersome notations, we focus on the random \mathbf{f}_i scenario, in which \mathbf{f}_i is independent of d_i . In this case $h(P(\mathbf{f}), d) = h(P(\mathbf{f}))$, lacking a dependence on d , and thus having no contribution to our desired d -scaling. In our analysis, it can, therefore, be ignored, as we only focus on J 's asymptotic scaling with d_i and d_j .

By inversion we arrive at

$$x(d) = R^{-1}(q), \quad (41)$$

providing the mean activity x_i of all nodes with weighted degree $d_i \in (d, d + \delta d)$. Finally, in the asymptotic limit of large d , the sub-polynomial contribution of $f(d)$ becomes negligible, allowing us to approximate q in (38) as

$$q \sim \mathcal{G}^{-1} \langle M_2(x) \rangle_{\odot}^{-1} d^{-1}, \quad (42)$$

capturing the inverse degree of nodes in $\mathcal{G}(d)$. Note that \mathcal{G} and $\langle M_2(x) \rangle_{\odot}$ are independent of d , and therefore, as $d \rightarrow \infty$, *i.e.* the network hubs, $q \rightarrow 0$.

1.1.2 Evaluating $\langle M_2(x) \rangle_{\odot}$

To link $\langle M_2(x) \rangle_{\odot}$ in (35) to the network A, G we use a mean-field approximation. We first define the weighted nearest neighbor activity as

$$\mathcal{X}_{\text{nn}} = \langle x \rangle_{\odot} = \frac{1}{N} \sum_{i=1}^N \frac{1}{d_i} \sum_{j=1}^N A_{ij} G_{ij} x_j, \quad (43)$$

and its corresponding nearest neighbor weighted degree as

$$\mathcal{D}_{\text{nn}} = \langle d \rangle_{\odot} = \frac{1}{N} \sum_{i=1}^N \frac{1}{d_i} \sum_{j=1}^N A_{ij} G_{ij} d_j. \quad (44)$$

Hence, the average nearest neighbor node is characterized by activity \mathcal{X}_{nn} and degree \mathcal{D}_{nn} . While \mathcal{X}_{nn} depends on the system's dynamics (16), \mathcal{D}_{nn} is fully determined by the weighted topology $A \otimes G$ through the network's weighted degree density $P(d)$. In the absence of degree correlations and under a symmetric A, G we have²

$$\mathcal{D}_{\text{nn}} = \frac{\langle d^2 \rangle}{\langle d \rangle}, \quad (45)$$

where $\langle d^n \rangle$ is the n th moment of $P(d)$. For a homogeneous network in which $P(d)$ is bounded we have $\mathcal{D}_{\text{nn}} \approx \langle d \rangle$, however, if the network is highly heterogeneous, *i.e.* $P(d)$ is fat-tailed - as indeed, many real networks are³ - we have $\mathcal{D}_{\text{nn}} \gg \langle d \rangle$. In case the network is not symmetrical, *i.e.* a directed A_{ij} or asymmetric weights $G_{ij} \neq G_{ji}$, we distinguish between the in/out degrees of all nodes as

$$d_{i,\text{in}} = \sum_{j=1}^N A_{ij} G_{ij}; \quad d_{i,\text{out}} = \sum_{j=1}^N A_{ji} G_{ji}, \quad (46)$$

obtaining²

$$\mathcal{D}_{\text{nn}} = \frac{\langle d_{\text{in}} d_{\text{out}} \rangle}{\langle d \rangle}, \quad (47)$$

incorporating a mixed moment - the average over the product $d_{i,\text{in}} d_{i,\text{out}}$.

More generally, in case the network also features degree correlations we use the conditional density function $P(d|d')$ to express the probability density to observe $d_i \in (d, d + \delta d)$, given that i 's neighbor has degree d' . This allows us to write⁴

$$\mathcal{D}_{\text{nn}} = \int_{d_{\text{min}}}^{\infty} \int_{d_{\text{min}}}^{\infty} dP(d|d')P(d') dd dd', \quad (48)$$

accounting for the potential degree dependence between neighboring nodes. In all cases, from (45) to the more general (48), under extreme degree-heterogeneity, \mathcal{D}_{nn} may diverge with system size as⁵

$$\mathcal{D}_{\text{nn}} \sim N^{\beta}, \quad (49)$$

with β determined by the network/weight heterogeneity.

We can now link $\langle M_2(x) \rangle_{\odot}$ in (35) to \mathcal{D}_{nn} and \mathcal{X}_{nn} , as, indeed, $\langle M_2(x) \rangle_{\odot}$ is designed to capture the mean value of $M_2(x)$ over all nearest neighbor nodes, namely nodes with typical degree \mathcal{D}_{nn} and activity \mathcal{X}_{nn} . We, therefore, approximate (35) as

$$\langle M_2(x) \rangle_{\odot} \approx M_2(\mathcal{X}_{\text{nn}}), \quad (50)$$

in which we swap the order of operations from $\langle M_2(x) \rangle$ to $M_2(\langle x \rangle)$. Such approximation becomes

exact in the limit where $M_2(x)$ is linear or when x_j are narrowly distributed. For example, in our Biochemical model we have $M_2(x_j) = x_j$, a linear function, and in our Epidemic model the activities x_j are bounded, hence narrowly distributed between zero and unity. Approximation (50) is also justified when $M_2(x)$ is sub-linear, *e.g.*, a saturating function that satisfies $M_2(x \rightarrow \infty) \rightarrow 1$. Such saturation is present, for instance, in our Regulatory and Population dynamics. Under these conditions, even if x_j are broadly distributed, $M_2(x_j)$ are more homogeneous, and hence their average is (roughly) concentrated around $M_2(\langle x \rangle)$. For a super-linear $M_2(x)$, combined with broadly distributed x_j , approximation (50) becomes inaccurate.

To evaluate $M_2(\mathcal{X}_{\text{nn}})$'s dependence on \mathcal{D}_{nn} we use (41) to write

$$R(\mathcal{X}_{\text{nn}}) = \frac{1}{\mathcal{G}f(\mathcal{D}_{\text{nn}})M_2(\mathcal{X}_{\text{nn}})\mathcal{D}_{\text{nn}}}, \quad (51)$$

where we substitute $\langle M_2(x) \rangle_{i,\odot}$ by $f(\mathcal{D}_{\text{nn}})M_2(\mathcal{X}_{\text{nn}})$ following approximations (34) and (50), and use the nearest neighbor degree \mathcal{D}_{nn} in place of d to express the inverse degree q in (38). We therefore arrive at

$$Z(\mathcal{X}_{\text{nn}}) = \frac{1}{\mathcal{G}f(\mathcal{D}_{\text{nn}})\mathcal{D}_{\text{nn}}} \equiv q_{\odot}, \quad (52)$$

where $Z(x) = R(x)M_2(x)$ is a dynamic function, fully determined by \mathbf{M} in (18). In (53) we use the notation q_{\odot} to signify the inverse degree (q) associated with the typical *neighborhood* (\odot). By inversion we obtain

$$\mathcal{X}_{\text{nn}} = Z^{-1}(q_{\odot}), \quad (53)$$

and hence

$$M_2(\mathcal{X}_{\text{nn}}) = M_2(Z^{-1}(q_{\odot})). \quad (54)$$

Similarly to $R(x)$, the dynamic function $Z(x)$ may also be non-invertible in case the system has multiple fixed-points. We treat this by considering the different branches of $Z(x)$, following a similar analysis to the one shown in Fig. 7 for $R(x)$. Below, in Sec. 3.2 we show in detail how we treat such non-invertibility, which arises naturally during our analysis of Regulatory dynamics.

To obtain the asymptotic scaling of $M_2(\mathcal{X}_{\text{nn}})$ on \mathcal{D}_{nn} we use the Hahn expansion⁶ to express $Z(x)$ in the form of a power series around $q_{\odot} \rightarrow 0$, *i.e.* $\mathcal{D}_{\text{nn}} \rightarrow \infty$. Hence we write

$$M_2(Z^{-1}(q_{\odot})) = \sum_{n=0}^{\infty} G_n q_{\odot}^{\Psi(n)}, \quad (55)$$

where $\Psi(n)$ is a set of real powers in ascending order with n . In the limit of large \mathcal{D}_{nn} (small q_{\odot}) the expansion in (55) is dominated by the leading power $\Psi(0)$, predicting that

$$M_2(\mathcal{X}_{\text{nn}}) \sim \mathcal{D}_{\text{nn}}^{\xi}, \quad (56)$$

where

$$\xi = -\Psi(0). \quad (57)$$

The exponent ξ is fully determined by the dynamic functions \mathbf{M} through the Hahn expansion in (55). It is independent of A, G , as well as of other microscopic parameters, such as the specific rate-constants \mathbf{f}_i or the interaction strength \mathcal{G} , used in (16), which are all encapsulated within the *coefficients* G_n , but have no impact on the *powers* $\Psi(n)$.

Using approximation (50) we substitute $M_2(\mathcal{X}_{\text{nn}})$ in (56), to replace the $\langle M_2(x) \rangle_{\odot}$ term in the denominator of Eq. (38), we write

$$q \sim \mathcal{D}_{\text{nn}}^{-\xi} d^{-1}. \quad (58)$$

Next we use these results, specifically (41) and (58), to obtain the terms of the Jacobian, J_{ij} and J_{ii} , and their dependence on \mathcal{D}_{nn} and d_i, d_j . Writing

$$J = (A - I) \otimes W, \quad (59)$$

as in Eq. (2) of the main text, we seek, separately, the weights of the diagonal (W_{ii}) and the off-diagonal ($W_{ij}, i \neq j$) terms.

1.2 Diagonal terms W_{ii}

Using (17) and (22) we write the diagonal Jacobian terms as

$$W_{ii} = \left. \frac{\partial F_i(\mathbf{x})}{\partial x_i} \right|_{\mathbf{x}=\mathbf{x}^*} = \left(M'_0(x_i, \mathbf{f}_i) + M'_1(x_i) \mathcal{G} \sum_{j=1}^N A_{ij} G_{ij} M_2(x_j) \right) \Big|_{\mathbf{x}=\mathbf{x}^*}, \quad (60)$$

where $M'_0(x) = \partial M_0 / \partial x$ and $M'_1(x) = \partial M_1 / \partial x$. Next we use (25) to express the sum on the r.h.s. obtaining

$$W_{ii} = M'_0(x_i, \mathbf{f}_i) \Big|_{\mathbf{x}=\mathbf{x}^*} + \mathcal{G} M'_1(x_i) d_i \langle M_2(x) \rangle_{i, \odot} \Big|_{\mathbf{x}=\mathbf{x}^*}, \quad (61)$$

in which we substitute the summation by the neighborhood average $\langle M_2(x) \rangle_{i, \odot}$. Finally, expressing the fixed-point \mathbf{x}^* via (29) and averaging over all nodes with degree $d \in (d, d + \delta d)$ as done in (31) - (38), we arrive at

$$W(d) = M'_0(R^{-1}(q)) + \mathcal{G} d M'_1(R^{-1}(q)) f(d) \langle M_2(x) \rangle_{\odot}, \quad (62)$$

capturing the average diagonal term W_{ii} , associated with a node $i \in \mathcal{G}(d)$. Note, that while the individual diagonal terms W_{ii} depend on the self-dynamic parameters \mathbf{f}_i , the averaging over all nodes in $\mathcal{G}(d)$ removes this dependence, as discussed above in Eq. (39). Indeed, $\mathcal{G}(d)$ is a macroscopic sample of nodes, and hence, collectively, it is characterized by the ensemble average $\langle \mathbf{f} \rangle$. Therefore, the parameter \mathbf{f}_i is omitted in (62), and the first term on its r.h.s should be read as shorthand for

$$M'_0(R^{-1}(q)) = M'_0(R^{-1}(q), \langle \mathbf{f} \rangle). \quad (63)$$

Next we use (40) to write $M_0(x) = -M_1(x)/R(x)$, which provides

$$M'_0(x) = -\frac{M'_1(x)}{R(x)} + \frac{M_1(x)R'(x)}{R^2(x)}. \quad (64)$$

Substituting (64) and (38) into (62) we arrive at

$$W(d) = -\frac{M'_1(R^{-1}(q))}{q} + \frac{M_1(R^{-1}(q))R'(R^{-1}(q))}{q^2} + \frac{M'_1(R^{-1}(q))}{q}, \quad (65)$$

where we used the fact that $R(R^{-1}(q)) = q$. Collecting all terms we write

$$W(d) = \frac{1}{q^2}Y(R^{-1}(q)), \quad (66)$$

where $Y(x) = M_1(x)R'(x)$. Similar to $Z(x)$ above, $Y(x)$ is a dynamic function fully determined by \mathbf{M} , independent of A or G .

To obtain the asymptotic scaling of $W(d)$ with d we, once again, use the Hahn expansion to express $Y(x)$ in the form of a power series around $q \rightarrow 0$, *i.e.* $d \rightarrow \infty$. Writing

$$Y(R^{-1}(q)) = \sum_{n=0}^{\infty} C_n q^{\Gamma(n)}, \quad (67)$$

we obtain the leading power in the expansion of $W(d)$ as $W(d) \sim q^{-2+\Gamma(0)}$, exact up to higher powers in q , which vanish under $q \rightarrow 0$. Using the scaling of Eq. (58), this predicts

$$W(d) \sim \mathcal{D}_{\text{nn}}^{\xi\mu} d^\mu, \quad (68)$$

where

$$\mu = 2 - \Gamma(0), \quad (69)$$

and ξ is taken from (57).

Equation (68), valid in the limit of large \mathcal{D}_{nn} and d , captures the typical magnitude of the diagonal terms W_{ii} , and their dependence on each node i 's degree d_i . The scaling exponents μ and ξ are fully determined by $\Gamma(n)$ in (67) and $\Psi(n)$ in (55), namely they are affected by the *powers* of the dynamic functions \mathbf{M} . At the same time μ and ξ are independent of the *coefficients* C_n, G_n , hence they are not sensitive to specific parameters, such as rate constants ($\mathbf{f}_i, \mathcal{G}$) in (16). The effect of A and G is encapsulated through \mathcal{D}_{nn} and d . While Eq. (68) provides the *scaling* with d , $W(d)$'s specific magnitude may, generally, depend on these coefficients, however for sufficiently large d , such dependencies have little impact on the spectrum of J . Finally, the sign of $W(d)$, positive or negative, is determined by $Y(x)$, which, in turn depends on $M_0(x)$ and $M_1(x)$. Stability can only be ensured in case $W(d) < 0$, *i.e.* negative self-feedback. Hence below we write

$$W(d) \sim C(\mathbf{f}, \mathcal{G}) \mathcal{D}_{\text{nn}}^{\xi\mu} d^\mu, \quad (70)$$

where $C > 0$, and set

$$J_{ii} = -W(d_i); \quad (71)$$

see our more detailed discussion of this and other related points in Sec. 1.4. Equation (71) describes our ensemble approximation: the *real* Jacobian diagonal terms are provided by (60), which is exact, and may be potentially distinct even for nodes with identical degrees. These *exact* terms are represented by symbols in Fig. 3 of the main text. Our analytically predicted Jacobians, on the other hand, approximate these exact terms by setting each diagonal entry via (71). This evaluates J_{ii} by substituting i 's weighted degree d_i into (70), yielding an identical entry for all nodes of similar degree. Such approximation is designed to capture J_{ii} 's ensemble average, namely

$$-W(d) = \frac{1}{|\mathcal{G}(d)|} \sum_{i \in \mathcal{G}(d)} J_{ii}, \quad (72)$$

the average diagonal Jacobian entry for nodes of degree $d_i \in (d, d + \delta d)$. This analytical construction is represented by the solid lines in Fig. 3 of the main text, and shown to accurately capture the exact J .

1.3 The off-diagonal terms W_{ij}

The off-diagonal Jacobian terms are given by

$$W_{ij} = \left. \frac{\partial F_i(\mathbf{x})}{\partial x_j} \right|_{\mathbf{x}=\mathbf{x}^*} = \frac{\partial}{\partial x_j} \left(M_0(x_i, \mathbf{f}_i) + M_1(x_i) \mathcal{G} \sum_{j=1}^N A_{ij} G_{ij} M_2(x_j) \right) \Big|_{\mathbf{x}=\mathbf{x}^*}. \quad (73)$$

Collecting only the terms that explicitly depend on x_j we obtain

$$\widetilde{W}_{ij} = M_1(x_i) A_{ij} M_2'(x_j) \Big|_{\mathbf{x}=\mathbf{x}^*}, \quad (74)$$

where

$$\widetilde{W}_{ij} = \frac{W_{ij}}{\mathcal{G} G_{ij}} \quad (75)$$

is the *weight-less* off-diagonal Jacobian term. Taking the fixed-point activities from (29) we obtain

$$\widetilde{W}_{ij} = M_1(R^{-1}(q_i)) A_{ij} M_2'(R^{-1}(q_j)). \quad (76)$$

Similarly to (72), here too we seek the average dependence of W_{ij} on the degrees d_i and d_j . Hence we consider the group $\mathcal{G}(d_1, d_2) = \{(i, j) | d_i \in (d_1, d_1 + \delta d_1); d_j \in (d_2, d_2 + \delta d_2); A_{ij} = 1\}$, comprising all links ($A_{ij} = 1$) between nodes with degrees around d_1, d_2 . We then average over the relevant Jacobian term as

$$\widetilde{W}(d_1, d_2) = \frac{1}{|\mathcal{G}(d_1, d_2)|} \sum_{(i,j) \in \mathcal{G}(d_1, d_2)} \widetilde{W}_{ij}, \quad (77)$$

allowing us to evaluate the magnitude of an average (non-zero) term whose row index is associated with a node of degree $d_i \in (d_1, d_1 + \delta d_1)$, and whose column index is associated with a node of degree $d_j \in (d_2, d_2 + \delta d_1)$. Using (74) we write

$$\widetilde{W}(d_1, d_2) = \frac{1}{|\mathcal{G}(d_1, d_2)|} \sum_{(i,j) \in \mathcal{G}(d_1, d_2)} M_1(x_i) A_{ij} M_2'(x_j) = \langle M_1(x_i) M_2'(x_j) \rangle_{\mathcal{G}(d_1, d_2)}, \quad (78)$$

a product average over all node pairs in $\mathcal{G}(d_1, d_2)$. In case the two activities x_i and x_j are weakly correlated, we can approximate the r.h.s. of (78) by factorizing the product average, writing it as $\langle M_1(x_i) \rangle_{\mathcal{G}(d_1, d_2)} \times \langle M_2'(x_j) \rangle_{\mathcal{G}(d_1, d_2)}$. Each of these averages can be then evaluated by

$$\langle M_1(x_i) \rangle_{\mathcal{G}(d_1, d_2)} \approx M_1(R^{-1}(q_1)) \quad (79)$$

$$\langle M_2'(x_j) \rangle_{\mathcal{G}(d_1, d_2)} \approx M_2'(R^{-1}(q_2)), \quad (80)$$

where we use the fact that in $\mathcal{G}(d_1, d_2)$ the activity x_i is on average $R^{-1}(q_1)$, *i.e.* $x(d_1)$ (31), and the activity x_j is $R^{-1}(q_2)$, namely $x(d_2)$. In reality, however, the two activities are, to some extent, correlated by virtue of being nearest neighbors ($A_{ij} = 1$). We therefore follow a similar track as in (34) and write (78) as

$$\widetilde{W}(d_1, d_2) \approx f(d_1, d_2) M_1(R^{-1}(q_1)) M_2'(R^{-1}(q_2)), \quad (81)$$

capturing the d_1, d_2 correlations via the sub-polynomial function $f(d_1, d_2)$.

We can now obtain the scaling of $\widetilde{W}(d_1, d_2)$ by examining the behavior of $M_1(R^{-1}(q_1))$ and $M_2'(R^{-1}(q_2))$ in the limit of large d_1 and d_2 , or subsequently small q_1, q_2 . We, therefore express these functions via the Hahn expansion as

$$M_1(R^{-1}(q)) = \sum_{n=0}^{\infty} K_n q^{\Pi(n)} \quad (82)$$

$$M_2'(R^{-1}(q)) = \sum_{n=0}^{\infty} L_n q^{\Theta(n)}, \quad (83)$$

and take only the leading term in the limit $q \rightarrow 0$, providing

$$\widetilde{W}(d_1, d_2) = f(d_1, d_2) K_0 q_1^{\Pi(0)} L_0 q_2^{\Theta(0)} + \dots \quad (84)$$

As we are only interested in the asymptotic scaling with d_1, d_2 we neglect all terms that do not contribute the scaling, namely $f(d_1, d_2), K_0$ and L_0 . Finally, substituting q with $\mathcal{D}_{\text{nn}}^{-\xi} d^{-1}$ as per Eq. (58), we obtain

$$\widetilde{W}(d_1, d_2) \sim \mathcal{D}_{\text{nn}}^{\xi(\nu+\rho)} d_1^\nu d_2^\rho \quad (85)$$

where

$$\nu = -\Pi(0), \quad \rho = -\Theta(0), \quad (86)$$

and ξ is taken from (57).

1.4 Piecing together the J_{ij} puzzle

We have now obtained the interplay between structure and dynamics, expressed through the magnitude of the diagonal/off-diagonal Jacobian entries, and their dependence on the network's degree distribution via d_i, d_j and \mathcal{D}_{nn} . This dependence is given in terms of asymptotic scaling relationships, as captured by the model dependent exponents μ, ν, ρ, ξ . This leaves a degree of freedom, determined by the specific parameters of each model to add an arbitrary coefficient as a pre-factor to the actual J terms. Indeed, writing an expression of the form $X(a) \sim a^\alpha$, as we have, *e.g.*, in Eqs. (68) and (85), should be taken to mean

$$X(a) = f(a)a^\alpha + \dots \quad (87)$$

where $f(a)$ is a sub-polynomial function, which is roughly constant, *i.e.* $f(a) \approx C$, and \dots represents *lower* powers of a , that are negligible in the asymptotic limit $a \rightarrow \infty$. Hence, all our derived scaling relationships are exact *up to* a multiplicative sub-polynomial pre-factor, and include only leading powers.

For the off-diagonal terms our derivation provided us with $\widetilde{W}(d_1, d_2)$, which is aggregated from the weight-less \widetilde{W}_{ij} of (75). To obtain the actual off-diagonal terms of J we must reintroduce the weights as $W_{ij} = \mathcal{G}G_{ij}\widetilde{W}_{ij}$, namely multiply (85) by $\mathcal{G}G_{ij}$. We can now piece all our results together to construct the complete Jacobian as appears in Eq. (23), rewriting it as

$$J_{ij} = A_{ij}W_{ij} - I_{ij}W_{ii} = -I_{ij}C\mathcal{D}_{\text{nn}}^{\xi\mu}d_i^\mu + \mathcal{G}A_{ij}G_{ij}\mathcal{D}_{\text{nn}}^{\xi(\nu+\rho)}d_i^\nu d_j^\rho, \quad (88)$$

where the first term on the r.h.s. represents the (negative) diagonal entries, and second term captures the off-diagonal entries, which are non-zero only if $A_{ij} = 1$; I is the identity matrix. As we are only interested in the sign of the principle eigenvalue, but not in its specific magnitude, we have the degree of freedom to multiply J by an arbitrary constant. We therefore normalize J by $\mathcal{G}^{-1}\mathcal{D}_{\text{nn}}^{-\xi(\nu+\rho)}$, providing

$$J_{ii} \sim -C\mathcal{D}_{\text{nn}}^\eta d_i^\mu \quad (89)$$

$$J_{ij} \sim d_i^\nu A_{ij}G_{ij}d_j^\rho \quad (90)$$

for the diagonal and off-diagonal terms respectively, with $\eta = \xi(\mu - \nu - \rho)$ and $C = C(\mathbf{f}, \mathcal{G})$ - recovering Eqs. (4) and (5) of the main text.

Equations (89) and (90) describe the asymptotic structure of the diagonal and off-diagonal Jacobian terms, as extracted from the general dynamics of Eq. (16). The resulting J is characterized by several distinct structural and dynamic inputs: A , the network topology, which determines the non-vanishing off-diagonal elements. Together with the link weights G it also determines the degrees d_i, d_j and the average neighbor degree \mathcal{D}_{nn} . The exponents

$$\Omega = (\eta, \mu, \nu, \rho) \quad (91)$$

are independent of the network topology, extracted from the dynamic functions \mathbf{M} , *i.e.* the interaction mechanisms driving Eq. (16). These exponents are universal in the sense that they

do not depend of the specific model *parameters*, but rather on the *model* itself, *e.g.*, Epidemic, Regulatory etc. The coefficient C , in contrast, is non-universal, and its value is determined by the specific rate-constants and time-scales driving Eq. (16), for example $P(\mathbf{f})$ or \mathcal{G} ; here we do not attempt to predict the magnitude of this coefficient. In the limit of sufficiently large d_i and d_j , and, where applicable - in the limit of large \mathcal{D}_{nn} , the specific finite value of C has negligible impact on the principal eigenvalue of J as we explicitly show in Sec. 2. Hence stability is asymptotically determined by the exponents Ω , irrespective of C . The meaning is that the *model* can be asymptotically stable or unstable, regardless of its specific *parameters*.

1.4.1 Impact of $P(d)$ and \mathcal{D}_{nn}

In this derivation we considered only the *scaling* of J on the weighted degrees d_i, d_j , and on the nearest neighbor degree \mathcal{D}_{nn} . We disregarded coefficients, such as C_n or G_n in (67) and (55), or sub-polynomial functions like $f(d)$ in (36). The rationale is that in the limit of large degrees the Jacobian spectrum is mainly impacted by these asymptotic scaling relationships, and has little dependence on finite size coefficients that do not scale with $d, \mathcal{D}_{\text{nn}}$, and hence also do not grow significantly as a function of system size N . Therefore, Eqs. (89) and (90) are especially relevant when $P(d)$ is fat-tailed, *e.g.*, scale-free, where the hub-degrees and the nearest neighbor degree can potentially diverge with N .

The role of \mathcal{D}_{nn} . While d_i is a node specific attribute, that captures a specific dependency between the i th diagonal term and i 's weighted degree, the pre-factor $\mathcal{D}_{\text{nn}}^\eta$ in (89) represents a network aggregated parameter, indeed - a *constant*, whose impact is often negligible in the asymptotic limit of large d . We include it in our analysis, however, because under extreme degree-heterogeneity, we may observe that \mathcal{D}_{nn} diverges as $\mathcal{D}_{\text{nn}} \sim N^\beta$ (49), and therefore *can* potentially impact the system's stability in the limit $N \rightarrow \infty$. For example, in a random scale-free network where $P(d) \sim d^{-\gamma}$, we can use $\mathcal{D}_{\text{nn}} = \langle d^2 \rangle / \langle d \rangle$ in (45) to obtain

$$\mathcal{D}_{\text{nn}} \sim \begin{cases} N & \gamma < 2 \\ N^{3-\gamma} & 2 \leq \gamma < 3 \\ \log(N) & \gamma \geq 3 \end{cases}, \quad (92)$$

which scales with N as long as $\gamma < 3$. There are, however, broad conditions, that arise quite naturally in many real systems, in which the \mathcal{D}_{nn} term in (89) can be neglected, significantly simplifying the stability analysis:

- **Finite \mathcal{D}_{nn} .** In case $\gamma \geq 3$, \mathcal{D}_{nn} no longer scales with N , it behaves as a constant and has no impact in the asymptotic limit. Under these conditions it suffices to write Eq. (89) as $J_{ii} \sim -C d_i^\mu$, with \mathcal{D}_{nn} effectively encapsulated within C .
- **Bounded activities.** In some models the activities x_i are bounded. For example, in spreading processes, from epidemics to cascading failures, the activities satisfy $0 \leq x_i \leq 1$. Under these conditions the leading power in the power-series expansion of (41) is zero, and hence $x(d \rightarrow \infty) \sim 1$. The result is that the nearest neighbor activity \mathcal{X}_{nn} , associated with degree \mathcal{D}_{nn} is itself bounded, and even if $\mathcal{D}_{\text{nn}} \rightarrow \infty$ *à la* Eq. (92), we still have $\mathcal{X}_{\text{nn}} \sim 1$. Consequently $M_2(\mathcal{X}_{\text{nn}})$ in (54) also approaches a constant value, and therefore the leading power in the expansion (55) is $\Psi(0) = 0$. This provides, based on Eq. (57), $\xi = 0$, which in turn leads to $\eta = 0$ in (89), again resulting in $J_{ii} \sim -C d_i^\mu$, independent of \mathcal{D}_{nn} .
- **Saturating $M_2(x)$.** Another common feature in many relevant models is that $M_2(x_j \rightarrow$

$\infty) \rightarrow 1$. This represents the saturating impact of node j on its nearest neighbor i , as frequently observed in regulatory processes or in population dynamics. Once again, we have $M_2(\mathcal{X}_{\text{nn}}) \sim 1$ in the limit of large \mathcal{X}_{nn} , providing $\xi = 0$, and consequently $\eta = 0$ in (89).

These rather frequent scenarios, observed, *e.g.*, in our Epidemic, Regulatory, Population and Power dynamics provide a simplifies J , in which $\eta = 0$, omitting \mathcal{D}_{nn} from the stability analysis. In Biochemical and Inhibitory we have $\eta \neq 0$, and hence the \mathcal{D}_{nn} term cannot be neglected.

The ensemble $\mathbb{E}(A, G, \Omega)$ summary

Starting from Eq. (16) we use $M_0(x)$, $M_1(x)$ and $M_2(x)$ to construct the functions

$$R(x) = -\frac{M_1(x)}{M_0(x)}, \quad Y(x) = M_1(x)R'(x), \quad Z(x) = R(x)M_2(x). \quad (93)$$

From these we extract the four relevant power-series expansions

$$\begin{aligned} M_2(Z^{-1}(x)) &= \sum_{n=0}^{\infty} G_n x^{\Psi(n)}, & Y(R^{-1}(x)) &= \sum_{n=0}^{\infty} C_n x^{\Gamma(n)}, \\ M_1(R^{-1}(x)) &= \sum_{n=0}^{\infty} K_n x^{\Pi(n)}, & M_2'(R^{-1}(x)) &= \sum_{n=0}^{\infty} L_n x^{\Theta(n)} \end{aligned} \quad (94)$$

whose leading powers determine the dynamic exponents $\Omega = (\eta, \mu, \nu, \rho)$ as

$$\mu = 2 - \Gamma(0), \quad \nu = -\Pi(0), \quad \rho = -\Theta(0), \quad \eta = -\Psi(0)(\mu - \nu - \rho). \quad (95)$$

To construct $J \in \mathbb{E}(A, G, \Omega)$ we first assign the network/weights A, G , then extract the weighted degrees d_i of all nodes and the nearest neighbor degree \mathcal{D}_{nn} from Eq. (44). The resulting J satisfies

$$J_{ii} \sim -C \mathcal{D}_{\text{nn}}^\eta d_i^\mu \quad (96)$$

$$J_{ij} \sim d_i^\nu A_{ij} G_{ij} d_j^\rho, \quad (97)$$

where the constant $C > 0$ is arbitrary.

1.5 J around a trivial fixed-point

Our derivation up to this point relied on the function $R_i(x_i) = -M_1(x_i)/M_0(x_i, \mathbf{f}_i)$, which becomes undefined in case $M_0(x_i, \mathbf{f}_i) = 0$. This represents a *trivial* fixed-point, in which the activities satisfy

$$x_i = M_0^{-1}(0, \mathbf{f}_i). \quad (98)$$

Returning to Eq. (24), we write

$$M_0(x_i, \mathbf{f}_i) + \mathcal{G} \sum_{j=1}^N A_{ij} G_{ij} M_1(x_i) M_2(x_j) = 0, \quad (99)$$

which, if $M_0(x_i, \mathbf{f}_i) = 0$, can only be solved by setting either $M_1(x_i) = 0$ for all i or $M_2(x_j) = 0$ for all j . In the first case we write

$$x_i = x = M_1^{-1}(0), \quad (100)$$

such that all activities independently satisfy $M_1(x_i) = M_1(x) = 0$, and in the second case we have

$$x_i = x = M_2^{-1}(0). \quad (101)$$

In principle such conditions may arise under a general x_i , including $x_i \neq 0$. However, having *all* x_i satisfy at least two of the conditions (98), (100) and (101) is extremely unlikely under a *natural* selection of $M_0(x)$, $M_1(x)$ and $M_2(x)$, unless one specifically designs these functions to sustain such solutions. Indeed, one must sets all links A_{ij} , weights G_{ij} and rate constants $\mathbf{f}_i, \mathcal{G}$, together with the functional form of $M_0(x)$, $M_1(x)$ and $M_2(x)$ to have a non-zero \mathbf{x}^* that simultaneously solves all N equations of (99). Such *fine-tuning*, indeed a specific and highly non-random design, is excluded from our derivation, which is centered around complex, typically random, and most often heterogeneous systems.

The natural exception to the above fine-tuned solution is the trivial solution $x_i = 0$ for all i , which, indeed, arises in many real-worlds systems, including ones examined in the present analysis. For example, in Epidemic dynamics, the healthy state $x_i = 0$ has $M_0(x_i, \mathbf{f}_i) = -f_i x_i = 0$, and $M_2(x_j) = x_j = 0$, hence satisfying (98) and (101). In Population 1, the null-state has $M_0(x_i, \mathbf{f}_i) = x_i(1 - x_1/f_i) = 0$, $M_1(x_i) = x_i = 0$ and $M_2(x_j) = F(x_j) = 0$, satisfying all three conditions simultaneously. Finally, in Inhibitory and Regulatory, the null-state has $M_0(x = 0, \mathbf{f}_i) = M_1(x = 0) = 0$ and $M_0(x = 0, \mathbf{f}_i) = M_2(x = 0) = 0$, respectively, once again satisfying two of the conditions (98) - (101). This specific state - the null state $\mathbf{x}^* = (0, \dots, 0)^\top$ - cannot be analyzed via the above derivation, and requires a dedicated treatment.

To obtain J around the null state we use (61) and (74) to write

$$W_{ii} = M_0'(0, \mathbf{f}_i) + \mathcal{G} M_1'(0) d_i M_2(0) \quad (102)$$

$$W_{ij} = \mathcal{G} M_1(0) A_{ij} G_{ij} M_2'(0). \quad (103)$$

Several distinct cases arise:

- **Case I.** In case $M_1'(0)$ and $M_2(0)$ are both non zero, we have the diagonal terms scaling as $W_{ii} \sim d_i$, corresponding to $\mu = 1$. Here, since $M_2(0) \neq 0$, the null-solution of (99) inevitably requires that $M_1(0) = 0$, *i.e.* condition (100). Consequently, the off-diagonal terms in (103) all vanish, indicating that the interactions, in this case, have no linear contribution, and are only expressed in the higher order nonlinear terms. In $\mathbb{E}(A, G, \Omega)$ this is captured by taking the limit $\nu, \rho \rightarrow -\infty$, deep within the asymptotically stable regime in case J_{ii} is negative, or the unstable regime if it is positive. As an example, we consider the dynamics $dx_i/dt = -f_i x_i - \mathcal{G} \sum_{j=1}^N A_{ij} G_{ij} x_i / (1+x_j)$, in which the interaction

is of deactivating nature. Using (102) we write $J_{ii} = -1 - \mathcal{G}d_i$, which, indeed, under large d_i , scales as $J_{ii} \sim -d_i^\mu$ with $\mu = 1$. The off-diagonal terms, in this dynamics vanish as per Eq. (103).

- **Case II.** If, however $M_2(0) = 0$, *i.e.* condition (101) we have both W_{ii} and W_{ij} independent of d_i, d_j , predicting $J \in \mathbb{E}(A, G, \Omega)$ with $\Omega = (0, 0, 0, 0)$. This captures an asymptotically unstable fixed point. We observe this, for example, in the healthy state of Epidemic dynamics. There we have $M'_0(0, \mathbf{f}_i) = f_i$, $M_2(0) = 0$ and $M_1(0)M'_2(0) = 1$. Together this leads to $W_{ii}, W_{ij} \sim \text{const}$, *i.e.* lacking any scaling with d_i and d_j . Indeed, we show in the Sec. 3.1 that the healthy state of the Epidemic model is asymptotically unstable, recovering a well-established result on the spread of epidemics on scale-free networks⁷.
- **Case III.** A third scenario is when both conditions (100) and (101) are satisfied, *i.e.* $M_1(0) = M_2(0) = 0$. The off-diagonal terms in (103) vanish in this case, indicating that the interactions are super-linear, having no linear component. The diagonal terms become $W_{ii} = M'_0(0, \mathbf{f}_i)$, independent of the network structure. Therefore, in such dynamics stability is fully determined by the sign of W_{ii} , unstable in case $M'_0(0, \mathbf{f}_i) \geq 0$ and stable otherwise. We encounter such conditions in Population 1, where $M_1(x) = x$ and $M_2(x) = x/(1+x)$, both zero when $x = 0$. The self-dynamics in this case has $M_0(x) = x(1-x/f_i)$, whose derivative around $x = 0$ provides $W_{ii} = 1 > 0$. This dynamics is, therefore, always unstable around the trivial fixed-point.

Note that Cases II and III are of different nature. While Case II is a specific member of $\mathbb{E}(A, G, \Omega)$, with all exponents being zero, Case III's instability is unrelated to $\mathbb{E}(A, G, \Omega)$. To understand this consider Epidemic's trivial state, which is in Case II, vs. that of Population 1, which is in Case III. The former can potentially be stable, if, for instance the recovery rate f_i is large. Its instability only emerges asymptotically in the limit of large and heterogeneous networks, *i.e.* our asymptotically unstable class. Therefore it is an integral system within our ensemble $\mathbb{E}(A, G, \Omega)$. Indeed, this form of asymptotic instability emerges from the interplay between topology $(P(d), N)$ and dynamics (Ω) , representing a direct outcome of our theoretical framework. Case III dynamics, in contrast, have an intrinsically unstable null state, even under low dimension (small N) or degree homogeneity ($P(d)$ bounded). Their null state instability, is, therefore, not driven by the topology/dynamics interplay, ingrained in our J -ensemble, but rather it is independent of topology, characteristic of $M'_0(0, \mathbf{f}_i)$ alone. Indeed, as we discuss in Sec. 3.3, in Population 1 the null state is always unstable, even in a one-dimensional system.

- **Case IV.** The final case is where $M'_0(0, \mathbf{f}_i) = M'_2(0) = 0$, which occurs when these functions are super-linear around $x = 0$. Under these conditions the linear approximation becomes irrelevant and higher order terms must be included to capture the fixed-point dynamics. As an example, we consider our Regulatory dynamics, having $M_0(x, \mathbf{f}_i) = -f_i x^a$, $M_1(x) = 1$ and $M_2(x) = x^h/(1+x^h)$. For $a, h > 1$ the first derivatives vanish around $x = 0$, and J is void. Consequently, under these conditions the null state Jacobian vanishes, and hence cannot be used to assess the system's stability. Such cases require specific treatment, independent of our formalism, which is, fortunately quite straightforward, as we demonstrate in our analysis of the Regulatory dynamics in Sec. 3.2.

To summarize, our analytical framework of (93) - (97) is designed to treat the non-trivial fixed-points of (16). If, however, the system exhibits also a null $\mathbf{x}^* = (0, \dots, 0)^\top$ state, we must treat this state specifically, following the case by case analysis presented above. Fortunately, the null

state Jacobians are straightforward to analyze, and can be done alongside our general analytical derivation.

2 Principle eigenvalue of $J \in \mathbb{E}(A, G, \Omega)$

While the principal eigenvalue λ of $J \in \mathbb{E}(A, G, \Omega)$ is difficult to obtain analytically, we find that simplification into a *star-network* can provide a rather reliable prediction, especially since we are only focused on whether λ is positive/negative, not on its specific value. We first distinguish between two families of dynamics: the first has $\mathbf{s} = 1$, describing cooperative interactions, in which the off-diagonal terms $J_{ij} > 0$. This is observed, for example, in Regulatory or in Epidemic, where j positively contributes to its neighbor i 's activity. The second option, $\mathbf{s} = 0$, describes adversarial interactions, where j ' activity has a negative impact on x_i . This can take the form of inhibition, such as in Inhibitory, where the larger is x_j the lower is i 's growth *rate*, or of direct reduction, such as in Biochemical, where the interaction of i and j is explicitly negative, with j directly depleting the i population via chemical binding.

The star-construction. The structure of J in (96) - (97) depends strongly on the network degrees through d_i, d_j and \mathcal{D}_{nn} . Therefore, the value of λ is driven by the limit of large d - and, specifically, in a degree-heterogeneous network, it is determined by the nearest neighbor degree \mathcal{D}_{nn} , which can potentially diverge with the system size N as

$$\mathcal{D}_{\text{nn}} \sim N^\beta. \quad (104)$$

As opposed to the *dynamic* exponents Ω , the exponent β is a *topological* exponent, determined by the network's weighted degree distribution $P(d)$. In a scale-free network, for example, β is extracted from (92).

To approximate this hub-periphery structure, below we focus on a star network, in which a single hub has a weighted degree of $d = \mathcal{D}_{\text{nn}}$. For a typical hub node, linked to many neighbors we write $d_i = \sum_{j=1}^N A_{ij} G_{ij} = \langle G \rangle \sum_{j=1}^N A_{ij}$, extracting the average weight $\langle G \rangle = \int GP(G) dG$ out of the sum. This is enabled thanks to the fact that, in the case of hubs, the summation in d_i covers a large sample of weights G_{ij} , and hence their sum converges to the mean. Using (19) this allows us to write the hub's unweighted degree as

$$k_i = \frac{1}{\langle G \rangle} d_i, \quad (105)$$

which in our star construction provides

$$k = \frac{1}{\langle G \rangle} \mathcal{D}_{\text{nn}} \sim N^\beta, \quad (106)$$

namely a single hub connected to k peripheral nodes. Note that the scaling with N remains unchanged as $\langle G \rangle$ is a constant, independent of network size.

Our star network captures the environment of a typical hub in, *e.g.*, a scale-free network. Indeed, such hubs in a scale-free environment can be viewed as a collection of weakly coupled *stars*, that are only sparsely linked to each other⁸. Under these conditions we have the $(k+1) \times (k+1)$ network

$$A = \begin{bmatrix} 0 & 1 & 1 & \dots & 1 \\ 1 & 0 & 0 & \dots & 0 \\ \vdots & & \ddots & & \vdots \\ 1 & 0 & 0 & \dots & 0 \end{bmatrix}, \quad (107)$$

capturing a single, highly connected node, surrounded by k small nodes.

2.1 Jacobians with positive weights $s = 1$

We now use (96) and (97), to construct the Jacobian of the star-network (107), which under cooperative interactions takes the form

$$J = -C\tilde{\kappa}_{\text{nn}}^\eta \begin{bmatrix} k^\mu & 0 & \dots & 0 \\ 0 & 1 & \dots & 0 \\ \vdots & & \ddots & \vdots \\ 0 & 0 & \dots & 1 \end{bmatrix} + \begin{bmatrix} 0 & k^\nu & \dots & k^\nu \\ k^\rho & 0 & \dots & 0 \\ \vdots & & \ddots & \vdots \\ k^\rho & 0 & \dots & 0 \end{bmatrix}, \quad (108)$$

where $C > 0$ and the off-diagonal terms are all positive. In (108) we used $\tilde{\kappa}_{\text{nn}}$ to express the nearest neighbor degree in our star construction, which is potentially distinct from \mathcal{D}_{nn} of the originally approximated scale-free network. Lacking an *a priori* estimate for this parameter we express it as

$$\tilde{\kappa}_{\text{nn}} \sim N^\alpha, \quad (109)$$

leaving us a degree of freedom to later tune α such that the prediction from our star construction best captures the observed results from a real scale-free network. Hence, β , characterizing the star-hub (k), is extracted from A via (104) and α is a tunable parameter, which we select for the star-model to best fit the complete scale-free network results.

We emphasize that the star approximation in (107) by no means captures the complete behavior of a real scale-free network, as indeed it represents but a crude representation of an isolated hub environment. However, our goal here is to examine stability vs. instability - a feature that only depends on the *sign* of the principal eigenvalue, not on its specific value, and is, therefore, insensitive to the detailed structure of A . As we show in Fig. 4 of the main text, the star approximation, while highly stylized, is, indeed, sufficient to capture this J characteristic.

To obtain the principal eigenvalue we solve the linear equation

$$J\mathbf{v} = \lambda\mathbf{v}. \quad (110)$$

Using the symmetry of (108), we seek a solution of the form $\mathbf{v} = (a, b, b, \dots, b)^\top$, allowing us to reduce (110) into

$$-C\tilde{\kappa}_{\text{nn}}^\eta k^\mu a + k k^\nu b = \lambda a \quad (111)$$

$$k^\rho a - C\tilde{\kappa}_{\text{nn}}^\eta b = \lambda b. \quad (112)$$

Note that in \mathbf{v} the specific values of a, b have no significance, only the ratio a/b , as we are only interested in the *direction* of the eigenvector, not its magnitude. We therefore arbitrarily set $a = 1$, allowing us to solve (111) - (112) and obtain

$$\lambda = \frac{1}{2} \left(-C\tilde{\kappa}_{\text{nn}}^\eta (k^\mu + 1) + \sqrt{C^2\tilde{\kappa}_{\text{nn}}^{2\eta} (k^\mu + 1)^2 - 4C^2\tilde{\kappa}_{\text{nn}}^{2\eta} k^\mu + 4k^{1+\nu+\rho}} \right), \quad (113)$$

where, of the two solutions, we selected only the one in which the square-root is added (rather than subtracted), as we seek the *largest* eigenvalue. Focusing on the limit

$$\lim_{N \rightarrow \infty} (\lambda), \quad (114)$$

we use (106) and (109) to rewrite (113) as

$$\begin{aligned} \lambda \sim & \frac{1}{2} \left(-CN^{\alpha\eta} (N^{\beta\mu} + 1) \right. \\ & \left. + \sqrt{C^2 N^{2\alpha\eta} (N^{\beta\mu} + 1)^2 + 4 \left[-C^2 N^{2\alpha\eta + \beta\mu} + N^{\beta(1+\nu+\rho)} \right]} \right), \end{aligned} \quad (115)$$

in which we replace $\tilde{\kappa}_{\text{nn}}$ and k by N^α and N^β , respectively. In (115) we ignore the pre-factors of the N -scaling, focusing only on the powers (α, β) , hence substituting the equality sign $=$ with the asymptotic scaling operator \sim (see our discussion leading to Eq. (87) in Sec. 1.4).

The case where $\mu > 0$. First we analyze λ under $\mu > 0$. Here, we write $N^{\beta\mu} \gg 1$, simplifying (115) in the limit $N \rightarrow \infty$ into

$$\lambda \sim \frac{1}{2} \left(-CN^{\alpha\eta + \beta\mu} + \sqrt{C^2 N^{2(\alpha\eta + \beta\mu)} + 4 \left[-C^2 N^{2\alpha\eta + \beta\mu} + N^{\beta(1+\nu+\rho)} \right]} \right). \quad (116)$$

Extracting the common terms out of the product we rewrite (116) as

$$\lambda \sim \frac{1}{2} CN^{\alpha\eta + \beta\mu} \left(-1 + \sqrt{1 + 4 \left(-N^{-\beta\mu} + \frac{1}{C^2} N^\sigma \right)} \right), \quad (117)$$

where

$$\sigma = \beta \left(1 + \nu + \rho - 2\mu - 2\frac{\alpha}{\beta}\eta \right). \quad (118)$$

Note that $N^{-\beta\mu} \leq 1$ in (117), as $\mu > 0$. Therefore, in case $\sigma \geq 0$, the N^σ term dominates the r.h.s. of the equation, providing, under $N \rightarrow \infty$,

$$\lambda \sim \frac{C}{\sqrt{C^2}} N^{\frac{1}{2}\sigma + \alpha\eta + \beta\mu}. \quad (119)$$

Using the fact that $C > 0$ it is guaranteed the λ in (119) is positive, *i.e.* the system is *unstable*.

Next we consider the case $\sigma < 0$. Under these conditions $N^\sigma \ll 1$, allowing us to expand the square-root in (117) to first order, providing

$$\lambda \sim \frac{1}{2}CN^{\alpha\eta+\beta\mu} \left(-1 + 1 + 2 \left(-N^{-\beta\mu} + \frac{1}{C^2}N^\sigma \right) \right) = -CN^{\alpha\eta} + \frac{1}{C}N^{\sigma+\alpha\eta+\beta\mu}. \quad (120)$$

We can rewrite this in the form of Eq. (8) of the main text, obtaining

$$\lambda \sim N^Q \left(1 - \frac{C}{N^S} \right), \quad (121)$$

where

$$Q = \sigma + \alpha\eta + \beta\mu \quad (122)$$

$$S = \sigma + \beta\mu. \quad (123)$$

As N^Q is guaranteed to be positive, the sign of λ depends on S : in case $S > 0$ the negative term in (121) satisfies $CN^{-S} \ll 1$, and hence we have $\lambda \sim N^Q > 0$, an unstable dynamics. If however $S < 0$, we have $-CN^{-S} \rightarrow -\infty$, predicting $\lambda < 0$, regardless of C , an asymptotically stable system. Consequently the system is stable as long as $S < 0$, which, using (123), and taking σ from (118), predicts the stability condition

$$\beta \left(1 + \nu + \rho - \mu - 2\frac{\alpha}{\beta}\eta \right) < 0. \quad (124)$$

This condition reduces stability into a small set of *relevant* parameters: β , characterizing the network topology A , and $\Omega = (\eta, \mu, \nu, \rho)$, associated with the dynamics \mathbf{M} . The non-universal parameter $C = C(\mathbf{f}, \mathcal{G})$ becomes irrelevant in the limit of sufficiently large N . Finally, α can be selected to tune the star approximation optimally to the case of a real scale-free A , as we do below. Note that condition (124) can also be expressed as $\sigma + \beta\mu < 0$. This implies that if $\sigma > \beta\mu$ the system is unstable. This instability condition already contains the previously obtained condition of $\sigma > 0$, that led to Eq. (119). Therefore, Eq. (124) is sufficient to characterize the system's stability.

Finally, the case $S = 0$ in (121) represents sensitive stability, in which λ 's value is not asymptotically defined, and rather it depends on the coefficient C . In this class, stability is no longer a characteristic of the dynamic *model*, but rather of its specific rate constants \mathbf{f}_i and \mathcal{G} , as encapsulated within C . A trivial example is when $\beta = 0$, *i.e.* a non fat-tailed $P(d)$, for example - Erdős-Rényi. Indeed, as we discuss in the main text, in such networks, stability can be tuned by the model parameters, lacking a defined asymptotic behavior.

The case where $\mu \leq 0$. Here, we have $N^{\beta\mu} \leq 1$, and hence Eq. (115) can be approximated by

$$\lambda \sim \frac{1}{2} \left(-CN^{\alpha\eta} + \sqrt{C^2N^{2\alpha\eta} + 4[-C^2N^{2\alpha\eta+\beta\mu} + N^{\beta(1+\nu+\rho)}]} \right), \quad (125)$$

leading to

$$\lambda \sim \frac{1}{2}CN^{\alpha\eta} \left(-1 + \sqrt{1 + 4 \left(-N^{\beta\mu} + \frac{1}{C^2}N^\omega \right)} \right), \quad (126)$$

where

$$\omega = \beta \left(1 + \nu + \rho - 2 \frac{\alpha}{\beta} \eta \right). \quad (127)$$

Once again, we have $N^{\beta\mu} \leq 1$, this time since $\mu < 0$. Therefore, as before, if $\omega > 0$, λ becomes dominated by the N^ω term, following

$$\lambda \sim \frac{C}{\sqrt{C^2}} N^{\frac{1}{2}\omega + \alpha\eta}, \quad (128)$$

which is always positive, *i.e. unstable*. If, however, $\omega < 0$, we use a linear approximation to write

$$\lambda \sim \frac{1}{2} C N^{\alpha\eta} \left(-1 + 1 + 2 \left(-N^{\beta\mu} + \frac{1}{C^2} N^\omega \right) \right) = -C N^{\alpha\eta + \beta\mu} + \frac{1}{C} N^{\omega + \alpha\eta}, \quad (129)$$

as before - a competition between a positive vs. a negative term. Collecting the powers we, once again, rewrite (129) in the form

$$\lambda \sim N^Q \left(1 - \frac{C}{N^S} \right), \quad (130)$$

where this time

$$Q = \omega + \alpha\eta \quad (131)$$

$$S = \omega - \beta\mu. \quad (132)$$

Stability is ensured if, for $N \rightarrow \infty$, the negative term dominates, namely if $S < 0$. Using (127) to express ω this provides

$$\beta \left(1 + \nu + \rho - \mu - 2 \frac{\alpha}{\beta} \eta \right) < 0, \quad (133)$$

recovering precisely the condition in (124).

Tuning α . The parameter α represents a degree of freedom, rooted in the fact that the star approximation captures an inaccurate depiction of a real scale-free network. This approximation can be optimized if we select α such that the star best captures the complete scale-free network environment. We find that setting

$$\alpha = \frac{\beta}{2} \quad (134)$$

provides the optimal approximation, accurately predicting stability $\sim 96\%$ of the time for our 2,881 unweighted networks, $\sim 94\%$ for our 2,290 networks with distributed weights, and $\sim 85\%$ in our 2,216 networks with negative links weights (Fig. 9). This completes the stability analysis, providing the stability classifier

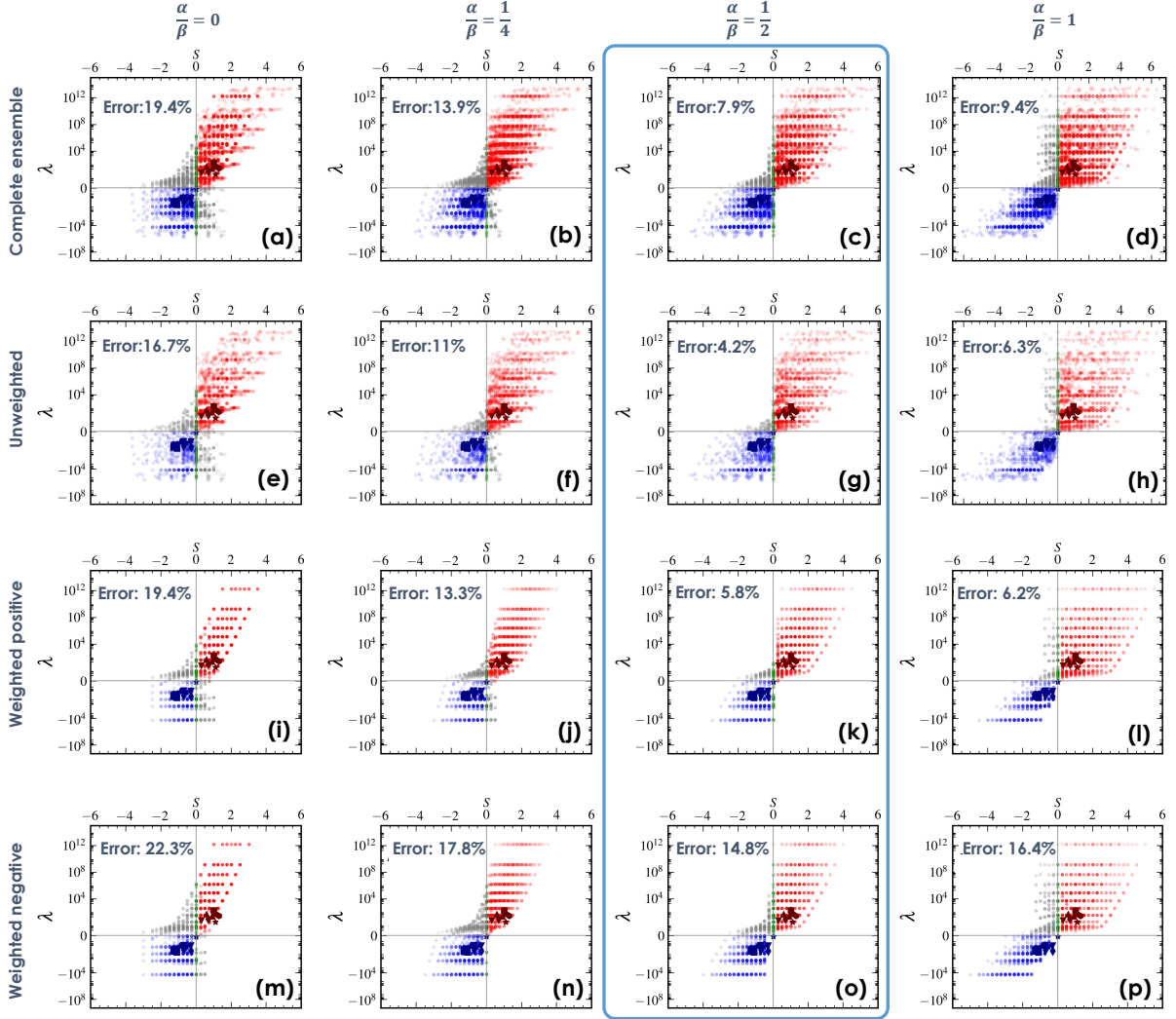


Figure 9: **Tuning the parameter α .** In Eqs. (124) and (133) we have the degree of freedom to set α/β for the star approximation to best predict the stability of complete scale-free networks. We used our ensemble of 7,387 J matrices (Fig. 4a of main text) to predict stability using different values of α/β . Quantifying the Error by the fraction of mis-classified J matrices (grey dots), we find that setting $\alpha/\beta = 1/2$ (blue frame) provides the optimal fit: securing a $\sim 96\%$ correct classification (Error= 4.2%) for unweighted networks, $\sim 94\%$ (Error= 5.8%) for weighted networks and $\sim 85\%$ (Error= 14.8%) for weighted and negative J .

$$S = \beta(1 + \nu + \rho - \mu - \eta), \quad (135)$$

as appears in Eq. (9) of the main text under $\mathbf{s} = 1$.

2.2 Jacobians with negative weights $\mathbf{s} = 0$

Adversarial interactions, in which J 's off-diagonal terms are negative confront us with more complex behaviors. Here, for example, i 's neighbor j has a negative impact on x_i , but its second neighbor m has an indirect positive effect, reducing x_j , and by that positively contributing to x_i . Our star approximation of (107), including only nearest neighbors, overlooks these indirect effects - and hence yields an identical outcome whether the interactions are cooperative, $\mathbf{s} = 1$, or adversarial, $\mathbf{s} = 0$. Therefore, to evaluate S under negative J_{ij} we consider a fully connected network of

$$k \sim N^\beta \quad (136)$$

nodes, *à la* May's original formulation⁹. This simplification may not allow us to fully evaluate the contribution of A , as, indeed, we have replaced the network by a single large clique, however, we are only interested in the stability of the *dynamics*, which remains independent of this simplifying assumption. With *all* nodes now having degree k , the resulting Jacobian takes the form

$$J = -Ck^\eta \begin{bmatrix} k^\mu & 0 & \dots & 0 \\ 0 & k^\mu & \dots & 0 \\ \vdots & & \ddots & \vdots \\ 0 & 0 & \dots & k^\mu \end{bmatrix} - \begin{bmatrix} 0 & k^{\nu+\rho} & \dots & k^{\nu+\rho} \\ k^{\nu+\rho} & 0 & \dots & k^{\nu+\rho} \\ \vdots & & \ddots & \vdots \\ k^{\nu+\rho} & k^{\nu+\rho} & \dots & 0 \end{bmatrix}, \quad (137)$$

in which both the diagonal and the off-diagonal terms are preceded by a minus sign.

For a matrix of the form (137) the principal eigenvector is $\mathbf{v} = (1, -1, 0, \dots, 0)^\top$, whose associated eigenvalue is

$$\lambda = -Ck^{\eta+\mu} + k^{\nu+\rho}. \quad (138)$$

Using (136) we rewrite (138) in the form

$$\lambda = N^Q \left(1 - \frac{C}{NS} \right), \quad (139)$$

where now

$$Q = \beta(\nu + \rho) \quad (140)$$

$$S = \beta(\nu + \rho - \mu - \eta). \quad (141)$$

Hence under adversarial interactions the stability classifier is different from (133), providing the stability condition

$$S = \beta (\nu + \rho - \mu - \eta) < 0, \quad (142)$$

namely Eq. (9) of the main text with $\mathbf{s} = 0$.

2.3 The role of topology vs. dynamics

The stability condition (135) is driven by five distinct exponents. The first four exponents $\Omega = (\eta, \mu, \nu, \rho)$ are determined by the dynamic model - Social, Regulatory, Population etc. - intrinsic to the system's inherent interaction mechanisms. These exponents are independent of the topology A or of microscopic model parameters, encapsulated within C , and are therefore *hardwired* into the system's dynamic behavior. For example, our formalism predicts that the SIS model (Epidemic) has $\Omega = (0, 1, -1, 0)$ (Sec. 3.1). This prediction is characteristic of the SIS model, namely it is an intrinsic feature of the SIS interaction mechanisms of infection and recovery. It is, therefore, insensitive to the specific rates of the model - predicting that Ω remains unchanged if, *e.g.*, a disease has a high or low infection rate, or if it is transmitted via physical contact or aerosols. These will impact the constant C in (96), but will have no impact on the universal scaling. Similarly, Ω is unaffected by A . Therefore, regardless of whether the disease spreads along the standard social network (Flu) or via sexual transmission (AIDS), as long as the *mechanism* is SIS (or any other mechanism for that matter) Ω remains the same. The remaining exponent in (135), β , on the other hand, is independent of the dynamics, and determined solely by A, G , specifically by the weighted degree distribution $P(d)$, capturing the divergence of \mathcal{D}_{nn} in the limit of large N . Hence, together, S captures the emergence of stability/instability as driven by the interplay of topology and dynamics.

3 Analyzing the dynamic models

To demonstrate our formalism we examined several commonly used dynamic models, as listed in Fig. 2 of the main text. Below we extract the exponents Ω and the stability classifier S for each of these models. The first five models are treated in this section, while the last two, Power and Population 2, which extend our application beyond the analytical framework of Sec. 1, are analyzed separately in Sec. 4.

3.1 Epidemic dynamics

As our first demonstration we model epidemic spreading via the Susceptible-Infected-Susceptible (SIS) model¹⁰, in which $x_i(t)$ captures the probability of infection of node i . Denoting the susceptible state by \mathcal{S} and the infected state by \mathcal{I} , the model includes the following transitions



capturing the processes of recovery at a rate f_i , and infection at the pairwise interaction rate G_{ij} . This gives rise to the dynamic equation¹¹

$$\frac{dx_i}{dt} = -f_i x_i(t) + \mathcal{G} \sum_{j=1}^N A_{ij} G_{ij} (1 - x_i(t)) x_j(t), \quad (145)$$

characterized by the dynamic functions $M_0(x_i, \mathbf{f}_i) = -f_i x_i$, in which \mathbf{f}_i comprises a single parameter $\mathbf{f}_i = \{f_i\}$, $M_1(x_i) = 1 - x_i$ and $M_2(x_j) = x_j$. The link weights G_{ij} capture the infection rate between all interacting individuals, and \mathcal{G} is the average infection rate.

Trivial state. First, we note that the SIS model exhibits a trivial fixed-point $\mathbf{x}^* = 0$, the *healthy* state, in which $M_0(0) = M_2(0) = 0$. Together this classifies the SIS model into Case II of Eqs. (102) and (103), hence predicting the null-state Jacobian to follow $J_{\in \mathbb{E}(A, G, \Omega)}$ with

$$\Omega = (0, 0, 0, 0). \quad (146)$$

Using Eq. (135) this provides $\mathcal{S} = \beta$, which for a fat-tailed $P(d)$, in which $\beta > 0$, predicts asymptotic instability.

With this prediction our formalism retrieves an already well-established result, that the epidemic threshold of the SIS model vanishes under a scale-free topology⁷. Therefore, regardless of the specific parameters, f_i, \mathcal{G} , the pandemic state is always the only stable fixed-point of this model when implemented on a scale-free A . This is precisely the meaning of our observation here that $\mathbf{x}^* = (0, \dots, 0)^\top$ is asymptotically unstable. However, while the original result was reported specifically for the Epidemic dynamics, using a dedicated analysis, in our formalism, this observation is but a special case of a broad class of potentially stable/unstable dynamics, all predictable via the $\mathbb{E}(A, G, \Omega)$ ensemble.

Non-trivial state/s. To obtain the relevant J ensemble for the non-zero fixed-point/s, we seek the exponents $\Omega = (\eta, \mu, \nu, \rho)$. We begin by translating \mathbf{M} into the relevant functions shown in (93), providing

$$R(x) = -\frac{M_1(x)}{M_0(x)} = \frac{1-x}{fx} \quad (147)$$

$$Y(x) = M_1(x)R'(x) = \frac{x-1}{fx^2} \quad (148)$$

$$Z(x) = R(x)M_2(x) = \frac{1}{f} - \frac{1}{f}x, \quad (149)$$

where we used $f = \langle f \rangle$ to denote the average recovery rate. Inverting $R(x)$ and $Z(x)$, we write

$$R^{-1}(x) = \frac{1}{fx+1}, \quad (150)$$

$$Z^{-1}(x) = 1 - fx, \quad (151)$$

allowing us to construct the Hahn expansions of (94) as

$$M_2(Z^{-1}(x)) = Z^{-1}(x) = 1 - fx \quad (152)$$

$$Y(R^{-1}(x)) = \frac{R^{-1}(x) - 1}{f \times (R^{-1}(x))^2} = -x - fx^2 \quad (153)$$

$$M_1(R^{-1}(x)) = 1 - R^{-1}(x) = \frac{fx}{fx + 1} = fx - f^2x^2 + f^3x^3 - \dots \quad (154)$$

$$M_2'(R^{-1}(x)) = 1. \quad (155)$$

Here both $R(x)$ and $Z(x)$ are invertible, and therefore, the system exhibits only a single fixed-point apart from $\mathbf{x}^* = (0, \dots, 0)^\top$. Each of the functions in (152) - (155) is expressed as a Hahn power-series, in some cases a finite polynomial, *e.g.*, (152) or (153), and in others an infinite series, where we only write the leading terms around $x \rightarrow 0$. Here, coincidentally, the last function (155) is a constant, *i.e.* a trivial power-series in which the only participating power is x^0 . We can list the relevant powers in these Hahn expansions as $\Psi(0) = 0, \Gamma(0) = 1, \Pi(0) = 1$ and $\Theta(0) = 0$, which, using (95) provides

$$\mu = 2 - \Gamma(0) = 1 \quad (156)$$

$$\nu = -\Pi(0) = -1 \quad (157)$$

$$\rho = -\Theta(0) = 0 \quad (158)$$

$$\eta = -\Psi(0)(\mu - \nu - \rho) = 0. \quad (159)$$

Consequently the stability classifier in (135) is $\mathcal{S} = \beta(1 - 1 + 0 - 1 - 0) = -\beta$, which for a fat-tailed $P(d)$ ($\beta > 0$) predicts the asymptotic stability of the pandemic state, indeed, reconfirming Ref.⁷.

3.2 Regulatory dynamics

We used the Michaelis-Menten model to capture gene regulation in sub-cellular networks¹². Here, Eq. (16) tracks the level of gene expression $x_i(t)$, as regulated via its interacting genes, providing

$$\frac{dx_i}{dt} = -f_i x_i^a(t) + \mathcal{G} \sum_{j=1}^N A_{ij} G_{ij} \frac{x_j^h(t)}{1 + x_j^h(t)}. \quad (160)$$

The self-dynamic term $M_0(x_i, \mathbf{f}_i) = -f_i x_i^a$ captures biochemical processes¹³, such as degradation ($a = 1$) or dimerization ($a = 2$). The interaction terms $M_1(x_i) = 1, M_2(x_j) = x_j^h / (1 + x_j^h)$ describe genetic activation, a *switch-like* dynamics, which ranges from $M_2(0) = 0$ to $M_2(x_j \rightarrow \infty) = 1$, capturing activation of gene i by gene j . The Hill coefficient h governs the rate of saturation of $M_2(x)$, often associated with the level of cooperation in gene regulation¹². The exponents a and h , are intrinsic to the interaction mechanisms, determined by the order of the relevant chemical reactions¹³, and are therefore taken to be uniform for all nodes/links. The parameters f_i, G_{ij} , on the other hand, capture the specific rates of all processes, which are potentially diverse across all nodes/links. Similarly, the average interaction rate \mathcal{G} is also subject to external perturbation by the cell's environmental conditions.

Trivial state. Regulatory dynamics exhibit a trivial solution $\mathbf{x}^* = (0, \dots, 0)^\top$, capturing cell-death. Following (102) and (103) we write

$$W_{ii} = af_i x^{a-1} \Big|_{x=0} \quad (161)$$

$$W_{ij} = A_{ij} w_{ij} \frac{hx^{h-1}}{(1+x^h)^2} \Big|_{x=0}. \quad (162)$$

Both terms vanish in case $a, h > 1$. This represents Case IV of Sec. 1.5, in which the linear regime is void. Under these conditions, the stability of the null state must be treated by resorting to higher orders, which are not within the scope of our formalism. Fortunately, thanks to the fact that the higher order expansion is around the trivial point $\mathbf{x}^* = (0, \dots, 0)^\top$, the analysis becomes straightforward. Indeed, for $x_i \rightarrow 0$, Eq. (160) approaches

$$\frac{dx_i}{dt} = -f_i x_i^a + \mathcal{G} \sum_{j=1}^N A_{ij} G_{ij} x_j^h \rightarrow \begin{cases} -f_i x_i^a & a < h \\ \mathcal{G} \sum_{j=1}^N A_{ij} G_{ij} x_j^h & a \geq h \end{cases}, \quad (163)$$

being dominated by the negative term if $a < h$, and by the positive term otherwise. For $a = h$, as the positive interaction term scales with d_i , having a sum over all of i 's neighbors, it will asymptotically dominate the dynamics. As a consequence the null state is stable if $a < h$ and unstable otherwise.

The remaining scenario is when $a = h = 1$, precisely the dynamics we analyze in the main text under Regulatory. Here (161) and (162) provide $W_{ii} = f_i$ and $W_{ij} = A_{ij} G_{ij}$, both independent of d_i, d_j . This corresponds to $J \in \mathbb{E}(A, G, \Omega)$, with

$$\Omega = (0, 0, 0, 0), \quad (164)$$

an asymptotically unstable fixed-point, as per Case II of Sec. 1.5. Therefore, while $\mathbf{x}^* = (0, \dots, 0)^\top$ may generally be stable, if the system is large and heterogeneous it will inevitably avoid this undesired state.

Non-trivial fixed-points. We now return to our formalism to analyze the stability of the non-vanishing states. First, we construct the three functions summarized in (93):

$$R(x) = -\frac{M_1(x)}{M_0(x)} = \frac{1}{fx^a} \quad (165)$$

$$Y(x) = M_1(x)R'(x) = -\frac{a}{fx^{a+1}} \quad (166)$$

$$Z(x) = R(x)M_2(x) = \frac{x^h}{f(x^a + x^{a+h})}, \quad (167)$$

where, once again, we use $f = \langle f \rangle$ to represent ensemble average over f_i . Inverting $R(x)$, we write

$$R^{-1}(x) = f^{-\frac{1}{a}} x^{-\frac{1}{a}}, \quad (168)$$

allowing us to construct the Hahn expansions (94)

$$Y(R^{-1}(x)) = -\frac{a}{f} \left(\frac{1}{fx} \right)^{-\frac{a+1}{a}} = af^{\frac{1}{a}} x^{\frac{a+1}{a}} \quad (169)$$

$$M_1(R^{-1}(x)) = 1 = x^0 \quad (170)$$

$$M_2'(R^{-1}(x)) = \frac{hf^{-\frac{h-1}{a}} x^{-\frac{h-1}{a}}}{\left(1 + f^{-\frac{h}{a}} x^{-\frac{h}{a}}\right)^2} = hf^{\frac{h+1}{a}} x^{\frac{h+1}{a}} - 2hf^{\frac{2h+1}{a}} x^{\frac{2h+1}{a}} + \dots \quad (171)$$

In each of these expansions we write the leading terms in the $x \rightarrow 0$ limit: in (169) and (170) the expansion features a single term, *i.e.* a pure monomial, and in (171) we show the first two terms of the relevant Hahn expansion. To obtain Ω we extract only the leading *powers* $\Gamma(0) = (a+1)/a$, $\Pi(0) = 0$, $\Theta(0) = (h+1)/a$, ignoring the *coefficients*, *e.g.*, $af^{1/a}$ or $hf^{(h+1)/a}$. We can now use (95) to extract the dynamic exponents as

$$\mu = 2 - \Gamma(0) = \frac{a-1}{a} \quad (172)$$

$$\nu = -\Pi(0) = 0 \quad (173)$$

$$\rho = -\Theta(0) = -\frac{h+1}{a}. \quad (174)$$

To obtain η we must calculate $M_2(Z^{-1}(x))$, requiring us to invert the function $Z(x)$ in (167). This becomes prohibitively complicated under a general a and h , however, as we are only focused on the leading powers of $M_2(Z^{-1}(x))$, we can advance using an asymptotic analysis. Similar to the trivial fixed-point analysis, we once again, distinguish between $a \geq h$ and $a < h$.

Regulatory dynamics under $a \geq h$. Under these conditions $Z(x)$ is monotonous and therefore invertible. For $x \rightarrow \infty$ we have $Z(x) \sim x^{-a}$, which approaches zero (Fig. 10a, blue). Therefore, the inverse $Z^{-1}(x)$ tends to infinity as $x \rightarrow 0$ (red). The form of this divergence can be obtained by mirroring the large x behavior of $Z(x)$, providing $Z^{-1}(x) \sim x^{-1/a}$. This enables us to construct the final Hahn expansion to leading order as

$$M_2(Z^{-1}(x)) \sim \frac{x^{-\frac{h}{a}}}{1 + x^{-\frac{h}{a}}} \sim 1 - x^{\frac{h}{a}} + \dots, \quad (175)$$

in which the leading power is $\Psi(0) = 0$. As a result, we obtain, using (95) our final exponent

$$\eta = -\Psi(0)(\mu - \nu - \rho) = 0. \quad (176)$$

Collecting the other exponents calculated above in (172) - (174), we derive the stability classifier

$$S = \beta \left(1 + 0 - \frac{h+1}{a} - \frac{a-1}{a} - 0 \right) = -\frac{h}{a}\beta < 0, \quad (177)$$

indicating that for $a \geq h$ the non-trivial fixed-point is asymptotically stable.

Regulatory dynamics under $a < h$. For $a < h$, the function $Z(x)$ in (167) is non-monotonous, its inverse is undefined, and hence the system can potentially reside in multiple fixed-points. As

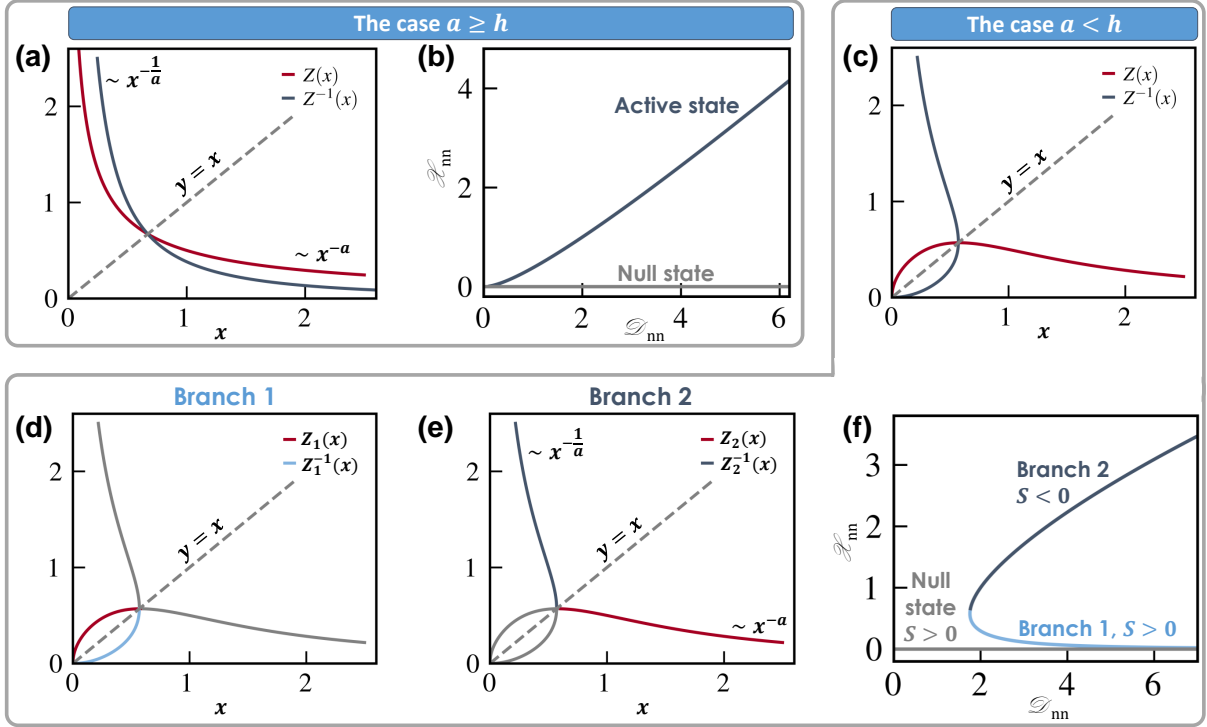


Figure 10: **Analyzing $Z(x)$ in Regulatory dynamics.** (a) $Z(x)$ in (167) vs. x (red) for $a \geq h$, set here to $a = 1, h = 1/2$. Here $Z(x)$ is monotonous and therefore we can obtain its inverse $Z^{-1}(x)$ for all x (blue). Using the fact that $Z(x \rightarrow \infty) \sim x^{-a}$, we can extrapolate that its inverse has $Z^{-1}(x \rightarrow 0) \sim x^{-1/a}$. (b) The nearest neighbor fixed-point activity \mathcal{X}_{nn} vs. \mathcal{D}_{nn} , as obtained for Regulatory dynamics (160) with $a > h$. Following Eq. (53), the limit $Z^{-1}(x \rightarrow 0)$ captured the active state (blue) in the limit of large \mathcal{D}_{nn} , predicting $\mathcal{D}_{nn} \sim \mathcal{X}_{nn}^{1/a}$. The null-state is also shown (grey). (c) For $a < h$, $Z(x)$ is not monotonous (red) and therefore $Z^{-1}(x)$ is undefined (blue). To treat this we divide $Z(x)$ into two branches: Branch 1 to the left of the maximum point; Branch 2 to its right. (d) In Branch 1 we have $Z_1(x \rightarrow 0) \sim x^{h-a}$ (red), providing $Z_1^{-1}(x \rightarrow 0) \sim x^{1/(h-a)}$ (light blue). (e) In Branch 2 we have $Z_2(x \rightarrow \infty) \sim x^{-a}$ (red), and hence $Z_2^{-1}(x \rightarrow 0) \sim x^{-1/a}$ (dark blue). (f) \mathcal{X}_{nn} vs. \mathcal{D}_{nn} under $a < h$. We observe three states: null-state (grey), active state (dark blue), intermediate state (light blue). Branch 1 has $Z_1^{-1}(x) \rightarrow 0$ in the limit of small x , describing a state in which \mathcal{X}_{nn} decreases with \mathcal{D}_{nn} . This corresponds to the intermediate state, for which we obtain $S > 0$, *i.e.* instability. Branch 2 has $Z_2^{-1}(x) \rightarrow \infty$, capturing a positive scaling between \mathcal{D}_{nn} and \mathcal{X}_{nn} . Therefore Branch 2 is related to the active state, which is asymptotically stable ($S < 0$).

an example, in Fig. 10c we present $Z(x)$ for an specific choice of $f = 1, a = 3/2, h = 2$, finding that it is, indeed, non-invertible. We therefore divide $Z(x)$ into its two branches, as shown in Fig. 7: Branch 1 - from $x = 0$ upto the maximum point, and Branch 2 - from the maximum point to $x \rightarrow \infty$. This allows us to construct the two functions, $Z_1(x)$ (Fig. 10d) and $Z_2(x)$ (Fig. 10e), each of which *is* invertible, and whose inverse function is associated with a distinct fixed-point of the system.

First we analyze $Z_1(x)$. As we are interested in the leading power of $M_2(Z_1^{-1}(x))$, we focus on the the behavior around $x \rightarrow 0$. Using (167) we write

$$Z_1(x \rightarrow 0) = x^{h-a} + \dots, \quad (178)$$

where we include only the leading term, and, for simplicity, set $f = 1$. We therefore have

$$Z_1^{-1}(x \rightarrow 0) = x^{\frac{1}{h-a}} + \dots, \quad (179)$$

and finally

$$M_2(Z_1^{-1}(x \rightarrow 0)) = x^{\frac{h}{h-a}} + \dots \quad (180)$$

This provides, for Branch 1, $\Psi(0) = h/(h-a)$, and consequently, taking μ, ν, ρ from (172) - (174), predicts

$$\eta = -\Psi(0)(\mu - \nu - \rho) = \frac{h(a+h)}{a(a-h)}. \quad (181)$$

Collecting all exponents we obtain

$$S = \beta \left(1 + 0 - \frac{h+1}{a} - \frac{a-1}{a} - \frac{h(a+h)}{a(a-h)} \right) = 2 \frac{h(a+1)}{a(h-a)}, \quad (182)$$

which, under the condition $a < h$, is guaranteed to be positive. Therefore, Branch 1 is asymptotically unstable.

The fixed-point captured by Branch 1 has $Z_1^{-1}(x \rightarrow 0) \rightarrow 0$. This captures a state in which the nearest neighbor activity \mathcal{X}_{nn} tends to zero as \mathcal{D}_{nn} is increased. Indeed in Eq. (53) we have $\mathcal{X}_{\text{nn}} = Z^{-1}(q_{\odot})$, in which $q_{\odot} \sim \mathcal{D}_{\text{nn}}^{-1}$ tends to zero in the limit $\mathcal{D}_{\text{nn}} \rightarrow \infty$, indicating that $Z_1^{-1}(x \rightarrow 0)$ captures the asymptotic behavior of \mathcal{X}_{nn} . This behavior, links Branch 1 to the intermediate state in the one-dimensional bifurcation diagram of Fig. 10f (light blue), which is, indeed, characterized by $\mathcal{X}_{\text{nn}} \rightarrow 0$. This state is unstable in the low-dimensional system, and as our formalism now shows, it is also unstable in the asymptotic limit, via our ensemble $\mathbb{E}(A, G, \Omega)$.

Next, we analyze Branch 2, $Z_2(x)$, capturing the part of $Z(x)$ to the right of the maximum point (Fig. 10e, red). Its asymptotic behavior is observed in the limit $x \rightarrow \infty$, where we have $Z_2(x) \sim x^{-a}$. Mirroring this behavior to the inverse $Z_2^{-1}(x)$, we have $Z_2^{-1}(x \rightarrow 0) \sim x^{-1/a}$ (dark blue), leading to

$$M_2(Z^{-1}(x)) \sim \frac{x^{-\frac{h}{a}}}{1 + x^{-\frac{h}{a}}} \sim 1 - x^{\frac{h}{a}} + \dots, \quad (183)$$

namely $\Psi(0) = 0$. Hence, for Branch 2 we have

$$\eta = -\Psi(0)(\mu - \nu - \rho) = 0, \quad (184)$$

which, together with (172) - (174), provides

$$S = \beta \left(1 + 0 - \frac{h+1}{a} - \frac{a-1}{a} - 0 \right) = -\frac{h}{a}\beta < 0, \quad (185)$$

predicting, for this branch, that it is asymptotically stable.

This branch, in which $Z^{-1}(x \rightarrow 0) \rightarrow \infty$ captures a state in which \mathcal{X}_{nn} increases with \mathcal{D}_{nn} , corresponding to the *active* state of Fig. 10f (dark blue). In a low-dimensional system, the stability of this state depends on the system's specific parameters, *i.e.* $\mathbf{f}_i, \mathcal{G}$. Yet, our formalism shows that this state becomes asymptotically stable for large heterogeneous networks.

3.3 Population 1 dynamics

We consider mutualistic eco-systems, such as plant-pollinator networks or microbial communities, in which the interacting species exhibit symbiotic relationships. The species populations follow the dynamic equation

$$\frac{dx_i}{dt} = x_i(t) \left(1 - \frac{x_i(t)}{f_i} \right) + \mathcal{G} \sum_{j=1}^N A_{ij} G_{ij} x_i(t) F(x_j(t)). \quad (186)$$

The self dynamics

$$M_0(x_i, \mathbf{f}_i) = x_i \left(1 - \frac{x_i}{f_i} \right) \quad (187)$$

captures logistic growth, driven by the single parameter f_i : when the population is small, the species reproduce at a rate proportional to x_i , yet, as x_i approaches the carrying capacity of the system f_i , growth is hindered by competition over limited resources¹⁴. The mutualistic interactions are captured by $M_1(x_i) = x_i$ and $M_2(x_j) = F(x_j)$, where $F(x_j)$ represents the *functional response*, describing the positive impact that species j has on species i . This functional response can take one of several forms¹⁵:

Type slowromancapi@: linear impact

$$F(x) = x. \quad (188)$$

Type slowromancapii@: saturating impact

$$F(x) = \frac{x}{1+x}. \quad (189)$$

Type slowromancapiii@: a generalization of Type slowromancapii@, where

$$F(x) = \frac{x^h}{1+x^h}. \quad (190)$$

In our simulations we used Type slowromancapii@ mutualistic interactions, therefore

$$M_2(x_j) = \frac{x_j}{1+x_j}. \quad (191)$$

For simplicity, we set the average carrying capacity to $\langle f \rangle = 1$.

Trivial state. Equation (186) has a trivial fixed-point $\mathbf{x}^* = (0, \dots, 0)^\top$, in which $M_0(x) = M_1(x) = M_2(x) = 0$. This corresponds to Case III in Sec. 1.5, in which the null-state is unstable. This instability, we emphasize, is different from our asymptotic instability of $S > 0$, as it is independent of network size (N) or of degree heterogeneity ($P(d)$). Indeed, even if we consider the one dimensional version of (186)

$$\frac{dx}{dt} = x \left(1 - \frac{x}{f} \right) + \mathcal{G} x F(x), \quad (192)$$

we find that $x = 0$ is unstable, independently of parameters f, \mathcal{G} . This is despite that fact that

the one-dimensional (192) is certainly not in the relevant asymptotic regime of $N \rightarrow \infty$ and $P(d)$ fat-tailed. Therefore, the null-state instability in this dynamics is unrelated to $\mathbb{E}(A, G, \Omega)$. Fortunately, the stability of this state can be directly analyzed without the need for our more advanced toolbox.

Non-trivial state. Next we analyze the non-vanishing fixed-point/s of (186) using our formalism. For $R(x), Y(x)$ and $Z(x)$ we have

$$R(x) = -\frac{M_1(x)}{M_0(x)} = \frac{1}{x-1} \quad (193)$$

$$Y(x) = M_1(x)R'(x) = -\frac{x}{(x-1)^2} \quad (194)$$

$$Z(x) = R(x)M_2(x) = \frac{x}{x^2-1}. \quad (195)$$

Inverting $R(x)$ and $Z(x)$, we write

$$R^{-1}(x) = \frac{x+1}{x}, \quad (196)$$

$$Z^{-1}(x) = \frac{1}{2x} \left(1 \pm \sqrt{1+4x^2}\right). \quad (197)$$

Note that, similar to Regulatory, here too, $Z(x)$ is non-invertible, and hence we have two branches (\pm) for $Z^{-1}(x)$. In this case, however, the *minus* branch corresponds to a purely negative fixed-point, which is physically irrelevant. Therefore, apart from the null fixed-point analyzed above, we are only left with the *plus* branch of (197). Taking this branch we construct the Hahn expansions of (94) as

$$M_2(Z^{-1}(x)) = \frac{Z^{-1}(x)}{1+Z^{-1}(x)} = \frac{1+\sqrt{1+4x^2}}{2x+1+\sqrt{1+4x^2}} = 1-x+\dots \quad (198)$$

$$Y(R^{-1}(x)) = -\frac{R^{-1}(x)}{(R^{-1}(x)-1)^2} = x+x^2 \quad (199)$$

$$M_1(R^{-1}(x)) = \frac{x+1}{x} = x^{-1}+1 \quad (200)$$

$$M_2'(R^{-1}(x)) = \frac{1}{(R^{-1}(x)+1)^2} = \frac{x^2}{4x^2+4x+1} = x^2-4x^3+\dots, \quad (201)$$

whose leading powers are $\Psi(0) = 0, \Gamma(0) = 1, \Pi(0) = -1$ and $\Theta(0) = 2$. Consequently, the dynamic exponents in (95) are

$$\mu = 2 - \Gamma(0) = 1 \quad (202)$$

$$\nu = -\Pi(0) = 1 \quad (203)$$

$$\rho = -\Theta(0) = -2 \quad (204)$$

$$\eta = -\Psi(0)(\mu - \nu - \rho) = 0. \quad (205)$$

	Epidemic	$\frac{dx_i}{dt} = -f_i x_i + \mathcal{G} \sum_{j=1}^N A_{ij} G_{ij} (1 - x_i) x_j$	$\Omega = (0, 1, -1, 0)$	$S = -\beta$
	Regulatory	$\frac{dx_i}{dt} = -f_i x_i^a + \mathcal{G} \sum_{j=1}^N A_{ij} G_{ij} \frac{x_j^h}{1 + x_j^h}$	$\Omega = \left(0, \frac{a-1}{a}, 0, -\frac{h+1}{a}\right)$	$S = -\frac{h}{a}\beta$
	Population 1	$\frac{dx_i}{dt} = x_i \left(1 - \frac{x_i}{f_i}\right) + \mathcal{G} \sum_{j=1}^N A_{ij} G_{ij} \frac{x_i x_j}{1 - x_j}$	$\Omega = (0, 1, 1, -2)$	$S = -\beta$
	Biochemical	$\frac{dx_i}{dt} = f_i - b_i x_i - \mathcal{G} \sum_{j=1}^N A_{ij} G_{ij} x_i x_j$	$\Omega = (-1, 1, -1, 0)$	$S = -\beta$
	Inhibitory	$\frac{dx_i}{dt} = x_i \left(1 - \frac{x_i}{f_i}\right) \left(\frac{x_i}{b_i} - 1\right) + \mathcal{G} \sum_{j=1}^N A_{ij} G_{ij} \frac{x_i}{1 - x_j}$	$\Omega = \left(-\frac{1}{2}, 1, \frac{1}{2}, -1\right)$	$S = -\beta$
	Power	$\frac{d^2 x_i}{dt^2} = f_i - b_i \frac{dx_i}{dt} + \mathcal{G} \sum_{j=1}^N A_{ij} G_{ij} \sin(x_j - x_i)$	$\Omega = (0, 1, 0, 0)$	$S = 0$
	Population 2	$\frac{dx_i}{dt} = x_i \left(1 - \frac{x_i}{f_i}\right) + \mathcal{G} x_i \frac{\sum_{j=1}^N A_{ij} G_{ij} x_j}{1 + \sum_{j=1}^N A_{ij} G_{ij} x_j}$	$\Omega = (0, 0, -2, 0)$	$S = -\beta$

Table 1: **Dynamic models - summary.** Our seven dynamic models and their associated exponents Ω , as calculated around their active fixed point \mathbf{x}_1 . For each model we also show the stability classifier S . The analysis of Power and Population 2, both beyond the scope of Eq. (16), appears in Sec. 4.

As analyzed in Sec. 1.4.1 we have, in Population 1, $\eta = 0$. This is due both to the *Bounded activities* ($0 < x_i < f_i$) and to the *Saturating* nature of the interaction function $M_2(x)$.

3.4 Biochemical dynamics

As a Biochemical model we consider protein-protein interactions (PPI), which are driven by three processes: $\phi \rightarrow P_i$, describing the synthesis of the i th protein P_i at a rate f_i ; $P_i \rightarrow \phi$, describing protein degradation at rate b_i ; $P_i + P_j \rightleftharpoons P_i P_j$ describing the binding and unbinding of a pair of interacting proteins at rates B_{ij} and U_{ij} respectively. The hetero-dimer $P_i P_j$ undergoes degradation $P_i P_j \rightarrow \phi$ at rate Q_{ij} . The dynamical equations for this system are^{13,16}

$$\frac{dx_i}{dt} = f_i - b_i x_i(t) + \sum_{j=1}^N U_{ij} x_{ij}(t) - \sum_{j=1}^N A_{ij} B_{ij} x_i(t) x_j(t) \quad (206)$$

$$\frac{dx_{ij}}{dt} = B_{ij} A_{ij} x_i(t) x_j(t) - (U_{ij} + Q_{ij}) x_{ij}(t), \quad (207)$$

where $x_i(t)$ is the concentration of P_i and $x_{ij}(t)$ is the concentration of the hetero-dimer $P_i P_j$. Under time-scale separation we assume that the hetero-dimer concentration is at steady-state, setting $dx_{ij}/dt = 0$ in (207). This provides us with

$$\frac{dx_i}{dt} = f_i - b_i x_i(t) - \mathcal{G} \sum_{j=1}^N A_{ij} G_{ij} x_i(t) x_j(t), \quad (208)$$

where the effective binding rate is $\mathcal{G}G_{ij} = Q_{ij}B_{ij}/(U_{ij} + Q_{ij})$. Hence, in the effective equation (208) we have $M_0(x_i, \mathbf{f}_i) = f_i - b_i x_i$, with parameters $\mathbf{f}_i = \{f_i, b_i\}$, $M_1(x_i) = x_i$ and $M_2(x_j) = x_j$. Denoting the average rates by $f = \langle f \rangle, b = \langle b \rangle$, we write the dynamic functions (93) as

$$R(x) = -\frac{M_1(x)}{M_0(x)} = \frac{x}{f - bx} \quad (209)$$

$$Y(x) = M_1(x)R'(x) = -\frac{fx}{(f - bx)^2} \quad (210)$$

$$Z(x) = R(x)M_2(x) = \frac{x^2}{f - bx}. \quad (211)$$

The inverse functions are, therefore

$$R^{-1}(x) = \frac{fx}{1 + bx} \quad (212)$$

$$Z^{-1}(x) = \frac{b}{2}x \left(-1 + \sqrt{1 + \frac{4f}{b^2x}} \right), \quad (213)$$

where in $Z^{-1}(x)$ we choose the positive solution, corresponding to the positive fixed-point of (208), similarly to Population 1 above. We can now compose the functions in (94), obtaining

$$M_2(Z^{-1}(x)) = Z^{-1}(x) = \sqrt{fx}^{\frac{1}{2}} + \frac{b^2}{8\sqrt{f}}x^{\frac{3}{2}} + \dots \quad (214)$$

$$Y(R^{-1}(x)) = -\frac{fR^{-1}(x)}{(f - bR^{-1}(x))^2} = fx + fbx^2 \quad (215)$$

$$M_1(R^{-1}(x)) = -\frac{fx}{1 + bx} = -fx + fbx^2 + \dots \quad (216)$$

$$M_2'(R^{-1}(x)) = 1, \quad (217)$$

allowing us to extract the leading powers as $\Psi(0) = 1/2, \Gamma(0) = 1, \Pi(0) = 1$ and $\Theta(0) = 0$. These powers provide the dynamic exponents via (95), providing, for Biochemical

$$\mu = 2 - \Gamma(0) = 1 \quad (218)$$

$$\nu = -\Pi(0) = -1 \quad (219)$$

$$\rho = -\Theta(0) = 0 \quad (220)$$

$$\eta = -\Psi(0)(\mu - \nu - \rho) = -1. \quad (221)$$

Here, since the interactions are adversarial, as indicated by the $-\mathcal{G}$ pre-factor preceding the interaction term in (208), we have $\mathbf{s} = 0$. Therefore, we use (142) to obtain the stability

classifier, providing us with $S = \beta(-1 + 0 - 1 + 1) = -\beta$, *i.e.* asymptotically stable.

3.5 Inhibitory dynamics

To model inhibition, *e.g.*, between genes¹² or between hosts and pathogens¹⁷, we use

$$\frac{dx_i}{dt} = x_i(t) \left(1 - \frac{x_i(t)}{f_i}\right) \left(\frac{x_i(t)}{b_i} - 1\right) + \mathcal{G} \sum_{j=1}^N A_{ij} G_{ij} x_i(t) \frac{1}{1 + x_j(t)}. \quad (222)$$

The self dynamics captures logistic growth, similar to Population 1, but here, also incorporating the Allee effect¹⁸, which balances competition with the potentially added benefit of the *tribe*. The competition is expressed in $M_0(x_i)$ through the negative growth occurring when $x_i > f_i$, *i.e.* when x_i exceeds the limited carrying capacity of the environment. This competition, however, is overcome by the enhanced growth at $b_i < x_i < f_i$, capturing the cooperative benefit of i from being surrounded by a greater i population. Hence, Eq. (222) is relevant under $b_i \leq f_i$, predicting suppressed growth when $0 < x_i < b_i$ or $x_i > f_i$, and positive growth in the range $b_i < x_i < f_i$. The interaction dynamics describes inhibition: i grows linearly with its instantaneous population x_i , but at a rate which approaches zero as $x_j \rightarrow \infty$. Consequently, the greater is x_j the lower is i 's reproduction rate.

Trivial state. In (222) the null state $\mathbf{x}^* = (0, \dots, 0)^\top$ has $M'_0(0) = -1$ and $M_2(0) = 1$, both non-zero. This adheres to Case I in Sec. 1.5, predicting $W_{ii} \sim -1 + d_i$ and $W_{ij} = 0$. Consequently, the null state is asymptotically unstable, as indeed we show in Fig. 5 of the main text.

Non-trivial state. To analyze the active state of (222) we first rewrite its self-dynamics as

$$M_0(x_i, \mathbf{f}_i) = -x_i + B_i x_i^2 - Q_i x_i^3, \quad (223)$$

where $B_i = (f_i + b_i)/f_i b_i$ and $Q_i = 1/f_i b_i$. Denoting $\langle B \rangle = B$ and $\langle Q \rangle = Q$, we construct the dynamic functions of (93), obtaining

$$R(x) = -\frac{M_1(x)}{M_0(x)} = \frac{1}{1 - Bx + Qx^2} \quad (224)$$

$$Y(x) = M_1(x)R'(x) = \frac{Bx - 2Qx^2}{(1 - Bx + Qx^2)^2} \quad (225)$$

$$Z(x) = R(x)M_2(x) = \frac{1}{1 + (1 - B)x + (Q - B)x^2 + Qx^3}. \quad (226)$$

The inverse function $R^{-1}(x)$ takes the form

$$R^{-1}(x) = \frac{B + \sqrt{B^2 - 4Q + \frac{4Q}{x}}}{2Q}, \quad (227)$$

where once again, we omit the negative branch, as it represents a negative, and hence irrelevant, fixed-point. In the limit $x \rightarrow 0$ we have

$$R^{-1}(x) \sim Q^{-\frac{1}{2}} x^{-\frac{1}{2}}. \quad (228)$$

Inverting $Z(x)$ in (226) is non-tractable analytically, however, as we only need to evaluate $Z^{-1}(x)$ in the limit of $x \rightarrow 0$, we can simplify the challenge, by seeking only the relevant leading terms. In Fig. 11 we show $Z(x)$ (blue) and its inverse $Z^{-1}(x)$ (red). Since $Z(x)$ is non-monotonic, its inverse is undefined, indeed showing several branches (Fig. 11b): Branch 1, the top branch, which diverges in the limit $x \rightarrow 0$, Branch 2, intermediate, and Branch 3, for which $Z^{-1}(x) < 0$. Of these, the only relevant branch is Branch 1, as it is the only one covering the $x \rightarrow 0$ regime. The meaning is that, while $Z(x)$ is non-invertible for all $x \in \mathbb{R}$, the limit $Z^{-1}(x \rightarrow 0)$ is well-defined, as the function is locally invertible around $x = 0$. Examining the corresponding branch in $Z(x)$ we observe that $Z^{-1}(x \rightarrow 0)$ is the mirror image of $Z(x \rightarrow \infty)$ (Branch 1 in Fig. 11a). Using (226) we write $Z(x \rightarrow \infty) \sim Q^{-1}x^{-3}$, and therefore we have, in the limit $x \rightarrow 0$

$$Z^{-1}(x) \sim Q^{-\frac{1}{3}}x^{-\frac{1}{3}}. \quad (229)$$

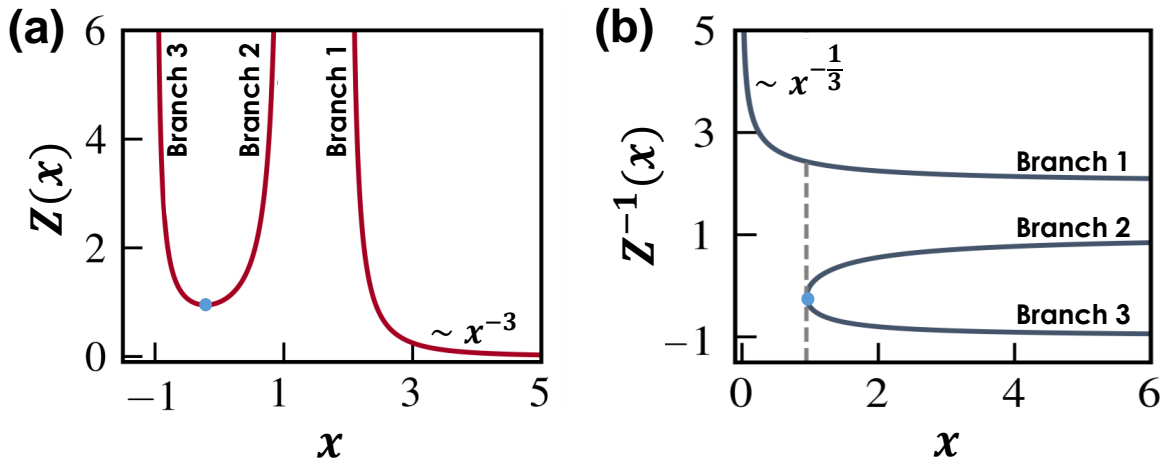


Figure 11: **Analyzing $Z(x)$ in Inhibitory dynamics.** (a) $Z(x)$ in (226) vs. x . The function is divided into three branches, separated by the extremum point (blue dot) and by the asymptotic divergence between Branch 2 and Branch 1. (b) $Z^{-1}(x)$ and its division into the three branches. To the right of the grey dashed line we observe overlapping solutions, and hence $Z^{-1}(x)$ is undefined. However, the limit $Z^{-1}(x \rightarrow 0)$ is well-defined, as in this regime, to the left of the dashed line, only Branch 1 is relevant. The limit $x \rightarrow 0$ in $Z^{-1}(x)$ is the mirror image of the limit $x \rightarrow \infty$ in $Z(x)$. Therefore, using the fact that $Z(x \rightarrow \infty) \sim x^{-3}$ we extrapolate $Z^{-1}(x \rightarrow 0) \sim x^{-1/3}$, as appears in Eq. (229).

With (228) and (229) at hand we can now construct the relevant dynamic functions of (94), obtaining

$$M_2(Z^{-1}(x)) = \frac{1}{1+Z^{-1}(x)} \sim \frac{1}{1+Q^{-\frac{1}{3}}x^{-\frac{1}{3}}} \sim x^{\frac{1}{3}} + \dots \quad (230)$$

$$\begin{aligned} Y(R^{-1}(x)) &= \frac{BR^{-1}(x) - 2Q(R^{-1}(x))^2}{(1 - BR^{-1}(x) + Q(R^{-1}(x))^2)^2} \\ &\sim \frac{BQ^{-\frac{1}{2}}x^{-\frac{1}{2}} - 2x^{-1}}{(1 - BQ^{-\frac{1}{2}}x^{-\frac{1}{2}} + x^{-1})^2} \sim x + \dots \end{aligned} \quad (231)$$

$$M_1(R^{-1}(x)) = R^{-1}(x) \sim x^{-\frac{1}{2}} + \dots \quad (232)$$

$$M_2'(R^{-1}(x)) = -\frac{1}{(1+R^{-1}(x))^2} \sim -\frac{1}{(1+Q^{-\frac{1}{2}}x^{-\frac{1}{2}})^2} \sim x + \dots \quad (233)$$

From here we extract the leading powers as $\Psi(0) = 1/3, \Gamma(0) = 1, \Pi(0) = -1/2$ and $\Theta(0) = 1$, which using (95), predicts

$$\mu = 2 - \Gamma(0) = 1 \quad (234)$$

$$\nu = -\Pi(0) = \frac{1}{2} \quad (235)$$

$$\rho = -\Theta(0) = -1 \quad (236)$$

$$\eta = -\Psi(0)(\mu - \nu - \rho) = -\frac{1}{2}. \quad (237)$$

The inhibitory nature of the dynamics is expressed in J through negative off-diagonal weights. This can be observed through (74), where the derivative $M_2'(x) < 0$, and hence \widetilde{W}_{ij} is negative. Therefore in Inhibitory we have $\mathbf{s} = 0$, the stability classifier follows (142) and, consequently, $S = \beta(1/2 - 1 - 1 + 1/2) = -\beta$, classifying the active state of Inhibitory as asymptotically stable.

Suppressed state. In addition to the inactive and active states of Inhibitory, this system also exhibits a *suppressed* fixed-point, in which the activities x_i become bimodal: $\sim 50\%$ of the nodes have $x_i \rightarrow 0$, and the remaining $\sim 50\%$ have x_i large, positively scaling with d_i . This state emerges as a consequence of the mutual inhibition between neighboring nodes, each pushing its neighbors towards lower activity. To understand this consider node a highly active node i with $x_i \gg 1$. This activity in (222) suppresses the growth rate of its neighbor j , leading to $x_j \ll 1$. Such suppressed x_j benefits j 's neighbors m , who will, consequently, also reach $x_m \gg 1$. As a result the system enters a bifurcated state, in which node i is active, its neighbors are suppressed, its next neighbors are active again and so on. This state breaks our assumed symmetry, in which all neighborhoods are considered similar, and hence cannot be analyzed via our formalism. Accordingly, its associated Jacobian is not covered by the $\mathbb{E}(A, G, \Omega)$ ensemble, therefore beyond the scope of our current analysis.

4 Extended dynamics

Our analytical framework is designed to predict the specific structure of $J \in \mathbb{E}(A, G, \Omega)$ for dynamic systems within the form of Eq. (16), as we have demonstrated on the five models of Sec. 3. The J -ensemble $\mathbb{E}(A, G, \Omega)$, however, is relevant also beyond Eq. (16), representing Jacobian patterns that may potentially emerge under more general conditions. Hence, while our analytically predicted Ω in Sec. 1 is limited to models within (16), the predicted scaling patterns themselves, together with their implications on stability, may cover a broader range of dynamical systems. To observe this we now consider three relevant models that allow us to test J beyond the scope of (16).

4.1 Power dynamics

Load balance in power systems requires synchronization between all generators and consumers, often tracked through the phases $x_i(t)$ of all nodes, following¹⁹

$$\frac{d^2 x_i}{dt^2} = f_i - b_i \frac{dx_i}{dt} + \mathcal{G} \sum_{j=1}^N A_{ij} G_{ij} \sin(x_j(t) - x_i(t)). \quad (238)$$

Here f_i is a node's power generation/consumption, depending on whether it is a generator/consumer, b_i is the damping coefficient, and the interaction is designed to synchronize phases x_i and x_j . The interaction strength is mediated by the conductivity of the i, j transmission line, as controlled by \mathcal{G} and G_{ij} . Equation (238) offers two generalizations to the dynamics of Eq. (16) - first, by including also a second derivative, and second, through its non-separable interaction mechanism, which cannot be expressed in the form $M_1(x_i)M_2(x_j)$. Still, as we show below, its perturbative behavior around the synchronized fixed-point continues to be characterized by a Jacobian within the family of $\mathbb{E}(A, G, \Omega)$.

The synchronized state has $x_i(t) = x_j(t)$ for all i, j , which, by shifting to the rotating frame, can be all set to zero, namely $\mathbf{x}^* = (0, \dots, 0)^\top$. Under a small fixed-point perturbation $\delta \mathbf{x}$ we have

$$\frac{d^2 \delta x_i}{dt^2} = -b_i \frac{d\delta x_i}{dt} + \mathcal{G} \sum_{j=1}^N A_{ij} G_{ij} \sin(\delta x_j(t) - \delta x_i(t)), \quad (239)$$

whose linear approximation becomes

$$\frac{d^2 \delta x_i}{dt^2} = -b_i \frac{d\delta x_i}{dt} + \mathcal{G} \sum_{j=1}^N A_{ij} G_{ij} (\delta x_j(t) - \delta x_i(t)) + O(\delta x^2). \quad (240)$$

Neglecting the nonlinear terms, Eq. (240) can be written as

$$\frac{d^2 \delta x_i}{dt^2} = -b_i \frac{d\delta x_i}{dt} + J_{ii} \delta x_i(t) + \sum_{\substack{j=1 \\ j \neq i}}^N J_{ij} \delta x_j(t), \quad (241)$$

where

$$J_{ii} = -\mathcal{G}d_i \quad (242)$$

$$J_{ij} = A_{ij}G_{ij} \quad (243)$$

is the system's Jacobian. The resulting Jacobian is precisely in the form of $J \in \mathbb{E}(A, G, \Omega)$, where $C(\mathbf{f}, \mathcal{G}) = \mathcal{G}$ and the exponents are $\mu = 1$ and $\eta = \nu = \rho = 0$. Under these conditions we have S in (135) equaling $S = \beta(1 + 0 + 0 - 1 - 0) = 0$, placing Power in the sensitive dynamics class. Note that in this system, due to the second derivative, J plays a different role as compared to its role in (16). Here J governs not just stability but also the system's potential oscillations around \mathbf{x}^* . Additionally, even if $\lambda > 0$, sufficient damping (b_i) may still stabilize the system. Still, our main goal is to show that even for this system, not covered by (16) we continue to observe $J \in \mathbb{E}(A, G, \Omega)$, further strengthening the importance and relevance of this previously unknown ensemble.

4.2 Non-additive dynamics

The structure of (16) assumes that the effect of a node's interacting partners is additive. This allows us to express the interaction as a summation over the nonlinear $M_2(x_j)$, namely $\sum_{j=1}^N M_2(x_j)$. In different contexts this may become a restrictive assumption. As an example we consider Population 2 dynamics, in which

$$\frac{dx_i}{dt} = x_i(t) \left(1 - \frac{x_i(t)}{f_i} \right) + x_i(t) \frac{\sum_{j=1}^N A_{ij}G_{ij}x_j(t)}{1 + \sum_{j=1}^N A_{ij}G_{ij}x_j(t)}, \quad (244)$$

replacing the $\sum_j M_2(x_j)$ structure of (16) by $M_2(\sum_j x_j)$, a non-additive form of interaction.

Once again, despite this system not being covered by our general analytical framework, we can still analyze it using a specific derivation. First, we use our mean-field approximation of (33) and (34) to write

$$\sum_{j=1}^N A_{ij}G_{ij}x_j = d_i \langle x \rangle_{\odot}, \quad (245)$$

substituting the sum by the nearest neighbor average. This allows us to express the *non-vanishing* fixed-point activity for a node $i \in \mathcal{G}(d_i)$ as

$$1 - x_i + \frac{d_i \langle x \rangle_{\odot}}{1 + d_i \langle x \rangle_{\odot}} = 0, \quad (246)$$

where, for simplicity we have taken $f_i = 1$. Extracting x_i from (246) we obtain

$$x_i = \frac{1 + 2d_i \langle x \rangle_{\odot}}{1 + d_i \langle x \rangle_{\odot}} \sim d_i^0, \quad (247)$$

namely that in the limit of large d_i , the fixed-point activities approach a constant and do not scale with degree.

Next, we seek the diagonal Jacobian terms J_{ii} associated with nodes $i \in \mathcal{G}(d_i)$ via

$$J_{ii} = \frac{\partial}{\partial x_i} \left(x_i(1 - x_i) + x_i \frac{\sum_{j=1}^N A_{ij} G_{ij} x_j}{1 + \sum_{j=1}^N A_{ij} G_{ij} x_j} \right), \quad (248)$$

providing us with

$$J_{ii} = 1 - 2x_i + x_i \frac{d_i \langle x \rangle_{\odot}}{1 + d_i \langle x \rangle_{\odot}}. \quad (249)$$

In (249) there are no terms that contribute to the scaling with d_i , as indeed $x_i \sim d_i^0$ and the fraction term on the r.h.s. approaches unity in the limit $d_i \rightarrow \infty$. Therefore, we obtain

$$J_{ii} \sim d_i^0, \quad (250)$$

predicting $\mu = 0$ in $\mathbb{E}(A, G, \Omega)$.

For the off-diagonal terms we write

$$J_{ij} = \frac{\partial}{\partial x_j} \left(x_i(1 - x_i) + x_i \frac{\sum_{m=1}^N A_{im} G_{im} x_m}{1 + \sum_{m=1}^N A_{im} G_{im} x_m} \right), \quad (251)$$

which we break down to the form

$$J_{ij} = \frac{\partial}{\partial x_j} \left(x_i(1 - x_i) + x_i \frac{A_{ij} G_{ij} x_j + \sum_{\substack{m=1 \\ m \neq j}}^N A_{im} G_{im} x_m}{1 + \sum_{m=1}^N A_{im} G_{im} x_m} \right). \quad (252)$$

Extracting the x_j partial derivative we obtain

$$J_{ij} = x_i A_{ij} G_{ij} \left(\frac{1 + \sum_{m=1}^N A_{im} G_{im} x_m - A_{ij} G_{ij} x_j - \sum_{\substack{m=1 \\ m \neq j}}^N A_{im} G_{im} x_m}{\left(1 + \sum_{m=1}^N A_{im} G_{im} x_m \right)^2} \right), \quad (253)$$

which after collecting all terms provides

$$J_{ij} = x_i A_{ij} G_{ij} \frac{1}{\left(1 + \sum_{m=1}^N A_{im} G_{im} x_m \right)^2}. \quad (254)$$

In (254) the only term that contributes to the scaling with d_i or d_j is the summation in the denominator. Using (245) we can express this summation as $\sum_{m=1}^N A_{im} G_{im} x_m = d_i \langle x \rangle_{\odot}$, leading to

$$J_{ij} = x_i A_{ij} G_{ij} \frac{1}{(1 + d_i(x)_\odot)^2}, \quad (255)$$

which in the limit $d_i \rightarrow \infty$ provides us with

$$J_{ij} \sim d_i^{-2}, \quad (256)$$

namely, an $\mathbb{E}(A, G, \Omega)$ Jacobian with $\nu = -2$ and $\rho = 0$. Therefore, despite not being within the form of (16) our Population 2 dynamics is also part of the broad $\mathbb{E}(A, G, \Omega)$ family with

$$\Omega = (0, 0, -2, 0). \quad (257)$$

This represents an asymptotically stable system with $S = \beta(1 - 2 + 0 - 0 - 0) = -\beta$.

4.3 Mixed dynamics

As our final example we consider dynamics with mixed positive/negative interactions. Our analytical derivation revolves around uniform interactions, either fully cooperative, such as Population 1,2 or Regulatory, or fully adversarial, such as Inhibitory or Biochemical. Some applications, however, involve a mixture of cooperative and adversarial interactions, requiring us to analyze signed networks in which $A_{ij} \in \{-1, 0, 1\}$. A classic example arises in population dynamics, which, in many cases, represent a mixture of mutualistic interactions, coexisting alongside competitive and predatory dynamics. Strictly speaking, under these conditions, the Jacobian J cannot be extracted from the $\mathbb{E}(A, G, \Omega)$ ensemble. Yet, as we next show, even then, our theory can still help us understand the emergence of stability.

Consider our Population 1 model

$$\frac{dx_i}{dt} = x_i(t) \left(1 - \frac{x_i(t)}{f_i} \right) + \sum_{j=1}^N A_{ij} G_{ij} x_i(t) \frac{x_j(t)}{1 + x_j(t)}, \quad (258)$$

in which now, the links include a random fraction $0 \leq \phi \leq 1$ of negative interactions ($A_{ij} = -1$) and a remaining $1 - \phi$ fraction of links that are positive ($A_{ij} = 1$). As the system evolves in time, the activities $x_i(t)$ are positively impacted by the cooperative interactions, but suppressed by the adversarial ones. Therefore, nodes with many negatively interacting partners will have their activities driven towards $x_i(t) \rightarrow 0$. The crucial point is that once a node reaches zero activity, it becomes extinct, and effectively removed from the network, together with its set of links. As a consequence the system will reach a steady state, in which the surviving nodes are biased towards positive d_i . *This represents a quite general, and most importantly, a naturally emerging organizing principle that leads real world networks to have a majority of positive links.*

To exemplify this, we constructed a scale-free A with $N = 6,000$ nodes and $L = 18,000$ links, of which a fraction $\phi = 0.1$ are negative, representing a 10% adversarial network. For simplicity, in this and the following simulations we set all parameters and link weights to unity, *i.e.* $\mathbf{f}_i = \mathcal{G} = G_{ij} = 1$. Starting from an arbitrary initial condition, we allowed the system (258) to naturally reach its fixed-point. During the process, whenever a specific activity reached $x_i(t) \leq \epsilon$ we set it permanently to zero (extinction), effectively removing it from the network; we used $\epsilon = 10^{-12}$. At its final state the network is reduced to $N = 5,981$ surviving nodes, featuring a (slight)

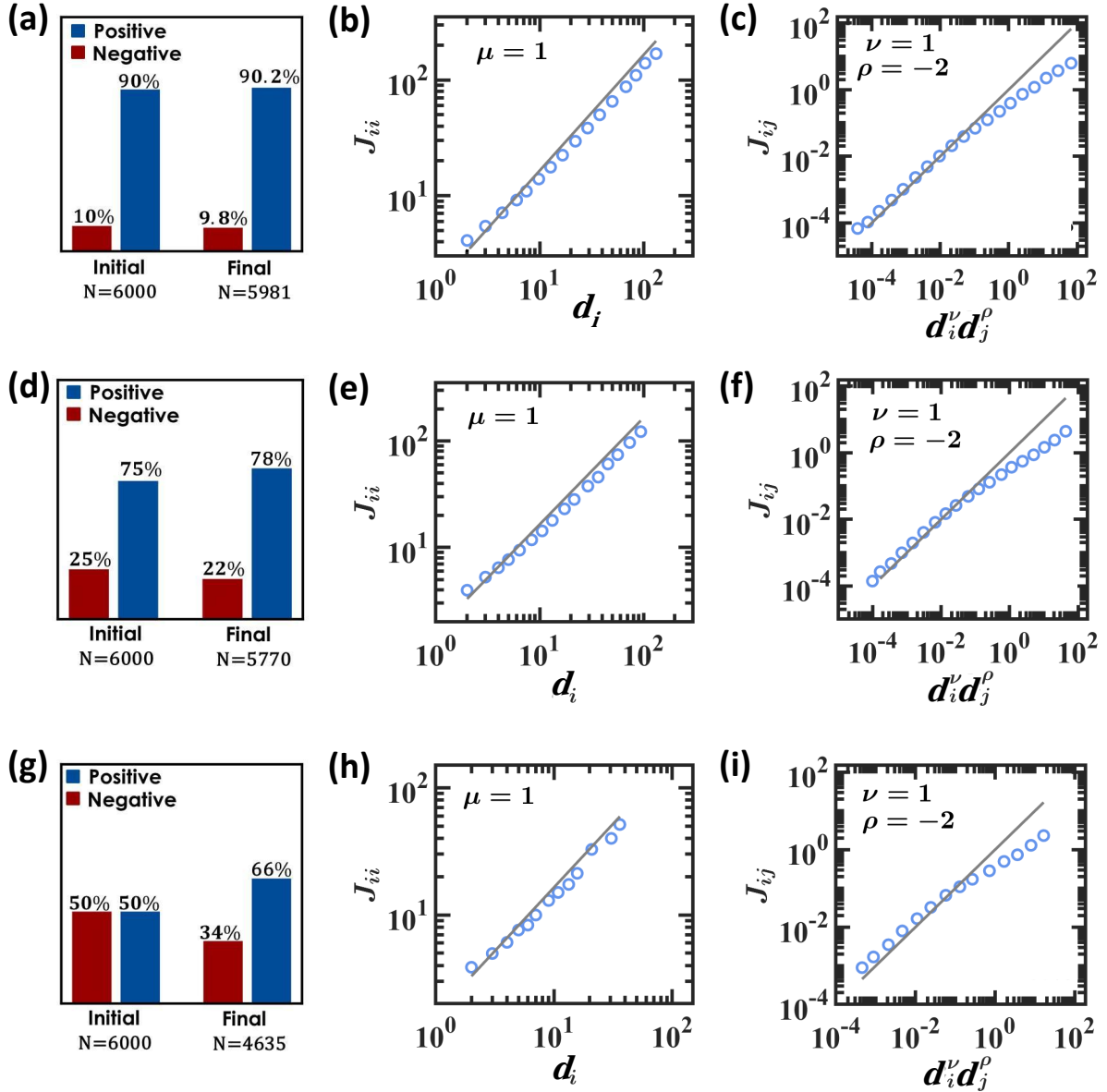


Figure 12: **Emerging stability under mixed interactions.** (a) Starting with a scale-free network A with 10% negative links, the system reaches a fixed-point in which most nodes with many negative links become extinct. As a result the surviving 5,981 node-network is slightly biased towards positive links (9.8% vs. the initial 10% negative). (b) The Jacobian matrix continues to follow the analytically predicted scaling $J_{ii} \sim d_i^\mu$, selectively for the (majority) of positive d_i . (c) Similarly the off-diagonal terms also follow the predicted $J_{ij} \sim d_i^\nu d_j^\rho$ (for $d_i, d_j > 0$). (d)-(f) Similar analysis for an initial 25% negative links. (g)-(i) Even under 50% negative links the surviving network Jacobian (4,635 nodes) can still be approximated by $\mathbb{E}(A, G, \Omega)$.

decrease in the fraction of negative links, from 10% to 9.8% (Fig. 12a). This is a minor effect, of course, however, as we increase the negative link fraction, ϕ , this positive-link bias becomes more pronounced. Indeed, under an initial condition where $\phi = 0.25$, the system reached a final state in which the negative links are reduced to 22% (Fig. 12d), and, finally, starting with a balanced positive-negative network ($\phi = 0.5$), we find, after pruning the extinct nodes, that the final surviving network is 66% positive (Fig. 12g).

For each of these three network, once reaching a fixed point, we extracted numerically their Jacobian matrix, as explained in Sec. 5.2. As expected, the resulting J matrices include both positive and negative weights, and hence, strictly speaking $J \notin \mathbb{E}(A, G, \Omega)$. However, thanks

to the pruning effect, the actual J matrices remain predominantly positive, and the majority of surviving nodes continue to have $d_i > 0$. Hence, while imperfect, we still observe that J follows (approximately) the scaling patterns of the $\mathbb{E}(A, G, \Omega)$ ensemble. Indeed, Fig. 12b,c,e,f,h,i confirms that, despite the inclusion of negative links, J_{ii} and J_{ij} continue to follow (96) and (97) with $\mu = 1, \nu = 1$ and $\rho = -2$, as predicted for Population 1.

Taken together, Secs. 4.1 - 4.3 exemplify that real-world Jacobians, under rather broad conditions, follow the scaling patterns predicted for $\mathbb{E}(A, G, \Omega)$. We wish to emphasize that we do not claim that this ensemble covers *all* network dynamics, as indeed, these sections provide just a few anecdotal examples beyond the coverage of Eq. (16). However, these examples do indicate the potential merit in further studying this Jacobian ensemble and its relevance to a potentially vast range of real-world dynamic applications.

5 Methods and data analysis

5.1 Numerical integration

To numerically test our predictions we constructed Eq. (16) for each of the systems in Sec. 3, using the appropriate network A, G (Scale-free, Erdős-Rényi, empirical, etc.). We then used a fourth-order Runge-Kutta stepper (Matlab's ode45) to numerically solve the resulting equations. Starting from an arbitrary initial condition $x_i(t = 0)$, $i = 1, \dots, N$ we allowed the system to reach steady-state by waiting for $\dot{x}_i \rightarrow 0$. To numerically realize this limit we implemented the termination condition

$$\max_{i=1}^N \left| \frac{x_i(t_n) - x_i(t_{n-1})}{x_i(t_n) \Delta t_n} \right| < \varepsilon, \quad (259)$$

where t_n is the time stamp of the n th Runge-Kutta step and $\Delta t_n = t_n - t_{n-1}$. As the system approaches a steady-state, the activities $x_i(t_n)$ become almost independent of time, and the numerical derivative $\dot{x}_i = x_i(t_n) - x_i(t_{n-1})/\Delta t_n$ becomes small compared to $x_i(t_n)$. The condition (259) guarantees that the maximum of \dot{x}_i/x_i over all activities $x_i(t_n)$ is smaller than the pre-defined termination variable ε . In our simulations, across the different dynamics we tested, we set $\varepsilon \leq 10^{-12}$, a rather strict condition, to ensure that our system is sufficiently close to the *true* steady-state.

5.1.1 Numerical analysis of Power dynamics

To analyze Power dynamics we used the Newton-Raphson method to extract the roots of

$$0 = f_i + \mathcal{G} \sum_{j=1}^N A_{ij} G_{ij} \sin(x_j(t) - x_i(t)), \quad (260)$$

providing the fixed-point of (238), under $\ddot{x}_i = \dot{x}_i = 0$. For a system with n_{gen} generators and n_{load} loads, we set $f_i = -1$ for load nodes and $f_i = n_{\text{load}}/n_{\text{gen}}$ for generators. This ensures a

global balance of power generation vs. demand. The global weight was set to $\mathcal{G} = 1$, and the link weights were also set uniformly to $G_{ij} = 1$, *i.e.* a binary network. In the empirical networks number of loads n_{load} vs. generators n_{gen} is specified in the data. For the model networks we used a balanced network with 50% generator and 50% loads, assigned at random. As our initial condition we extracted x_i from a uniform distribution, seeking an initial condition in which the system converges to a fully positive solution. This was satisfied for $x_i \sim U(0.8, 1.5)$ for the model networks and for $x_i \sim U(3.5, 4.5)$ for the empirical ones. Using the obtained roots $\mathbf{x} = (x_1, \dots, x_N)^\top$ we constructed the relevant Jacobian matrix as explained below in Sec. 5.2.

5.2 Numerically estimating J

Once the steady state $\mathbf{x} = (x_1, \dots, x_N)^\top$ is reached we construct the *numerical* Jacobian by substituting the numerically obtained states x_i into (60) and (74). This represents the system's *actual* stability matrix, as obtained for each dynamics on the relevant network. For example, consider our Epidemic model in Eq. (145), where $M_0(x) = -f_i x_i$, $M_1(x_i) = 1 - x_i$ and $M_2(x) = x_j$, and hence $M'_0(x) = -f_i$, $M'_1 = -1$ and $M'_2 = 1$. Once we obtain \mathbf{x} we introduce all numerically calculated x_i into W_{ii} and W_{ij} , which for Epidemic take the form

$$W_{ii} = -f - \mathcal{G} \sum_{j=1}^N A_{ij} G_{ij} x_j \quad (261)$$

and

$$W_{ij} = \mathcal{G} A_{ij} G_{ij} (1 - x_i). \quad (262)$$

This construction, directly from the numerically obtained fixed-point \mathbf{x}^* is *exact*, incorporating all the potential confounding factors of the real-world system, from the fine-structure and potential degree-correlations in A , to the random distribution of \mathbf{f}_i and G_{ij} , or the varying interaction strength \mathcal{G} . In Fig. 3 of the main text we compare the scaling of these numerically estimated W_{ii} and W_{ij} vs. the theoretically predicted ensemble $\mathbb{E}(A, G, \Omega)$, as provided by (96) and (97).

5.3 Logarithmic binning

Our main theoretical prediction focuses on scaling relationships, such as $W(d) \sim d^\mu$, which we observe by their linear slope in a log-log plot (*e.g.*, Fig. 3 of main text). To construct such plots we employed logarithmic binning²⁰. First we divide all nodes into B bins

$$\mathbb{B}(b) = \left\{ i \in \{1, \dots, N\} \left| c^{b-1} < \frac{d_i}{d_{\min}} \leq c^b \right. \right\}, \quad (263)$$

where $b = 1, \dots, B$, c is a constant and $d_{\min} = \min_{i=1}^N d_i$ is the minimal weighted degree in $A \otimes G$. In (263) the b th bin includes all nodes i whose weighted degree d_i is between $d_{\min} c^{b-1}$ and $d_{\min} c^b$. The parameter c is selected such that the unity of all bins $\cup_{b=1}^B \mathbb{B}(b)$ includes all nodes, hence we set $c^B = d_{\max}/d_{\min}$. Therefore, the first bin $b = 1$ is bounded from below by d_{\min} , and the final bin bounded from above by d_{\max} . Dividing the nodes according to (263) generates exponentially growing bins in d_i , which are *linear* in $\log d_i$, allowing to naturally observe the scaling in the logarithmic plots.

After dividing all nodes into bins, we plot the average degree of the nodes in each bin

$$d_b = \langle d_i \rangle_{i \in \mathbb{B}(b)} = \frac{1}{|\mathbb{B}(b)|} \sum_{i \in \mathbb{B}(b)} d_i \quad (264)$$

versus the average $W(d)$ term of nodes in that bin

$$W(d_b) = \langle W_{ii} \rangle_{i \in \mathbb{B}(b)} = \frac{1}{|\mathbb{B}(b)|} \sum_{i \in \mathbb{B}(b)} W_{ii}. \quad (265)$$

In a similar fashion we plot $W_{ij} \sim d_i^\nu G_{ij} d_j^\rho$, this time applying the binning to $W_{ij}^{\text{Theory}} = d_i^\nu G_{ij} d_j^\rho$, instead of to d_i . Therefore, the bins are defined as

$$\mathbb{B}(b) = \left\{ (i, j) \mid A_{ij} = 1, c^{b-1} < \frac{W_{ij}^{\text{Theory}}}{W_{\min}} \leq c^b \right\}, \quad (266)$$

such that in each bin we include all node pairs whose product $d_i^\nu d_j^\rho$ is within a given range. Similarly to (263) we set $W_{\min} = \min(W_{ij}^{\text{Theory}})$, and select c such that the entire range of W_{ij}^{Theory} is covered. As above, we then plot the average *real* W_{ij} in each bin vs. the theoretically predicted W_{ij}^{Theory} . Specifically, these averages take the form

$$W^{\text{Real}}(b) = \langle W_{ij} \rangle_{(i,j) \in \mathbb{B}(b)} = \frac{1}{|\mathbb{B}(b)|} \sum_{(i,j) \in \mathbb{B}(b)} W_{ij} \quad (267)$$

and

$$W^{\text{Theory}}(b) = \langle d_i^\nu d_j^\rho \rangle_{(i,j) \in \mathbb{B}(b)} = \frac{1}{|\mathbb{B}(b)|} \sum_{(i,j) \in \mathbb{B}(b)} W_{ij}^{\text{Theory}}, \quad (268)$$

where W_{ij} in (267) is constructed via Sec. 5.2.

5.4 Model and empirical networks

To test our predictions we used model and real networks, as summarized below:

ER. An Erdős-Rényi random network with $N = 6,000$ nodes and an average degree of $\langle d \rangle = 6$. Weights were added using $G_{ij} \sim \mathcal{N}(1.0, 0.1)$, a normal distribution function with mean $\mu = 1.0$ and variance $\sigma^2 = 0.1$. Note that this weight distribution allows for a small number of negative weights, hence testing out predictions under a coexistence of a majority positive along side a small minority of negative links.

SF. A binary scale-free network with $N = 6,000$ nodes, average degree $\langle d \rangle = 6$, and degree distribution following $P(d) \sim d^{-\gamma}$ with $\gamma = 2.5$. Under this distribution we have $\mathcal{D}_{\text{nn}} \sim N^\beta$ with $\beta = 0.6$, allowing us to examine our asymptotic limits (which require $\beta > 0$).

SF1. Using the underlying topology of SF we added weights G_{ij} , extracted from a normal distribution with mean $\mu = 1.0$ and variance $\sigma^2 = 0.1$, *i.e.* $G_{ij} \sim \mathcal{N}(1.0, 0.1)$. Also here we do not limit the weights from becoming negative.

SF2. Using the underlying topology of SF we added weights G_{ij} , from a scale-free probability density function $P(G) \sim G^{-\alpha}$ with $\alpha = 3$. Hence, SF2 represents an extremely heterogeneous

	Epidemic	$\mathbf{f}_i = \{f_i\}$	$f_i \sim \mathcal{N}(\mu, \sigma^2), \mu = 1.0, \sigma^2 = 0.1, f_i \geq 0.1$
	Regulatory	$\mathbf{f}_i = \{f_i\}$	$f_i \sim \mathcal{N}(\mu, \sigma^2), \mu = 1.0, \sigma^2 = 0.1, f_i \geq 0.1$
	Population 1	$\mathbf{f}_i = \{f_i\}$	$f_i \sim \mathcal{N}(\mu, \sigma^2), \mu = 1.0, \sigma^2 = 0.1, f_i \geq 0.1$
	Biochemical	$\mathbf{f}_i = \{f_i, b_i\}$	$f_i, b_i \sim \mathcal{N}(\mu, \sigma^2), \mu = 1.0, \sigma^2 = 0.1, f_i, b_i \geq 0.1$
	Inhibitory	$\mathbf{f}_i = \{f_i, b_i\}$	$b_i \sim \mathcal{N}(\mu, \sigma^2), \mu = 1.0, \sigma^2 = 0.1, b_i \geq 0.1, f_i = 2b_i$
	Power	$\mathbf{f}_i = \{f_i, b_i\}$	$f_i = \begin{cases} -1 & \text{For consumers} \\ \frac{n_{\text{load}}}{n_{\text{gen}}} & \text{For generators} \end{cases}, b_i = 1$
	Population 2	$\mathbf{f}_i = \{f_i\}$	$f_i \sim \mathcal{N}(\mu, \sigma^2), \mu = 1.0, \sigma^2 = 0.1, f_i \geq 0.1$

Table 2: **Model parameters.** For each of our dynamic models we summarize the dynamic parameters used in our simulations. For example, in Epidemic the recovery rate was extracted from a truncated normal distribution with mean $\mu = 1.0$ and variance $\sigma^2 = 0.1$. To avoid the irrelevant scenario of a negative recovery rate we truncated this distribution at $f_i \geq 0.1$. Biochemical, Inhibitory and Power have two parameters $\mathbf{f}_i = (f_i, b_i)$. In Inhibitory the Allee effect required $f_i > b_i$ for all species. To ensure this we extracted b_i from a truncated normal distribution, the set $f_i = 2b_i$. In Power the loads were set to -1 for consumer nodes, then the generation we gauges to ensure a balanced network.

network, featuring both scale-free topology and scale-free weights.

UCIonline. An instant messaging network from the University of California Irvine²¹, capturing 61,040 transactions between 1,893 users during a $T = 218$ day period. Connecting all individuals who exchanged messages throughout the period, we obtain a network of 1,893 nodes with 27,670 links, exhibiting a fat-tailed degree distribution. Here weights G_{ij} are taken from a scale-free probability density function $P(G) \sim G^{-\alpha}$ with $\alpha = 3$, once again examining conditions of extreme heterogeneity.

Email Epoch. This dataset monitors $\sim 3 \times 10^5$ emails exchanged between 3,185 individuals over the course of ~ 6 months²², giving rise to a scale-free social network with 31,885 binary links. Here too weights G_{ij} were extracted from a scale-free probability density function $P(G) \sim G^{-\alpha}$ with $\alpha = 3$.

PPI1. The yeast scale-free protein-protein interaction network, consisting of 1,647 nodes (proteins) and 5,036 undirected links, representing chemical interactions between proteins²³. Weights were assigned via $G_{ij} \sim \mathcal{N}(1.0, 0.1)$.

PPI2. The human protein-protein interaction network, a scale-free network, consisting of $N = 2,035$ nodes (proteins) and $L = 13,806$ protein-protein interaction links²⁴. Here too, Weights were assigned via $G_{ij} \sim \mathcal{N}(1.0, 0.1)$.

Microbial 1. To construct microbial networks we collected data on 844 microbial species and 283 associated metabolites²⁵. This allowed us to construct an 844×283 directed bipartite network B whose links capture the production and consumption of metabolites among the microbial species: $B_{im} = 1$ if species i produces metabolite m ; $B_{mi} = 1$ if species i consumes metabolite m ($i = 1, \dots, 844$; $m = 1, \dots, 283$). We then used

$$K_{ij} = \frac{\sum_{m=1}^{283} B_{mi} B_{mj}}{\sum_{m=1}^{283} B_{mi}} \quad (269)$$

to construct a weighted directed complementarity network. In this network the links connect species that compete over the same metabolites. The link weights capture the strength of the competition, quantifying the fraction of i 's consumed metabolites (denominator) on which it must compete with j (numerator). The resulting K has a small fraction of isolated species, hence we consider only its giant connected components, which includes $N = 737$ microbial species linked through $L = 113,350$ competitive interactions.

Microbial 2. Using B above we now construct a mutualistic network via

$$K_{ij} = \frac{\sum_{m=1}^{283} B_{jm} B_{mi}}{\sum_{m=1}^{283} B_{mi}}, \quad (270)$$

now describing the fraction of i 's consumption (denominator) produced by j (numerator). Here, the connected component remains with $N = 496$ nodes and $L = 43,964$ links.

The two networks are of different nature: Microbial 1 is adversarial, relevant *e.g.*, for Inhibitory, while Microbial 2 is cooperative, naturally fitting our Population 1/2 dynamics. Still, for the purpose of examining our theoretical predictions, and mainly for confronting them with empirically observed networks, we applied our Population 1/2 dynamics on both Microbial 1 and 2, despite the fact that the former, is, perhaps, less relevant.

Power grid 1. Power network of Great Britain country, consisting of $N = 2,224$ nodes and $L = 2,804$ links. The nodes are split into 394 generators and 1,830 consumer loads. This network data is publicly available at <http://www.nationalgrid.com>

Power grid 2. Polish Power network known as case2383²⁶⁻²⁸. It consists of $N = 2,383$ nodes, 327 of which are generators and the remaining 2,056 are the consumer loads. These loads and generators are linked through $L = 2,886$ transmission lines. This data is provided by Roman Korab roman.korabat@polsl.pl.

References

- [1] B. Barzel and A.-L. Barabási. Universality in network dynamics. *Nature Physics*, 9:673 – 681, 2013.
- [2] J. Gao, B. Barzel and A.-L. Barabási. Universal resilience patterns in complex networks. *Nature*, 530:307—312, 2016.
- [3] G. Caldarelli. *Scale-free networks: complex webs in nature and technology*. Oxford University Press, New York, 2007.
- [4] S. Boccaletti, V. Latora, Y. Moreno, M. Chavez and D.-U. Hwang. Complex networks: Structure and dynamics. *Physics Reports*, 424:175–308, 2006.
- [5] M.E.J. Newman. *Networks - an introduction*. Oxford University Press, New York, 2010.
- [6] L. Schmetterer and K. Sigmund (Eds.). *Hans Hahn Gesammelte Abhandlungen Band 1/Hans Hahn Collected Works Volume 1*. Springer, Vienna, Austria, 1995.
- [7] R. Pastor-Satorras and A. Vespignani. Epidemic spreading in scale-free networks. *Phys. Rev. Lett.*, 86:3200–3203, 2001.
- [8] H.I. Schreier, Y. Soen and N. Brenner. Exploratory adaptation in large random networks. *Nature Communications*, 8:14826, 2017.
- [9] R.M. May. Will a large complex system be stable? *Nature*, 238:413 – 414, 1972.
- [10] R. Pastor-Satorras, C. Castellano, P. Van Mieghem and A. Vespignani. Epidemic processes in complex networks. *Rev. Mod. Phys.*, 87:925–958, 2015.
- [11] P.S. Dodds and D.J. Watts. A generalized model of social and biological contagion. *Journal of Theoretical Biology*, 232:587–604, 2005.
- [12] G. Karlebach and R. Shamir. Modelling and analysis of gene regulatory networks. *Nature Reviews*, 9:770–780, 2008.
- [13] B. Barzel and O. Biham. Binomial moment equations for stochastic reaction systems. *Phys. Rev. Lett.*, 106:150602–5, 2011.
- [14] R.M. May. Simple mathematical models with very complicated dynamics. *Nature*, 261: 459–467, 1976.
- [15] C.S. Holling. Some characteristics of simple types of predation and parasitism. *The Canadian Entomologist*, 91:385–398, 1959.
- [16] E.O. Voit. *Computational Analysis of Biochemical Systems*. Cambridge University Press, New York, NY, 2000.
- [17] D. Wodarz, J.P. Christensen and A.R. Thomsen. The importance of lytic and nonlytic immune responses in viral infections. *Trends in Immunology*, 23:194–200, 2002.
- [18] W.C. Allee and E.S. Bowen. Studies in animal aggregations: Mass protection against colloidal silver among goldfishes. *Journal of Experimental Zoology*, 61:185–207, 1932.

- [19] G. Filatrella, A. Nielsen and N. Pedersen. Analysis of a power grid using a Kuramoto-like model. *Eur. Phys. J. B*, 61:485–491, 2008.
- [20] S. Milojević. Power-law distributions in information science: making the case for logarithmic binning. *Journal of the American Society for Information Science and Technology*, 61:2417–2425, 2010.
- [21] T. Opsahl and P. Panzarasa. Clustering in weighted networks. *Social Networks*, 31:155–163, 2009.
- [22] J.-P. Eckmann, E. Moses and D. Sergi. Entropy of dialogues creates coherent structures in e-mail traffic. *Proc. Natl. Acad. Sci. USA*, 101:14333–7, 2004.
- [23] H. Yu *et al.* High-quality binary protein interaction map of the yeast interactome network. *Science*, 322:104–110, 2008.
- [24] J.F. Rual *et al.* Towards a proteome-scale map of the human protein–protein interaction network. *Nature*, 437:1173–1178, 2005.
- [25] R. Lim, J.J.T. Cabatbat, T.L.P. Martin, H. Kim, S. Kim, J. Sung, C.-M. Ghim and P.-J. Kim. Large-scale metabolic interaction network of the mouse and human gut microbiota. *Scientific Data*, 7:1–8, 2020.
- [26] R.D. Zimmerman, C.E. Murillo-Sánchez and R.J. Thomas. MATPOWER: Steady-state operations, planning, and analysis tools for power systems research and education. *IEEE Transactions on power systems*, 26:12–19, 2010.
- [27] A.E. Motter, S.A. Myers, M. Anghel and T. Nishikawa. Spontaneous synchrony in power-grid networks. *Nature Physics*, 9:191–197, 2013.
- [28] T. Nishikawa and A.E. Motter. Comparative analysis of existing models for power-grid synchronization. *New Journal of Physics*, 17:015012, 2015.